Fall 2018

Fe(II)-catalyzed transformation of ferrihydrite associated with natural organic matter

Zhe Zhou
University of Iowa

FE(II)-CATALYZED TRANSFORMATION OF FERRIHYDRITE ASSOCIATED WITH NATURAL ORGANIC MATTER

by

Zhe Zhou

A thesis submitted in partial fulfillment
of the requirements for the Doctor of Philosophy
degree in Civil and Environmental Engineering in the
Graduate College of
The University of Iowa

December 2018

Thesis Supervisors: Professor Michelle M. Scherer
Assistant Research Scientist Drew E. Latta

To my parents and Nan for all their support

外 师 造 化， 中 得 心 源。

——张璪 （唐）

Sufficient observation and learning from nature inspires deeper comprehension of the mind.

Zao Zhang (Tang dynasty)

ACKNOWLEDGEMENTS

This was an unexpected journey at the beginning, and it turns out to be one of the best experiences I have ever had. There are a long list of people who helped me to make it so enjoyable. First, I owe much gratitude to my advisor Professor Michelle M. Scherer, who gives me tremendous help and support in research and life. She has set a great example for me as researcher and professor. If I become a professor in the future, I would like my students to evaluate me as what I feel about Michelle. Many thanks also go to our research scientist Dr. Drew E. Latta. His great personality and comprehensive knowledge provided me invaluable guidance throughout my study. I am so grateful to finish my PhD study under their advising. A big thank-you goes out to all of my committee members for their contributions to this work, I am indebted to have their instructions and comments during my study. Thank you to all the students in Scherer lab. I will always remember those struggles and happiness experienced with Luiza and John, and the happy faces of Thomas, Olivia, Amina and many others. You guys make the lab work more enjoyable. I deeply appreciate the great environment made by all the faculty, staff and students to work in. As a Chinese student in this kind of political environment, I am so grateful to work with a group of people that are open, receptive and respectable. The people I met here make me understand the real image of civilization and the causes that make the United States become such a beautiful country. I will let more people in China know the kindness I received here and built more bridges not wall between two counties.

From my deepest heart, I would like to acknowledge the tremendous contributions from my family, who give me the support and love without any reservation. During the writing of my thesis, my parents are experiencing one of the hardest times in their life, they still give me selfless support and comfort as always, that's some love and energy I received incomparable to anything. I also want to note the encouragement given by my grandfather. I could not meet him for the last time

but I always remember his expectation on me. Finally, I want to express my appreciation to Nan, my soulmate and wife, for experiencing all these things with me. Your appearance warms my world and gives all the comforts I would ever need. A special thank you for all the sacrifice you made for me and the family. I love you!

ABSTRACT

The association between natural organic matter (NOM) and iron (Fe) minerals was widely found in soil and sediments and has been shown to impact the fate of Fe minerals and NOM. Ferrihydrite, a ubiquitous Fe mineral, serves as important sink for NOM and rapidly transforms to secondary Fe minerals in the presence of Fe(II). The associated NOM has been found to influence the Fe(II)-catalyzed ferrihydrite transformation pathway, but it remains unclear how various NOM affects this transformation and the implication. This study specifically investigates how different species of NOM affect Fe(II)-catalyzed ferrihydrite transformation under different C/Fe ratios. A series of Fe isotope tracer experiments were conducted to measure Fe atom exchange and electron transfer between aqueous Fe(II) and ferrihydrite in the presence of diverse NOM species. The fate of Ni during Fe(II)-catalyzed transformation of NOM-Fh coprecipitate was also investigated.

Ferrihydrite was found less susceptible to Fe(II)-catalyzed transformation with increasing C/Fe ratio and fulvic acids and Suwannee River NOM (SRNOM) in the coprecipitates need lower C/Fe ratio than humic acids to completely inhibit formation of secondary Fe minerals. At C/Fe ratios where ferrihydrite transformed to secondary minerals, goethite was dominant in ferrihydrite coprecipitated with humic acids, whereas lepidocrocite was favored in ferrihydrite coprecipitated with fulvic acids and SRNOM. Adsorbed SRNOM may be more inhibitive than coprecipitated SRNOM on Fe(II)-catalyzed ferrihydrite transformation under similar C/Fe ratios. Despite no secondary mineral transformation at high C/Fe ratios, Mössbauer spectra indicated electron transfer still occurred between Fe(II) and ferrihydrite coprecipitated with fulvic acid and SRNOM. In addition, isotope tracer experiments revealed that a significant fraction of structural Fe(III) in the ferrihydrite mixed with the aqueous phase Fe(II) (~85%). After reaction with Fe(II), Mössbauer

spectroscopy indicated some subtle changes in the crystallinity, particle size or particle interactions in the coprecipitate.

The effect of coprecipitated SRNOM on Ni(II) distribution during Fe(II)-catalyzed ferrihydrite transformation was investigated with adsorbed Ni(II) and coprecipitated Ni(II). Ni(II) adsorbed on ferrihydrite was more resistant to acid extraction after Fe(II)-catalyzed transformation and suggested that structural incorporation of Ni into secondary Fe minerals occurred. With coprecipitated SRNOM, ferrihydrite did not transform to secondary minerals in the presence of Fe(II) but extensive Fe atom exchange between aqueous Fe(II) and structural Fe(III) still occurred. Limited change in Ni stability was observed, suggesting there was only small portion of Ni redistributed in the presence of Fe(II). Pre-incorporated Ni(II) in Ni-SRNOM-Fh coprecipitate was partially released (6-8 %) in the presence of Fe(II), but the distribution of remaining Ni(II) in the solid did not change measurably. Our observation suggests that the presence of SRNOM limited the redistribution of Ni most likely because of limited transformation of ferrihydrite to secondary minerals.

PUBLIC ABSTRACT

Iron is the fourth most abundant elements in the Earth's crust and can be found as Fe oxides in virtually all soils and sediments. These Fe oxides normally exist as tiny particles in natural environment and can associate with so many critical components in soil, such as natural organic matter (NOM), trace metals and nutrients. Despite the association with Fe minerals was widely found for many natural substances, the interactions between them and the implication to chemicals' behavior in nature remain poorly understood. Our goal is to better understand the interaction between Fe oxides and the key components in natural environment to help environmental engineers and soil scientists address important site contamination and soil health issues. This work specifically focused on the interactions between Fe oxide, NOM and a trace metal (nickel), which aids the understanding of carbon cycle that will impact climate change and the fate of trace metals that impact groundwater safety.

Recently, several worldwide investigations have shown significant amount of NOM in soil and sediments is directly associated with Fe oxides. Associating with Fe oxides can improve the stability of NOM and reduce its release as CO_2 into the air suggesting that Fe oxides may play a critical role in global carbon cycle and climate change. Reducing environments are common in soil and sediment and it has been known for decades that some Fe oxides can be transformed to different Fe oxides under reducing environment which may affect the stability of associated NOM. Our study showed that the association of Fe oxides with NOM can improve the stability of Fe oxides and inhibit transformation to other minerals. More specifically, the species of NOM and the ways NOM bonded to Fe oxides were found to have different effects on the activity of Fe oxide. Our results suggest that NOM and Fe oxides association formed in different types of soil or sediments may have behave differently under reducing environment and provide additional

evidence that understanding the geochemistry of Fe oxides is critical to understanding carbon and trace metal preservation.

TABLE OF CONTENTS

LIST OF TABLES

LIST OF FIGURES

CHAPTER 1: INTRODUCTION

The Biogeochemical Fe Cycle

As the final product of nuclear fusion of stars, Iron (Fe) is one of the dominant elements in the universe (1, 2). Not surprisingly, Fe is also one of the most abundant elements on earth and occupies essential roles in important natural processes including the origin of life (3-5). Specifically, the active redox properties of Fe result in Fe having a significant role in elemental geochemical cycles and microbial respiration. It has been well established that association with Fe minerals controls the mobility, bioavailability and overall fate of many elements, such as carbon, phosphate, nitrate and most trace metals.

Iron can exist in multiple oxidation states with the most commonly found oxidation states in natural environments being ferrous (Fe(II)) and ferric (Fe(III)). The redox transition between Fe(II) and Fe(III) is referred to as the Fe redox cycle and is mediated by multiple microbial and chemical reactions as illustrated in **Figure 1.1**. Abiotic and microbial Fe(II) oxidation by oxygen are the most common pathways to form Fe(III) or Fe(III) minerals (6-10). Fe(II) oxidation by photoferrotrophs, N species, manganese and other natural oxidants have also been demonstrated in the laboratory and observed in natural soil and sediments (11). Due to the low solubility of Fe(III), most oxidized Fe(II) precipitates as Fe(III) minerals. Fe(III) reduction has also been widely observed in natural environments by dissimilatory Fe reduction bacteria (12, 13), photochemical Fe(III) reduction (14) and other abiotic reduction by electron doped humic substances or sulfide species (15-17). The multitude of abiotic and microbial mediated reactions result in active dynamic cycling between Fe(II) and Fe(III) and allow both oxidation states to coexist in a wide variety of environments (18, 19).

The coexistence of Fe(II) and Fe(III) minerals forms one of the most influential redox couples in soil and groundwater chemistry (20). The Fe(II)-Fe(III) redox couple has been linked to the mobility and fate of trace metals, nutrients and groundwater pollutants that closely associate with Fe minerals (21-24). The Fe redox couple has also been shown to affect stability and bioavailability of Fe minerals themselves (25, 26). The reaction between Fe(II) and Fe(III) minerals was originally conceptualized simply as adsorption of Fe(II) onto the surface of Fe(III) minerals (27-29). Adsorption of Fe(II) on Fe(III) minerals became of more interest as it became clear that sorbed Fe(II) reduced a variety of groundwater pollutants (27, 29, 30). The prevailing hypothesis was that this was due to the increased reduction potential of sorbed Fe(II) relative to aqueous Fe(II) (27, 31). Increased reactivity was, at the beginning, attributed to increased electron density in Fe(II) atoms or the formation of some specific surface species (32-34). However, observations comparing the competitive sorption of Fe(II) and trace metals, such as Co^{2+} and Ni^{2+} that with similar atomic size, found that Fe(II) uptake was three times more than other metals, and surprisingly, the presence of Fe(II) also increased the uptake of Ni^{2+}, Co^{2+} and Cu^{2+} (28, 35-37). Based on these observations, a different perspective of Fe(II)-Fe(III) interaction involving an electrochemical reaction emerged (28).

Over the next decade, direct laboratory observation of electron transfer between Fe(II) and Fe(III) mineral was achieved using the isotope specificity of ^{57}Fe Mössbauer spectroscopy (38, 39). ^{57}Fe Mössbauer spectroscopy only recognizes ^{57}Fe isotope, other Fe isotopes, such as ^{56}Fe, are transparent in ^{57}Fe Mössbauer spectroscopy. Capitalizing on the isotope specificity, Fe minerals made with ^{57}Fe were reacted with $^{56}Fe(II)$. The emerging of a $^{57}Fe(II)$ doublet in ^{57}Fe Mössbauer spectroscopy indicated that an electron was transferred from $^{56}Fe(II)$ into $^{57}Fe(III)$ and reduced it to $^{57}Fe(II)$, which provided direct evidence that Fe(III) minerals were reduced by

aqueous Fe(II). Fe minerals were also made with ^{56}Fe, including goethite, hematite and magnetite, and reacted with ^{57}Fe(II) (38, 40, 41). Since ^{56}Fe is transparent to ^{57}Fe Mössbauer spectroscopy, the ^{56}Fe mineral does not have any Mössbauer signal. After reaction with ^{57}Fe(II), the presence of a sextet that was consistent with the Fe mineral present indicates aqueous ^{57}Fe(II) was oxidized by Fe(III) and transferred into structural ^{57}Fe(III). These Fe isotope and Mössbauer spectroscopy based experiments provide compelling evidence that electron transfer occurs between Fe(II) and Fe(III) minerals which provided an alternative conceptual model for explaining sorbed Fe(II) reactivity than simply an increased reduction potential of adsorbed Fe(II). It was, however, still unclear what the fate of injected electron was and how this facilitated adsorption of some trace metals in the presence of Fe(II).

Additional isotope experiments were designed to explore the fate of the injected electron and the movement of Fe(II) and Fe(III). Fe has four stable isotopes, including ^{54}Fe, ^{56}Fe, ^{57}Fe and ^{58}Fe, and some radioactive isotopes (For example ^{55}Fe, half-life = 1004 days). Using inductively-coupled plasma mass spectrometry (ICP-MS) or multi-collector ICP-MS (MC-ICP-MS) the relative abundance of Fe isotopes in different samples can be measured. This allowed experiments to be designed that use Fe isotopes as tracers to track Fe atom movement during the redox cycle of aqueous Fe(II) and Fe(III) minerals. Some early studies used ^{55}Fe as tracer by synthesizing Fe(III) minerals enriched with ^{55}Fe and measured the release of ^{55}Fe during the reaction with Fe(II) (26, 42). Isotopic mixing was observed for ferrihydrite, lepidocrocite and goethite, indicating extensive Fe atom exchange occurred between aqueous Fe(II) and those Fe(III) minerals. More recently, ^{57}Fe enriched aqueous Fe(II) was applied to track Fe atom exchange with Fe minerals that has natural abundance (~ 2.1% of ^{57}Fe, 91.8% of ^{56}Fe) (43-47). In addition, these experiment measured the isotope composition in aqueous Fe over time, as well as the solid Fe mineral and

even extracted Fe(II), giving more details about the Fe isotope mixing process. Based on these experiments, a conceptual model for the reaction of Fe(II) and Fe(III) minerals was proposed named the redox-driven conveyor belt (**Figure 1.2**) (44). The conceptual model included five steps: Fe(II) sorption, electron transfer, oxide growth, electron bulk conduction, and Fe reductive dissolution (44). Electron conduction in bulk was directly supported with the observation in hematite where Fe(II) oxidation and Fe(III) dissolution occurred at different crystal faces in the presence of aqueous Fe(II) (48). The electron migration through goethite surfaces was suggested to proceed by short path length along specific directions (49), no particle size change in goethite was observed by our group (44), but a recent study showed anisotropic morphological changes occurred during the recrystallization of goethite, resulting in an increase in particle width (50). The electrons injected by Fe(II) can also be localized in a trapping site as suggested by a revised conceptual model (51).

To better explain the Fe isotope mixing data, serval models were suggested to describe the Fe atom movement between aqueous Fe(II) and Fe minerals. We have evolved from a linear model (42) to non-linear models that better describe the Fe atom exchange process (52). A homogenous model was suggested based the assumption that exchanged solid would go further exchange with aqueous Fe(II) and finally reach a homogenous Fe isotope distribution (53). But a recent study found a decreasing susceptibility of goethite to further exchange with aqueous Fe(II) and a hybrid model was suggested to include the exchange and burial situations that may happen during Fe atom exchange (54). Despite the efforts of us and many others, it remains a challenge to explain the Fe isotope mixing data and describe the Fe atom exchange process.

Fe atom exchange between aqueous Fe(II) and Fe minerals is coupled with Fe mineral dissolution and reprecipitation process, during which the recrystallization of Fe mineral occurred

(51). The extent of Fe atom exchange, or Fe mineral recrystallization, varies between different Fe minerals and brought disparate impacts on the recrystallized solids. For goethite, the Fe(II)-catalyzed recrystallization did not show significant change in its crystal size or stability (52), similar as magnetite and hematite where lower percent of Fe atom exchange observed (43, 46). But for some Fe minerals that were poorly crystallized, Fe(II)-catalyzed recrystallization dramatically changes the morphology of solid as it transforms into secondary Fe minerals coupled with a complexed Fe atom mixing process (26, 42, 55). In this situation, the Fe(II)-catalyzed mineral recrystallization was normally called as Fe mineral transformation. Among those Fe minerals that are subject to Fe(II)-catalyzed transformation, ferrihydrite may be the one get most attention.

Fe (II)-catalyzed Ferrihydrite Transformation

Ferrihydrite, a short-range ordered Fe hydroxide, is widely spread in soils and sediments. It can be easily precipitated at high pH and was normally the first Fe mineral to form (56, 57). Due to its low crystallinity, ferrihydrite is thermodynamically unstable and can be transformed into more crystallized Fe minerals by aging at high temperature or under reducing environment (58-61). Significant research has been done to understand the ferrihydrite transformation pathway in the last two decades (55, 61-64). Specifically, the Fe(II)-catalyzed ferrihydrite transformation pathway has been investigated under a wide range of conditions. Fe(II) concentration and Fe(II)/Fe(III) ratio have been found to have the most significant influence on the rate of ferrihydrite transformation and the identity of secondary Fe minerals formed (55, 64, 65). At high Fe(II) loading (> 1.0 mmol Fe(II)/g ferrihydrite), magnetite was observed coupled with the formation of goethite and small percentage of lepidocrocite; at low Fe(II) loading, magnetite disappeared and the lepidocrocite growth increased (55, 64). One study suggested that continuous exposure to Fe(II)

would eventually transform lepidocrocite into goethite (62). Lepidocrocite was also suggested as the precursor of goethite during the mineral transformation, but it is not necessary for the formation of goethite. Ligands also affect the rates and ratios of secondary Fe minerals formation (55). Chloride resulted in relatively slower ferrihydrite transformation than sulfate, and lepidocrocite was more favorable in the presence of chloride. Bicarbonate inhibited the formation of magnetite and resulted in more accumulation of goethite (55).

The mechanism behind ferrihydrite transformation, however, remains unclear. One study suggested that attached Fe(II) can transfer electrons into ferrihydrite and form a "reactive ferrihydrite" phase before the formation of secondary Fe minerals (62). Another study using 6-line ferrihydrite speculated that ferrihydrite needs to coagulate and grow through Ostwald ripen during the reaction with Fe(II), and the mineral transformation would not start until the particles exceeded a certain size (66). The Fe(II)-catalyzed ferrihydrite transformation becomes even more complicated in natural environments as ferrihydrite normally associate with lots of substances in the soil or sediments, such as natural organic matter.

The Interaction of Natural Organic Matter and Fe Minerals

Natural organic matter (NOM) in soil and sediments has received increasing attention because of accumulating concerns about atmospheric CO_2 concentration. As one of the most important carbon reservoirs, NOM in soil stores 2-3 times that of carbon than atmospheric CO_2 (67), which directly impacted the carbon cycle between soil and air and may control the CO_2 concentration (68). The stability of NOM in soil is also critical in the carbon cycle. According to several investigations, significant portions of NOM in soil and sediments were directly associated with Fe phase (69, 70). This NOM and Fe association was reported to inhibit microbial degradation of NOM and increase carbon stability in soil (71, 72), which would further affect global carbon

cycle and climate change. In addition, the associated NOM would alter the properties and behavior of Fe minerals and affect other elements that closely associated with Fe phase (73-75).

NOM can associate with Fe minerals through adsorption and coprecipitation. Adsorption of NOM to Fe minerals has been extensively studied (76-78). NOM is a mixture of various molecular structures and the adsorption mechanisms vary depending on the characteristic and proportion of the key functional groups in NOM (79). Interactions between NOM and Fe minerals include but are not limited to electrostatic interaction, van der Waals interaction, ligand exchange, hydrophobic interaction, H-bonding, chelation and cation bridging (79). NOM fractionation occurred during adsorption to Fe minerals and large and intermediate size NOM fractions were preferentially adsorbed by Fe oxides (76, 77). Adsorbed NOM was also found to facilitate aggregation of Fe minerals and reduce Fe mineral reactivity (80, 81).

Compared to adsorption, coprecipitation of NOM and Fe mineral is a more dominant process in sediments (82-84). During the Fe redox cycle, ferrihydrite is normally the first Fe(III) mineral to form and coprecipitate with surrounding NOM and is why most of the studies about NOM-Fe mineral coprecipitates focused on the NOM-Ferrihydrite coprecipitate. Coprecipitation can lead to more carbon retained by ferrihydrite and stronger carbon stability than adsorption (75). The surface area of the NOM-Fh coprecipitate significantly decreased due to the facilitated aggregation and surface blockage by coprecipitated NOM. Even though the particle size of the NOM-Fh coprecipitate increased compared to pure ferrihydrite, the crystal size of ferrihydrite in the coprecipitate was reduced by coprecipitated NOM (73).

The effect of NOM on Fe(II)-catalyzed ferrihydrite transformation is of growing interest because it not only impacts the stability of associated NOM but also affects the fate of trace metals and nutrients that associate with ferrihydrite. From previous studies, we know NOM can inhibit

Fe(II)-catalyzed ferrihydrite transformation (42, 85, 86), however, the mechanism behind this inhibition is unclear. In addition, little is known about the effect of NOM species on this Fe(II)-catalyzed ferrihydrite transformation, which is important because there exists diverse NOM compositions in different soils. A direct comparison between adsorbed OM and coprecipitated OM on Fe(II)-catalyzed ferrihydrite transformation has also not been done nor has the implications of these reactions to the fate of trace metals been investigated.

Objectives and Hypotheses

The overall objective of my work is to explore the effect of NOM on Fe(II)-catalyzed ferrihydrite transformation and its implication to trace metal cycling. I investigated the impact of different NOMs on ferrihydrite transformation pathways, and tracked electron transfer and Fe atom exchange between aqueous Fe^{2+} and structural Fe^{3+} during these reactions. I also compared the influence of coprecipitated NOM and adsorbed NOM on ferrihydrite transformation at different C/Fe ratios. In addition, the effect of NOM on Ni redistribution during Fe(II)-catalyzed ferrihydrite transformation was also investigated. My work has four main objectives addressing multiple specific hypotheses as outlined below.

Objective 1: Quantify rates of Fe^{2+}-catalyzed ferrihydrite mineral transformation in the presence of different NOM.

Hyp. 1a: Ferrihydrite coprecipitated with fulvic acid will transform to secondary minerals slower in the presence of Fe^{2+} than ferrihydrite coprecipitated with humic acid at given similar C/Fe ratio.

Hyp. 1b: Ferrihydrite will transform to secondary minerals slower in the presence of Fe^{2+} when NOM is adsorbed on the surface compared to coprecipitated NOM.

Hyp 1c: Freeze dried and wet ferrihydrite will have different transformation rate and pathway in the presence of Fe(II).

Objective 2: Determine if NOM affects the extent of Fe atoms exchanged during Fe^{2+}-catalyzed ferrihydrite mineral transformation.

Hyp. 2a: The extent of Fe atom exchange between aqueous Fe^{2+} and ferrihydrite will decrease as the C/Fe ratio increases.

Hyp. 2b: Fe atom exchange between aqueous Fe^{2+} and ferrihydrite will be slower in the presence of adsorbed NOM than coprecipitated NOM.

Objective 3: Measure whether NOM affects electron transfer between aqueous Fe^{2+} and structural Fe^{3+} in ferrihydrite.

Hyp. 3a: The amount of electron transferred from aqueous Fe^{2+} to Fe^{3+} in ferrihydrite will be reduced by NOM and will increase as the initial Fe(II) concentration increases.

Hyp. 3b: Electron transfer between aqueous Fe^{2+} and ferrihydrite will be less with adsorbed NOM than coprecipitated NOM given similar Fe^{2+}/Fe^{3+} and C/Fe ratio.

Objective 4: Evaluate whether Ni redistributes in OM-Fh association during Fe^{2+}-catalyzed ferrihydrite recrystallization.

Hyp. 4a: The presence of NOM will reduce the amount of Ni sorbed by ferrihydrite.

Hyp. 4b: Fe^{2+}-catalyzed recrystallization of ferrihydrite will redistribute adsorbed Ni and increase its stability even without the formation of secondary Fe minerals.

Hyp. 4c: Associated NOM will reduce the release of pre-incorporated Ni during Fe^{2+}-catalyzed ferrihydrite recrystallization.

Thesis Overview

My thesis consists of three main chapters which address the objectives and hypotheses listed above. Chapter 2 addresses the effect of NOM species on Fe(II)-catalyzed ferrihydrite transformation including whether electron transfer and Fe atom exchange occur and what these finding suggest about inhibition mechanism of NOM. Chapter 2 was recently published in *Environmental Science & Technology* (87). Chapter 3 explores the inhibition of humic acid and fulvic acid over a wider range of C/Fe ratios. The impact of coprecipitated OM and adsorbed OM on Fe(II)-catalyzed ferrihydrite transformation were also compared in this chapter. Chapter 4 addresses the objective 4 by introducing Ni into NOM and ferrihydrite coprecipitates through adsorption or coprecipitation, and characterizing the Ni distribution during ferrihydrite recrystallization.

In Chapter 2, Different species of NOM were used to synthesize NOM-Fh coprecipitates. Those coprecipitates were reacted with different Fe(II) to track mineral transformation, electron transfer and Fe atom exchange. The comparison of different NOM on ferrihydrite transformation dynamics and electron transfer was carried out. A elaborate investigation was carried out to understand the Fe atom exchange process between aqueous Fe(II) and NOM-Fh coprecipitate. This chapter has been published on Environmental Science & Technology at September 7, 2018 (DOI: 10.1021/acs.est.8b03407)

In chapter 3, I expanded the experimental conditions in NOM-Fh association. The difference of humic acid and fulvic acid on ferrihydrite transformation were further explored at different C/Fe ratios. The adsorbed and coprecipitated SRNOM were compared in the perspective of ferrihydrite mineral transformation and Fe atom exchange. The fate of NOM during Fe(II)-

catalyzed ferrihydrite transformation was explored. This chapter will be extended and prepare for submission to peer-reviewed journal.

Chapter 4 focused on the effect of coprecipitated NOM on Ni distribution during Fe(II)-catalyzed ferrihydrite transformation. Ni adsorption by ferrihydrite with or without NOM were compared in the presence of Fe(II). The distribution of Ni after Fe(II) treatment were investigated through extraction experiments. Pre-incorporated Ni in ferrihydrite and NOM-Fh coprecipitate were also prepared and reacted with aqueous Fe(II). The Ni distribution before and after Fe mineral recrystallization was characterized through acid dissolution. Fe atom movement in these studies was tracked with ^{57}Fe labeled Fe(II).

Appendix A shows the study comparing the transformation pathway of wet ferrihydrite and freeze dried ferrihydrite in the presence of aqueous Fe(II). The results indicates the dry and wet cycle experienced by ferrihydrite in nature will affect Fe(II)-catalyzed transformation pathway. Appendix B contains some preliminary data I obtained to investigate the role of defects on metal sorption by goethite. The relationship between Fe atom exchange and metal incorporation was also discussed. Appendix C contains a manuscript in preparation for submission to a peer-reviewed journal in which we explore the effect of NOM on stable Fe isotope fractionation. In this work, I designed and carried out the experiments and assisted with the explanation of mineral characterization data. Appendix D contains a manuscript that has been submitted to peer-reviewed journal in which I provided Mössbauer spectroscopy characterization and analysis of the natural samples.

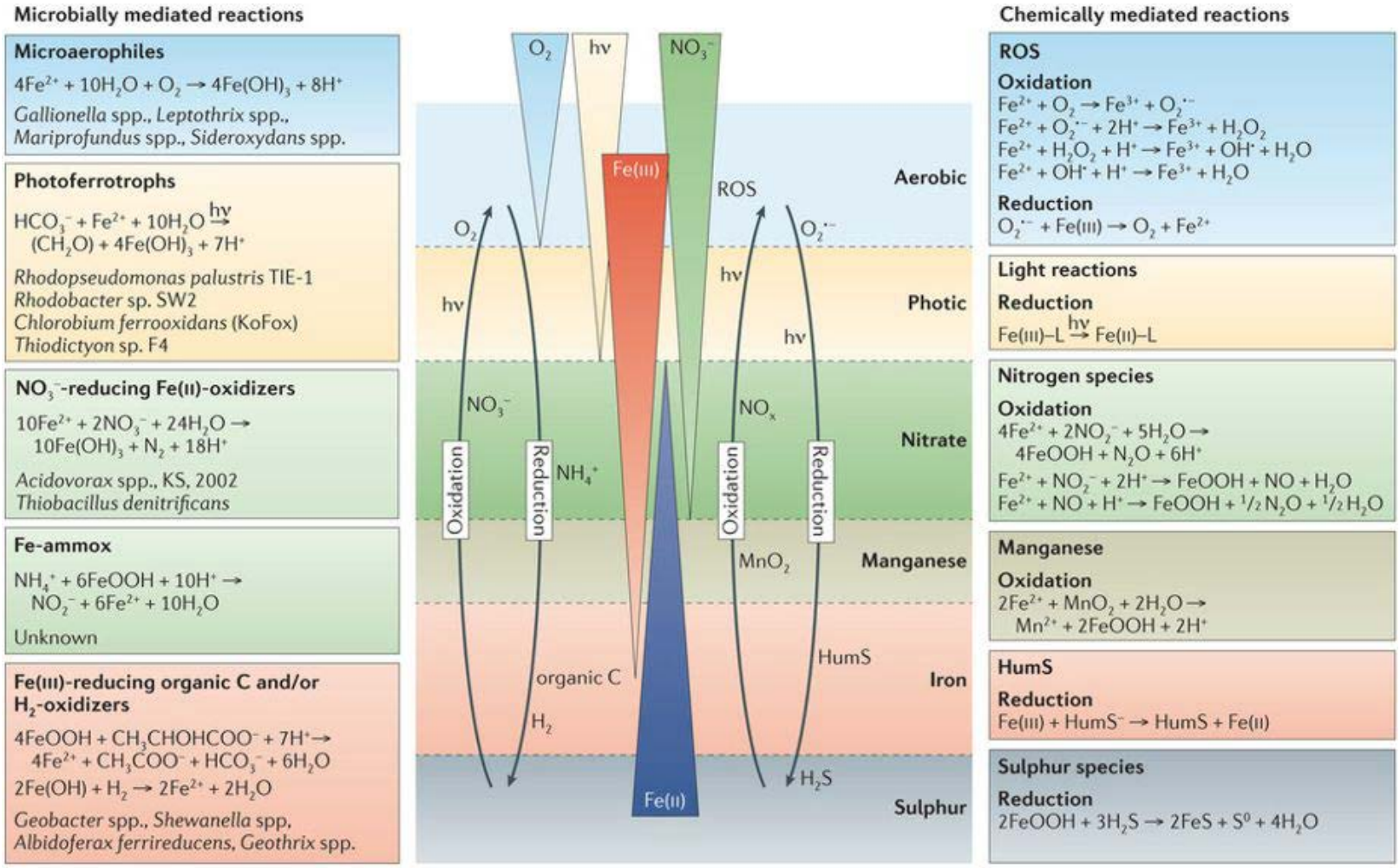

Figure 1.1. Microbially and chemically mediated reactions that constitute the biogeochemical Fe cycle (11).

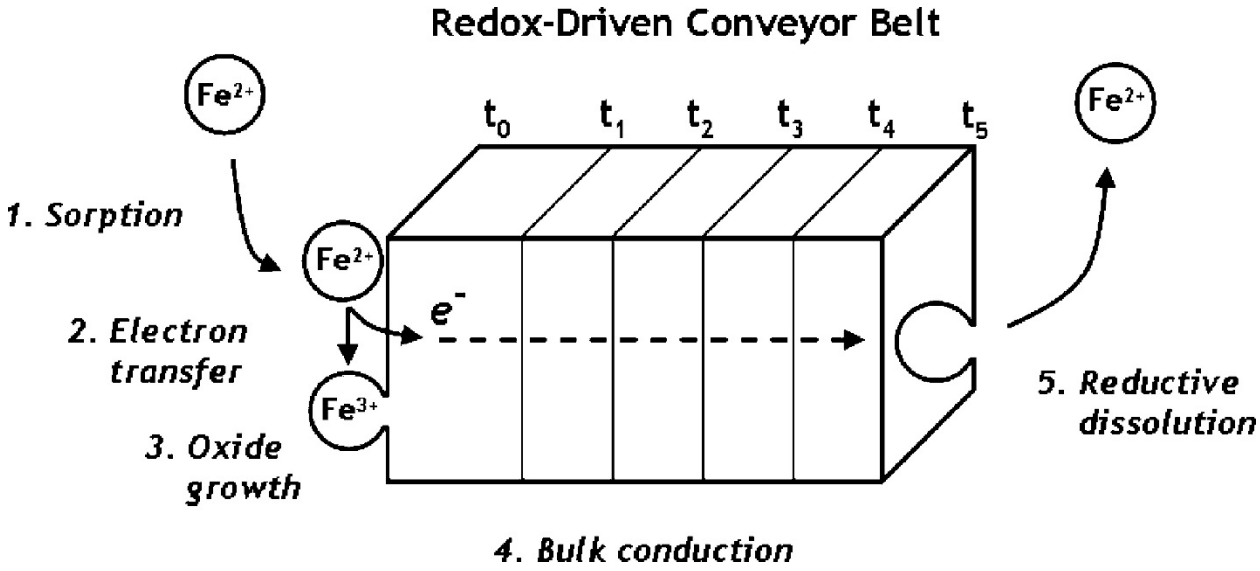

Figure 1.2. Conceptual model for the five steps associated with the redox-driven conveyor belt mechanism to explain how bulk goethite Fe(III) atoms and aqueous Fe(II) can become completely mixed via growth and dissolution at separate goethite surface sites. The left surface may be considered a reference plane in the original goethite crystal at the start of the process (t0), and through growth on the left and dissolution on the right, this reference plane will migrate over time ($t_0 \rightarrow t_5$) until time t_5, at which point 100% atom exchange has occurred (44).

CHAPTER 2: FE(II)-CATALYZED TRANSFORMATION OF ORGANIC MATTER-FERRIHYDRITE COPRECIPITATES (87)

Abstract

Ferrihydrite is a common Fe mineral in soils and sediments that rapidly transforms to secondary minerals in the presence of Fe(II). Both the rate and products of Fe(II)-catalyzed ferrihydrite transformation have been shown to be significantly influenced by natural organic matter (NOM). Here we used enriched Fe isotope experiments and ^{57}Fe Mössbauer spectroscopy to track the formation of secondary minerals, as well as electron transfer and Fe mixing between aqueous Fe(II) and ferrihydrite coprecipitated with several types of NOM. Ferrihydrite coprecipitated with humic acids transformed primarily to goethite after reaction with Fe(II). In contrast, ferrihydrite coprecipitated with fulvic acids and Suwannee River NOM (SRNOM) resulted in no measurable formation of secondary minerals. Despite no secondary mineral transformation, Mössbauer spectra indicated electron transfer still occurred between Fe(II) and ferrihydrite coprecipitated with fulvic acid and SRNOM. In addition, isotope tracer experiments revealed that a significant fraction of structural Fe in the ferrihydrite mixed with the aqueous phase Fe(II) (~ 85%). After reaction with Fe(II), Mössbauer spectroscopy indicated some subtle changes in the crystallinity, particle size or particle interactions in the coprecipitate. Our observations suggest that ferrihydrite coprecipitated with fulvic acid and SRNOM remains a highly dynamic phase even without ferrihydrite transformation.

Introduction

Organic matter (OM) in soils and sediments is often associated with iron (Fe) minerals (69, 70). The close association between organic matter and Fe minerals influences Fe mineral properties and behavior as well as the availability of organic matter carbon in soils. For example, carbon associated with Fe minerals in soils has recently been shown to be protected from microbial mineralization (88, 89). The significant influence of Fe minerals on carbon availability in soils makes it important to understand Fe mineral –OM reactions to better predict and mitigate climate change and soil health (90-92).

Ferrihydrite is an Fe(III) mineral that is often found associated with organic matter and is ubiquitous in both soils and sediments (93-95). Ferrihydrite associated with has been shown to lead to smaller crystal sizes and more defects (94, 96, 97). Despite the smaller crystal sizes, however, ferrihydrite in the presence of OM tends to have smaller surface areas compared to pure ferrihydrite, which has been attributed to OM blocking surface sites and facilitating aggregation (75, 96). In addition to the physical changes in both crystal size and surface area, OM is has also been shown to inhibit the crystallization of ferrihydrite and transformation to secondary minerals (42, 86, 98).

While ferrihydrite on its own is metastable and will slowly transform to secondary minerals such as hematite and goethite, transformation is rapidly accelerated in the presence of dissimilatory Fe(III)-reducing bacteria (DIRB) and Fe(II) (61, 62, 99). Which secondary Fe minerals form (e.g., lepidocrocite, goethite, or magnetite) has been found to depend on multiple factors including Fe(II) concentrations, pH, and anions or other impurities (55, 62, 100). In general, Fe(II)/Fe(III) ratio seems to have the largest influence with higher Fe(II) concentrations leading to goethite and

magnetite, whereas lepidocrocite tends to be more prevalent at lower Fe(II) concentrations (55, 62). Lepidocrocite formation also appears to be favored in the presence of chloride (55, 100).

Since both Fe(II), which accelerates ferrihydrite transformation, and OM, which inhibits ferrihydrite transformation, are often present together in reducing environments, recent studies have explored how OM influences both DIRB and Fe(II)-catalyzed ferrihydrite mineral transformation (42, 86, 101-103). Organic matter that was coprecipitated or adsorbed with ferrihydrite has been found to inhibit Fe(II)-catalyzed ferrihydrite mineral transformation (42, 86, 103). For example, ferrihydrite coprecipitated with OM extracted from the O horizon of an Ultisol resulted in less transformation with higher C/Fe ratio. At C/Fe ratios equal to or greater than 1.6, no ferrihydrite transformation was observed (86). Adsorbed fulvic acid also resulted in significant inhibition of ferrihydrite transformation (C/Fe ratio 4.18) (42). The bio-reduction of ferrihydrite can also be altered by OM. Coprecipitated OM was found to reduce ferrihydrite bio-reduction rates (101). Some studies, however, found that coprecipitated humic acid reduced ferrihydrite bio-reduction rates at low C/Fe ratios ($\leqslant$ 0.8) but enhanced the extent of bio-reduction at high C/Fe ratios ($\geq$ 1.8) (104, 105).

While these studies clearly show that OM influences the transformation of ferrihydrite in the presence of both DIRB and Fe(II), and at high enough C/Fe ratios can even completely inhibit Fe(II)-catalyzed ferrihydrite transformation, it remains unclear how OM inhibits Fe(II)-catalyzed ferrihydrite transformation. Some have suggested that OM inhibits electron transfer between Fe(II) and ferrihydrite which then prevents ferrihydrite from transforming to secondary minerals (42, 86). It has also been shown Fe atom exchange between aqueous Fe(II) and structural Fe(III) is less in the presence of OM and some have suggested that the inhibition of atom exchange may be responsible for less ferrihydrite transformation (42, 103). Here, we directly evaluate whether Fe

electron transfer and atom exchange between Fe(II) and ferrihydrite are inhibited in the presence of OM. Specifically, we used ^{57}Fe Mössbauer spectroscopy and Fe isotope tracers to measure Fe electron transfer and atom exchange between aqueous Fe(II) and ferrihydrite coprecipitated with five different organic matters. Our findings indicate that both Fe electron transfer and atom exchange occur between Fe(II) and ferrihydrite coprecipitated with OM even when no secondary mineral transformation is observed.

Material and Methods

OM - Ferrihydrite Coprecipitates Synthesis and Characterization

Five organic matters (OMs) were used in this study to prepare OM-ferrihydrite (OM-Fh) coprecipitates, including Pahokee Peat humic acid (PPHA), Elliot Soil humic acid (ESHA), Pahokee Peat fulvic acid (PPFA), Suwannee River fulvic acid (SRFA), and Suwannee River natural organic matter (SRNOM). All of the OMs were purchased from International Humic Substances Society (IHSS, St. Paul, MN) and used without further treatment. The carbon percent and main functional group compositions in OMs, as reported by IHSS (106), are descripted in **Table 2.1**. To produce OM-Fh coprecipitates, appropriate masses of OMs were dissolved in 1 L deionized water at pH 9.0 under vigorous stirring. The solution pH was adjusted back to pH 7.0 before the adding of 1 g ferric nitrate ($Fe(NO_3)_3 \cdot 9H_2O$) to generate an initial molar C/Fe ratio of 1.6. The mixed solution was re-adjusted to pH 7.5 with 1 M KOH to form OM-Fh coprecipitates under stirring. The coprecipitates were centrifuged and washed with deionized water twice. The C lost from solution and C content in the final coprecipitates were measured using a TOC analyzer (TOC-V and SSM-5000A, Shimadzu). The final C/Fe ratios in the coprecipitates were listed in **Table 2.2**. The solids were transferred into an anaerobic glovebox filled with mixed gas (7% H_2

and 93% N_2) and dispersed in deionized water by sonicator. All OM-Fh coprecipitates were used as wet within 7 days.

The solids were characterized by X-ray diffraction (XRD, Rigaku Mini Flex II) and with ^{57}Fe Mössbauer spectrometer (Web Research Inc., Edina, MN) equipped with closed-cycle cryostat (CCS-850 System, Janis Research Co., Wilmington, MA), similar as we described before (107). Ferrihydrite was the only Fe mineral detected by XRD and Mössbauer spectroscopy. The specific surface area of freeze dried SRNOM-Fh (C/Fe = 1.2) coprecipitate was determined by N_2 adsorption BET analysis (Quantachrome Nova 1200) and was found to be 15.5 $m^2 g^{-1}$, which was smaller than pure ferrihydrite (269 $m^2 g^{-1}$) but consistent with published studies (86, 96).

Secondary Mineral Transformation Experiments

All experiments were done in an anaerobic glovebox. Deionized water were degassed with N_2 over 2 hours and equilibrated in the glovebox at least overnight before using. Natural isotopic abundance Fe(II) stock solutions (denoted ^{NA}Fe(II), ~100 mM) were made by dissolving ^{NA}Fe(0) in hydrochloric acid (107).

To investigate the effect of coprecipitated OMs on Fe(II)-catalyzed ferrihydrite transformation, we reacted 2 mM ^{NA}Fe(II) with different OM-Fh coprecipitates in 15 mL piperazine-N,N'-bis (ethanesulfonic acid) (PIPES) buffer (10 mM, pH 7.0). Lower buffer concentration to 1 mM was tried but the system pH cannot hold. Coprecipitate solids loadings were set at ~10 mM Fe(III) in all the reactors. Reactors were placed on an end-over-end rotator and sampled over 14 days. Aqueous Fe(II) concentrations were measured during the reaction using the 1,10-phenantroline method (108). The reacted solids were collected with glass microfiber filters (Whatman) and characterized on the filter with XRD and Mössbauer spectroscopy. No background subtraction has been applied to XRD pattern due to the weak signal of ferrihydrite and

background from the filter. Based on the results of XRD, we fit Mössbauer spectra using the Recoil software (Ottawa, Canada) to determine the percent of secondary Fe minerals in the reacted Fe solids (109).

Electron Transfer Experiments

To track the electron transfer between Fe(II) and ferrihydrite with coprecipitated OMs, we reacted ^{56}Fe(II) with some OM-Fh coprecipitates under similar conditions as mineral transformation experiments. An ^{56}Fe(II) stock solution (~99.8% ^{56}Fe) was made by dissolving ^{56}Fe(0) powder (Isoflex, San Francisco, CA, USA) in concentrated HCl, as with ^{NA}Fe(0). All OM-Fh coprecipitates were reacted in 10 mM PIPES buffer (pH 7.0) with or without 2 mM ^{56}Fe(II) over 1 day, the reacted coprecipitates were collected on glass filters and characterized with ^{57}Fe Mössbauer spectroscopy.

For a subset of reactors containing SRNOM-Fh (C/Fe = 1.2) and PPFA-Fh (C/Fe = 1.4) coprecipitates, we varied the initial ^{56}Fe(II) concentration from 2 to 5 mM. The coprecipitates reacted with ^{56}Fe(II) for 1 and 7 days. After reaction, half of the reacted solid was totally dissolved by 4 M HCl, and we measured Fe(II) and total Fe concentrations in the dissolved solution using 1,10-phenanthroline. Another half of the solid from same batch was characterized with ^{57}Fe Mössbauer spectra at 77 K. The solids were sealed with Kapton tape in glovebox before transferring to the Mössbauer spectrometer. We used Recoil to fit the Mössbauer spectra.

Isotope Mixing Experiments

Fe isotope mixing experiments between aqueous Fe(II) and OM-Fh coprecipitates were conducted under similar conditions as the mineral transformation study. Instead of ^{NA}Fe(II), we reacted ^{57}Fe enriched Fe(II) (~95% ^{57}Fe, Isoflex) with SRNOM-Fh (C/Fe = 1.2) coprecipitate at Fe(II)/Fe(III) ratio of 0.2. The initial Fe(II) concentration and isotope composition were measured

before adding the SRNOM-Fh (C/Fe = 1.2) coprecipitate. Triplicate reactors were allowed to react for 1 hour, 1 day, 7 days and 14 days. At each time point, 2 mL of suspension was collected and centrifuged. The supernatant was filtered through a 0.22 μm filter and acidified with 10 μL concentrated HCl. The solids were subjected to Fe(II) extraction with 10 mM piperazine-N,N′-bis (3-propanesulfonic acid) (PIPPS) buffer at pH 3.5 over 20 minutes. The extracted solids were dissolved by 4 M HCl. The remaining suspension in the vials was filtrated through the glass filter to collect the solid for XRD characterization.

Fe(II) and total Fe concentration in the filtered supernatant, extraction solution, and dissolved solids over time were measured with 1,10-phenantroline. Fe isotope composition analysis in aqueous, extracted and solid phase Fe was performed with a quadrupole inductively coupled plasma-mass spectrometer (ICP-MS, Agilent 7900) using He gas in collision cell mode to remove isobaric interferences (predominantly $^{40}Ar^{16}O$ and $^{40}Ar^{16}O^{1}H$) for ^{56}Fe and ^{57}Fe. Sample preparation and measurement methods were same as we described before (52).

To investigate the isotope distribution in ^{57}Fe(II)-treated SRNOM-Fh (C/Fe = 1.2) coprecipitates, we did sequential extractions as a function of reaction time, similar as previous studies (110, 111). Solids were resuspended in 0.1 M HCl for 5 minutes and centrifuged to get the supernatant as extraction 1, following another 10 minutes extraction using same acid and method for extraction 2. An additional 3 extractions were done in 0.2 M HCl for 10 minutes each. Finally, the residual solid after the 5 sequential extractions was totally dissolved with 4 M HCl. The Fe concentrations and isotope composition in each extraction were measured, as above.

Results and Discussion

Fe(II)-catalyzed Mineral Transformation of OM-Fh Coprecipitates

To evaluate if organic matter influences Fe(II)-catalyzed mineral transformation of ferrihydrite, we coprecipitated five different soil organic matters with ferrihydrite. We included two humic acids (PPHA and ESHA), two fulvic acids (PPFA and SRFA) and one natural organic matter (SRNOM) at an initial C/Fe ratio of 1.6. Ferrihydrite is the only Fe mineral found in these coprecipitate by XRD and Mössbauer spectra. We also compared the SRNOM-Fh (C/Fe = 1.2) Mössbauer spectra to ferrihydrite prepared without OM present (**Figure 2.1**). At 77 K (and above) the Mössbauer spectra of ferrihydrite and SRNOM-Fh (C/Fe = 1.2) after synthesis are an Fe(III) doublet (CS = 0.47 mm/s, and QS = 0.73 and 0.76 mm/s, respectively). In the absence of OM, ferrihydrite began to order to a sextet at 25 K in contrast to SRNOM-Fh (C/Fe = 1.2) which remained predominantly a doublet at 25 K, indicating that the superparamagnetic blocking temperature (T_B) is higher for ferrihydrite alone than for SRNOM-Fh (C/Fe = 1.2) consistent with previous observations of NOM-Fh coprecipitates (86, 96). We also observed that all Fe(III) in the OM-Fh coprecipitate was magnetically ordered at T = 14 K, suggesting the majority of Fe(III) was present as ferrihydrite rather than Fe(III)-OM complexes which would likely occur as a doublet. Note that in contrast to previous work (86, 96), we did not observe a large change in the quadrupole splitting of SRNOM-Fh (C/Fe = 1.2) coprecipitates as a function of C/Fe ratio (data not shown).

Reaction with 2 mM Fe(II) at pH 7.0 resulted in similar amounts of Fe(II) sorbed on the five different coprecipitates (17 to 23 μmol) (**Table 2.2**). About 60-80% of the ferrihydrite coprecipitated with humic acids transformed to secondary minerals after two weeks as estimated by relative areas from Mössbauer Spectroscopy (**Figure 2.2**). Mössbauer parameters of the secondary mineral are consistent with goethite (CS = 0.48 mm/s, QS = -0.24 mm/s, H = 48-49

mm/s) (95) and XRD confirmed goethite as the primary secondary mineral (**Figure 2.3 and 2.4**). In contrast, the ferrihydrite coprecipitated with fulvic acids (PPFA and SRFA), as well as SRNOM that is enriched with fulvic content, remained ferrihydrite after two weeks of reaction with Fe(II) (**Figure 2.2**). XRD patterns and Mössbauer spectroscopy indicated no measurable formation of secondary Fe minerals (**Figure 2.3 and 2.5**).

Our results are consistent with previous observations of inhibition of ferrihydrite transformation in the presence of organic matter. Sorption of SRFA onto ferrihydrite at a high OM concentration and C/Fe ratio (150 mg/L SRFA, C/Fe = 4.2) inhibited ferrihydrite transformation substantially (42). At a lower SRFA concentration and C/Fe ratio (25 mg/L, C/Fe = 0.7), ferrihydrite transformed to goethite and lepidocrocite (42). Organic matter extracted from highly weathered, acidic soil (Ultisol) coprecipitated with ferrihydrite also resulted in less ferrihydrite transformation as the C/Fe ratio increased and no secondary minerals were observed at C/Fe greater than 1.6 (which is similar to the 1.2 to 1.6 C/Fe ratio used here) (86). The Ultisol extracted organic matter was composed of abundant carboxyl C with only a small amount of aromatic and phenolic C making it more similar to fulvic acid OM than humic acid OM (75, 86). More recently, coprecipitated polygalacturonic acid (PGA) and OM in freshwater flocs comprised predominantly of ferrihydrite and lepidocrocite was also found to inhibit ferrihydrite transformation around C/Fe ratio of 2.5 (103).

While the presence of organic matter as sorbed, coprecipitated, or in natural flocs has been shown to inhibit Fe(II)-catalyzed ferrihydrite mineral transformation (42, 86, 103), the mechanism of inhibition is still questionable and it is unclear why higher fulvic content inhibits ferrihydrite transformation more than humic acids. Some possible explanations for why fulvic acids inhibit transformation more then humic acids may be due to differences in (*i*) amount of Fe(II) sorption,

(*ii*) OM molecular weights (MW), or (*iii*) carboxylic content of OM. Fulvic acids have higher carboxylic contents compared to humic acids (**Table 2.1**) and it has been suggested that the carboxylic groups can bind strongly to ferrihydrite surfaces via ligand exchange, or associate with Fe(II) and prevent the direct complexing with structural Fe(III) and thus reduce the rate of Fe(II) oxidation (112-115). Previous results with a soluble OM extracted from Ultisol with a high carboxylic content, however, resulted in substantial ferrihydrite transformation at C/Fe ratio 1.2, which suggests that carboxylic content may not be the controlling factor in whether ferrihydrite transformation occurs or not (75, 86). Different amounts of sorbed Fe(II) between humic and fulvic ferrihydrite coprecipitates is also an unlikely explanation as we observed similar amounts of Fe(II) sorbed by fulvic and humic coprecipitates (20 ± 3μmol, **Table 2.2**). We speculate that molecular weight differences in fulvic and humic acids may play an important role. Fulvic acids have lower MW than humic acids and tend to have higher charge density, and interaction with fulvic acids may inhibit ferrihydrite aggregation and growth via Ostwald ripening (66, 79, 116-119). Regardless, it is clear from our data that OM with high fulvic contents inhibits Fe(II)-catalyzed ferrihydrite transformation to secondary minerals more than humic acids.

Fe(II)-ferrihydrite Electron Transfer in the Presence of Organic Matter

To explore how fulvic acid and SRNOM inhibit Fe(II)-catalyzed ferrihydrite transformation, we used ^{57}Fe Mössbauer spectroscopy to determine if Fe(II)-Fe(III) electron transfer still occurred when ferrihydrite was coprecipitated with PPFA, SRFA, and SRNOM. Previous studies inferred that OM suppressed electron transfer from less sorption of Fe(II) on the ferrihydrite surface and that inhibited electron transfer was responsible for why ferrihydrite transformed less with OM present (42, 86). Here, we reacted naturally abundant OM-Fh coprecipitates with ^{56}Fe(II) (which is invisible in Mössbauer spectroscopy). After reaction with

^{56}Fe(II), we observed a high velocity peak emerge with Mössbauer parameters consistent with an Fe(II) doublet (CS = 1.16±0.05 mm/s and QS = 2.93±0.06 mm/s) (**Figure 2.6)** (38, 120). The presence of an Fe(II) doublet in the Mössbauer spectra indicates that some of the ^{57}Fe(III) in the naturally abundant ferrihydrite coprecipitates (2.3% ^{57}Fe) was reduced and that electron transfer occurred between aqueous Fe(II) and ferrihydrite coprecipitated with the different OM. We assume that the proportion of ^{57}Fe(II) reduced is the same as the proportion of ^{56}Fe(III) and the overall Fe(III). Unfortunately, the Mössbauer spectra cannot distinguish whether the Fe(II) doublet represents sorbed Fe(II), structural Fe(II), or Fe(II) complexed with OM. The Mössbauer spectra from the labeled isotope experiment, does, however, provide conclusive evidence that Fe(II) reduced Fe(III) in the ferrihydrite coprecipitate structure. Using a similar approach we also previously observed electron transfer between Fe(II) and goethite with adsorbed organic carbon (121, 122). Electron transfer between Fe(II) and ferrihydrite in the presence of OM is also consistent with biological reduction of ferrihydrite at high C/Fe ratio (16, 104). Despite clear evidence for electron transfer between Fe(II) and the OM-Fh coprecipitates, both the Mössbauer spectra and XRD indicate no secondary Fe minerals formed.

To test whether sorbing more Fe(II) (and possibly having more electron transfer) might be needed to induce Fe(II)-catalyzed ferrihydrite transformation in presence of OM, we reacted the SRNOM-Fh (C/Fe = 1.2) coprecipitate with higher concentrations of ^{56}Fe(II) (up to 5 mM). As the aqueous Fe(II) concentration increased, a similar Fe(II) doublet emerged with increasing relative areas (**Figure 2.7**). The increase in relative area of the Fe(II) doublet indicates more ^{57}Fe(III) in the ferrihydrite was reduced, however, no secondary Fe mineral was observed after seven days of reaction based on the Mössbauer spectra and XRD patterns (**Figure 2.8**). We also varied initial Fe(II) concentration in PPFA-Fh coprecipitate reactors and similarly observed no mineral

transformation (**Table 2.2**). Our results provide compelling evidence that OM is not inhibiting secondary mineral transformation of ferrihydrite by suppressing electron transfer between Fe(II) and ferrihydrite as previously suggested (42, 86).

To probe whether Fe(II) was complexing or reacting with the OM, we measured how much of the sorbed Fe(II) underwent electron transfer and reduced Fe(III) in the ferrihydrite structure. To do this, we compared the relative area of the Fe(II) doublet from the Mössbauer spectra to the percent of Fe(II) measured with 1,10-Phenanthroline method in the dissolved coprecipitates (**Figure 2.9**). The strong agreement between the percent of Fe(II) in the ferrihydrite (the relative area of the doublet) and the percent Fe(II) by dissolution indicated that nearly all of the sorbed Fe(II) reduced Fe(III) in ferrihydrite such that there is a 1:1 apparent stoichiometry between Fe(II) sorbed and Fe(III) in ferrihydrite reduced. The 1:1 electron transfer stoichiometry confirms that the SRNOM did not inhibit electron transfer from sorbed ^{56}Fe(II) to ferrihydrite nor did the SRNOM bind Fe(II) and prevent it from participating in electron transfer. The OM may still, however, be participating by serving as an electron shuttle between the Fe(II) and ferrihydrite as has been previously suggested for dissimilatory Fe reduction (16, 104).

Fe Mixing Between Aqueous Fe(II) and OM-Fh Coprecipitate

Another possible explanation for the lack of ferrihydrite transformation in the presence of OM may be that OM inhibits the release of the Fe(II) from the ferrihydrite structure (i.e., if no dissolution occurs, then reprecipitation as a secondary mineral does not occur). To test whether Fe(II) release and mixing occurs between aqueous Fe(II) and the SRNOM-Fh (C/Fe = 1.2), we used an Fe isotope tracer approach similar to our previous work with other Fe minerals.(121) We reacted ^{57}Fe enriched aqueous Fe(II) (~95% ^{57}Fe) with SRNOM-Fh (C/Fe = 1.2) made from natural abundant Fe (~2.3% ^{57}Fe) and tracked the Fe concentrations and isotope composition over time in

the aqueous phase, an extracted phase, and the residual solid (**Figure 2.10**). Fe(II) recovery from the three phases gave near complete mass balance over the course of the experiment (90-94%) (**Figure 2.11**). Fe isotope compositions changed over time in all three phases with ^{57}Fe in the aqueous phase decreasing from 95% to 42% within 2 hours accompanied by a rapid increase ^{57}Fe in the residual solid (from 2.3% to 13%) (**Figure 2.10, Table 2.5**). This initial rapid isotope mixing was followed by a slower mixing over the next 14 days with both the aqueous phase and solid residual ^{57}Fe contents approaching the calculated completely mixed ^{57}Fe value of 17.5% (19 and 18%, respectively). The extracted Fe(II) had a similar isotope composition to the aqueous Fe(II) suggesting that the aqueous phase equilibrated with the extracted Fe similar to what we previously observed with goethite (52). As expected, we observed rapid and near complete mixing of the isotope tracer in ferrihydrite without OM (**Figure 2.12**) (26, 42).

The substantial decrease in ^{57}Fe in the aqueous phase and increase in the SRNOM-Fh (C/Fe = 1.2) solid ^{57}Fe indicates that Fe atoms mixed between the two phases despite no observable secondary mineral transformation. While our work is not directly comparable to others because of differences in OM used, C/Fe ratios, and coprecipitate treatment, the near complete isotope mixing we observed in the presence of OM is not consistent with other recent observations. For example, precipitating ferrihydrite with a model OM (polygalacturonic acid – PGA) or adsorbing OM (SRFA) on ferrihydrite were both shown to inhibit Fe atom exchange (42, 103). Precipitating ferrihydrite with PGA resulted in only 15% estimated Fe atom exchange compared to 100% in the absence of PGA (103), and sorption of 150 mg/L SRFA was also shown to lower the extent of Fe isotope exchange (42). In both cases, the reduced Fe atom exchange was suggested to explain the lack of ferrihydrite mineral transformation in the presence of PGA or OM. Note that both the PGA and SRFA experiments were with higher C/Fe ratios (2.5 and 4.2, respectively) than the 1.2 C/Fe

ratio used here. Higher C/Fe ratios inhibit ferrihydrite mineral transformation more (42, 82, 86, 101). which may explain why more inhibition of atom exchange was observed in these studies. Another potentially important variable in our work is that we did not freeze-dry our OM-Fh coprecipitates. Freeze drying changes the aggregation state and structure of ferrihydrite and has been implicated in reduced Fe atom exchange (42, 123).

The extensive mixing of the isotope tracer we observed for SRNOM-Fh (C/Fe = 1.2) suggests that a significant fraction of the SRNOM-Fh (C/Fe = 1.2) recrystallized without transformation to any secondary minerals. Quantifying the extent of recrystallization, however, is challenging. Multiple approaches have been used to estimate the percent of solid recrystallized (see a recent review of recrystallization models) (53). Modeling approaches have evolved from using a simple linear isotope mixing model (also referred to as the fractional approach) (42, 44) to a non-linear model that accounts for the different amounts of Fe in the aqueous and solid phase (also referred to as the homogeneous model) (46, 52, 53, 124). An alternative, stochastic simulation-based approach that assumes a linked 1:1 transfer of Fe atoms between solution and the solid has also been used to successfully interpret the isotope data and successfully reproduces the measured ~10^{-5} s^{-1} reductive dissolution rate of goethite (125).

While the non-linear, homogeneous models is a better approach than the linear model, it still requires the assumption that Fe atoms that have participated in exchange can further exchange with aqueous phase and result in a homogeneous isotope distribution in the solid phase. Our previous sequential extraction data with goethite, however, suggested that the isotopes were not homogenously distributed in the solid phase, but rather that a ^{57}Fe gradient developed in the goethite solids (52). To account for a heterogeneous distribution within the solid, a heterogeneous has been proposed where equilibration between the exchanged solids and aqueous phase is not

assumed (53, 54). The heterogeneous model, however, requires information on the spatial distribution of the isotopes in the solid which is analytically difficult to obtain (53). Recent work, however, with hematite and Atom Probe Tomography (APT) suggest that APT is a promising approach for mapping isotope distribution in solids (126). Since we do not have direct measurements of the spatial distribution in the SRNOM-Fh (C/Fe = 1.2) coprecipitates, we used a sequential extraction approach to evaluate whether we could reasonably assume homogeneous distribution of the isotopes in the SRNOM-Fh (C/Fe = 1.2) coprecipitate. More specifically, we sequentially extracted SRNOM-Fh (C/Fe = 1.2) before and after reaction with Fe(II) and measured Fe isotope composition in each extraction (**Figure 2.13**). Although we cannot definitely determine what portion of the particle we are extracting, it seems a reasonable first approximation to assume that the sequential extractions are removing Fe atoms from progressively deeper within the bulk structure. After two hours of reacting with ^{57}Fe(II), a clear gradient in ^{57}Fe isotope concentration is apparent as more Fe was extracted. The initial extracted Fe was close to the ^{57}Fe isotope composition of the aqueous Fe and decreases but never reaches the initial ^{57}Fe composition of the SRNOM-Fh (C/Fe = 1.2) coprecipitate (**Table 2.6**). After longer Fe(II) reaction times (1, 7, and 14 days), the ^{57}Fe isotope gradient became less. By fourteen days, the ^{57}Fe approached a more homogeneous distribution throughout the extracted solid. Based on the relatively homogeneous distribution of ^{57}Fe in the SRNOM-Fh (C/Fe = 1.2) suggested by the extraction data at 14 days, we used the non-linear, homogeneous model to estimate that 85 ± 3% of Fe atoms in the SRNOM-Fh (C/Fe = 1.2) exchanged and recrystallized by 14 days. Note we did not estimate the extent of recrystallization over time as the sequential extraction data suggest the isotopes are heterogeneously distributed in the solids. We found it surprising to observe such extensive

recrystallization of the SRNOM-Fh (C/Fe = 1.2) after reaction with Fe(II) given that we did not observe any measurable formation of secondary minerals with XRD or Mössbauer spectroscopy.

SRNOM-Fh (C/Fe = 1.2) Before and After Reaction with Fe(II)

To further probe whether there might be more subtle changes in the SRNOM-Fh (C/Fe = 1.2) particles in the absence of transforming to secondary minerals, we collected Mössbauer spectroscopy temperature profiles before and after Fe(II)-catalyzed recrystallization. The temperature profiles revealed some difference in the blocking temperature (T_B) which is where the ferrihydrite transitions from a superparamagnetic state to an antiferromagnetic state and ferrihydrite doublet transitions to a sextet (127, 128). The T_B for SRNOM-Fh (C/Fe = 1.2) is higher (close to 25K) after reacting with Fe(II) compared to SRNOM-Fh (C/Fe = 1.2) aged in buffer without Fe(II) (**Figure 2.14**). Plotting the distribution of the hyperfine field also reveals a shift towards a larger hyperfine field both with aging and in the presence of Fe(II) with a larger shift observed in the presence of Fe(II) (**Figure 2.17**). The higher T_B and shift to a larger hyperfine field as well as a more narrow distribution of the SRNOM-Fh (C/Fe = 1.2) hyperfine field after reaction with Fe(II) may be due to increased crystallinity, particle size, or particle aggregation through particle-particle magnetic exchange interactions (128-130). These possible changes are also consistent with slightly slower Fe dissolution rates of SRNOM-Fh (C/Fe = 1.2) after reaction with Fe(II) (**Figure 2.18**). In addition, we also visually observed the SRNOM-Fh (C/Fe = 1.2) particles settled more in the presence of Fe(II) which suggests increased particle size or aggregation (**Figure 2.19**). We caution that while the changes in blocking temperature, hyperfine field, and dissolution rates are consistent with increased particle size, crystallinity, or aggregation, we cannot definitely conclude what is responsible for the changes. It is, however, clear from the Mössbauer

spectroscopy temperature that Fe(II)-catalyzed recrystallization does alter the SRNOM-Fh (C/Fe = 1.2) particles to some extent even though no secondary minerals form.

Environmental Implications

Our finding of extensive mixing of SRNOM-Fh (C/Fe = 1.2) during reaction with Fe(II) suggests that ferrihydrite may be even more dynamic than we thought under reducing conditions and interact extensively with surrounding fluid even when no secondary minerals are observed to form. This finding of a "hidden" pathway for ferrihydrite-fluid mixing, where no secondary mineral formed but the blocking temperature changed, may have interesting implications for the stability of carbon associated with ferrihydrite in soils and natural flocs (86, 131) and the notion of soil carbon preservation by Fe minerals (86, 132). In addition, the extensive mixing we observed raises questions about the fate of other elements associated with ferrihydrite when exposed to redox cycling (133, 134). For example, others have found that Fe(II)-catalyzed recrystallization of goethite and hematite can redistribute heavy metals, such as Ni, Pb and Cr, between the mineral structure and the mineral surface (134, 135). The extensive mixing we observed for SRNOM-Fh (C/Fe = 1.2) and aqueous Fe(II) raises the interesting question of whether a similar redistribution may occur for recrystallized ferrihydrite even in the absence of secondary Fe mineral transformation.

Finally, our results clearly demonstrate that ferrihydrite transformation to more stable minerals is influenced by the nature of the organic matter present during ferrihydrite formation. Based on our results and those of others (42, 86), we speculate that ferrihydrite formed in the presence of fulvic acids or fulvic acids enriched OM may be more resistant to transformation than ferrihydrite formed in the presence of humic-like OM. In nature, the stability of OM-Fh

precipitates would likely be impacted by geological setting (aquatic vs. terrestrial) as well as precipitation (well-flushed soils vs. not), and time (131, 136, 137).

Table 2.1. Properties of different natural organic matter compiled from IHSS website (106) unless otherwise noted.

Sources	C (%)	Carboxyl [b] (%)	Phenolic[b] (%)	Aromatic[c] (%)	Aliphatic[c] (%)
Suwannee River Fulvic Acid[a]	52.3	11.2	2.8	22	35
Suwannee River NOM	50.7	11.2	2.5	23	27
Elliot Soil Humic Acid[a]	59.5	8.3	1.9	41	27
Pahokee Peat Humic Acid	56.4	9.0	1.9	47	19
Pahokee Peat Fulvic Acid[d]	51.3	10.6	5.4	40.4	17.1

a. humic acid and fulvic acid are operationally defined based on their solubility at different pH ranges;
b. Measured by titration using 0.1 M NaOH. Carboxyl is the charge density (meq/g C) at pH 8.0; Phenolic is two times the change in charge density (meq/g C) between pH 8 and pH 10;
c. Analyzed from NMR peak area percentages.
d. Pahokee Peat Fulvic Acid data is from reference cited here (138).

Table 2.2. Summary of Fe(II) experimental results with OM-Fh coprecipitates.

OC Source	C/Fe Nominal	C/Fe TOC[a]	Solid C Content (%)[b]	Fe(II) Initial (µmol)	Fe(II) Sorbed (µmol)	End Minerals[c]
PPHA	1.6	1.6	17.7	31.1	20.4	G
ESHA	1.6	1.6	17.7	30.6	20.3	G
SRFA	1.6	1.1	11.3	32.7	19.7	Fh
PPFA				31.5	22.5	Fh
	1.6	1.4	15.9	58.1	27.6	Fh
				88.7	30.1	Fh
SRNOM				30.5/30.11	16.7/19.4[d]	Fh
	1.6	1.2	13.9	59.7	26.4	Fh
				81.9	26.8	Fh

a. C/Fe ratio calculated from C content measured by TOC analyzer and total Fe content measured by dissolution and quantification with 1,10-phenanthroline;
b. Calculated from C/Fe ratio, ferrihydrite was calculated as FeOOH;
c. G = goethite; Fh = ferrihydrite.
d. Two different batches of SRNOM-Fh (C/Fe = 1.2) used in ET and AE study, In ET study, 16.7 µmol Fe(II) was sorbed; In AE study, we have slightly more Fe(II) sorbed.

Table 2.3. Mössbauer spectral parameters derived from fitting samples in Figure 2.4.

OM-Fh	Reaction time (day)	Component	Relative area (%)	Center shift, CS (mm/s)	QS or 2ε [b] (mm/s)	σ(Δ)[c] (mm/s)	Hyperfine field, H (Tesla)	χ_v^2
PPHA-Fh (1.6)	0	Fe(III) doublet	100	0.47	0.76	0.35		1.6
	1	Fe(II) doublet	4.07(.47)	1.28	3.17	0.38		2.9
		Fe(III) doublet	51.70(.46)	0.46	0.69	0.15		
		Goethite	44.23(.45)	0.48	-0.22	48.63	0.94	
	14	Fe(II) doublet	3.54(.34)	1.13	3.39	0.13		2.4
		Fe(III) doublet	39.94(.43)	0.46	0.70	0.25		
		Goethite	56.52(.44)	0.48	-0.23	48.98	0.73	
ESHA-Fh (1.6)	0	Fe(III) doublet	100	0.47	0.76	0.33		1.6
	1	Fe(II) doublet	3.76(.33)	1.28	3.19	0.41		2.9
		Fe(III) doublet	28.91(.29)	0.47	0.71	0.12		
		Goethite	67.33(.36)	0.48	-0.23	48.23	2.16	
	14	Fe(II) doublet	8.27(.74)	1.26	3.92	2.21		3.1
		Fe(III) doublet	19.69(.39)	0.42	0.7	0.29		
		Goethite	72.05(.68)	0.48	-0.22	49.04	0.97	

a value in parenthesis reflects the error (1σ) in determination of the relative area for each component
b QS = quadrupole splitting; 2ε = quadrupole shift parameter in sextet
c σ(Δ) = standard deviation of quadrupole splitting component

Table 2.4. Mössbauer spectral parameters derived from fitting SRNOM-Fh (C/Fe = 1.2) samples reacted with different amount of Fe(II).

Initial Fe(II) (mM)	**Component**	**Relative area (%)**	**Center shift, CS (mm/s)**	**Quadrupole splitting, QS or 2ε [b] (mm/s)**	**σ(Δ)[c] (mm/s)**	**χ_ν^2**
2	Fe(II) doublet	12.02(.62)	1.16	3.0	0.89	1.82
	Fe(III) doublet	87.98(.62)	0.47	0.70	0.33	
4	Fe(II) doublet	14.56(.81)	1.21	2.90	0.70	1.42
	Fe(III) doublet	85.44(.61)	0.46	0.68	0.33	
5	Fe(II) doublet	17.29(.53)	1.12	2.90	0.90	2.24
	Fe(III) doublet	82.71(.53)	0.45	0.68	0.34	

a value in parenthesis reflects the error (1σ) in determination of the relative area for each component
b 2ε = quadrupole shift parameter in sextet
c σ(Δ) = standard deviation of quadrupole splitting component

Table 2.5. Summary of Fe isotope data during reactions between aqueous Fe(II) and SRNOM-Fh coprecipitate (C/Fe = 1.2) at pH 7.0.

Time (d)	Aqueous				Extract[a]				Solid			
	Fe(II) (μmole)	$f^{57}Fe$	$f^{56}Fe$	$f^{54}Fe$	Fe(II) (μmole)	$f^{57}Fe$	$f^{56}Fe$	$f^{54}Fe$	Fe (μmole)	$f^{57}Fe$	$f^{56}Fe$	$f^{54}Fe$
0	30.11(0.42)	0.95(0.006)	0.026(0.006)	0.001(0)	NA	NA	NA	NA	152.7(3.41)	0.02(0)	0.92(0.001)	0.055(0)
0.083	11.72(1.0)	0.42(0.007)	0.53(0.007)	0.028(0)	13.9(0.66)	0.38(0.016)	0.57(0.015)	0.03(0.001)	139.04(6.02)	0.13(0.002)	0.82(0.002)	0.043(0)
1	10.36(0.10)	0.30(0.002)	0.65(0.002)	0.034(0)	13.0(0.25)	0.29(0.002)	0.67(0.003)	0.035(0)	145.75(8.78)	0.16(0.001)	0.79(0.001)	0.042(0)
7	10.45(0.48)	0.19(0.002)	0.75(0.001)	0.046(0)	12.32(0.34)	0.19(0.002)	0.76(0.002)	0.046(0)	139.43(4.37)	0.17(0.005)	0.78(0.005)	0.048(0)
14	10.68(0.91)	0.19(0.001)	0.75(0.001)	0.046(0)	11.94 (0.50)	0.19(0.002)	0.76(0.002)	0.046(0)	132.83(2.59)	0.18(0.002)	0.78(0.002)	0.048(0.001)

a. Around 80% of sorbed Fe(II) was extracted by this extraction method, less than 3% of Fe in the extraction was Fe(III).

Table 2.6. Fe mass and isotope composition in each fraction during the sequential extraction to SRNOM-Fh (C/Fe ratio 1.2) reacted with ^{57}Fe(II) over different time.

Fe(II) treated time (d)	Fraction	Fe(II) (μmol)	Fe(III) (μmol)	Total Fe (μmol)	^{57}Fe percent (%)	^{57}Fe mass (μmol)	Sum of ^{57}Fe mass (μmol)	Percent of Fe mass recovered (%)
0	aqueous	30.9(0.3)	-	_-	94.6(0.3)	29.2	32.9	98.1
	extract 1	0	11.2	11.2(0.3)	2.6(0.03)	0.3		
	extract 2	0	20.2	20.2(0.1)	2.6(0.03)	0.5		
	extract 3	0	28.4	28.4(0.3)	2.6(0.005)	0.7		
	extract 4	0	28.4	28.4(0.2)	2.6(0.003)	0.7		
	extract 5	0	19.9	19.9(0.1)	2.6(0.01)	0.5		
	residual	0	32.9	32.9(0.1)	2.6(0.02)	0.8		
0.08	aqueous	13.6(0.2)	-	-	33.6(0.1)	4.6	34.3	96.9
	extract 1	15.2(0.3)	8.5	23.7(0.3)	31.6(0.2)	7.5		
	extract 2	0.6(0.1)	15	15.6(0.1)	23.4(0.1)	3.7		
	extract 3	0.1(0.3)	25.3	25.4(0.3)	18.7(0.1)	4.7		
	extract 4	0.4(1.3)	24.6	25(1.3)	16.6(0.1)	4.2		
	extract 5	0(0.3)	16.1	16.1(0.3)	15.6(0.04)	2.5		
	residual	1.9(0.8)	47.1	49(0.8)	14.7(0.1)	7.2		
1	aqueous	13.1(0.3)	-	-	25.8(0.1)	3.4	32.2	93.8
	extract 1	13.5(0.2)	9	22.5(0.8)	25.4(0.03)	5.7		
	extract 2	0.5(0.1)	9.5	10(0.5)	22.1(0.1)	2.2		
	extract 3	0.8(0.7)	16.3	17.1(0.7)	19.6(0.03)	3.4		
	extract 4	0.4(0.04)	23.6	24(1.6)	18.2(0.1)	4.4		
	extract 5	0.1(0.06)	10.4	10.5(0.2)	17.2(0.5)	1.8		
	residual	3.2(0.1)	62.3	65.5(1.2)	17.3(0.03)	11.3		
7	aqueous	12.9(0.4)	-	-	22.2(0.04)	2.9	30.1	92.8
	extract 1	13.4(0.4)	6.1	19.5(0.6)	22.3(0.2)	4.3		
	extract 2	1.5(0.04)	11	12.5(0.7)	20.3(0.05)	2.5		
	extract 3	0.1(0.1)	6	6.1(0.2)	19.3(0.1)	1.2		
	extract 4	0.2(0.2)	6.9	7.1(0.3)	18.6(0.1)	1.3		
	extract 5	0.1(0.1)	8.3	8.4(0.1)	18(0.4)	1.5		
	residual	2.3(0.1)	87.7	90(0.6)	18.2(0.2)	16.4		
14	aqueous	12.4(0.1)	-	-	20.2(0.1)	2.5	29.9	93.6
	extract 1	13.2(0.3)	6.1	19.3(0.4)	19.9(0.1)	3.8		
	extract 2	0.3(0.1)	5.2	5.5(0.5)	18.3(1.1)	1.0		
	extract 3	0.2(0.03)	9.2	9.4(0.1)	18(0.1)	1.7		
	extract 4	0.1(0.06)	10.4	10.5(1.1)	16.9(0.5)	1.8		
	extract 5	0.1(0.04)	10.7	10.8(0.3)	16.9(0.1)	1.8		
	residual	2.8(0.2)	92.6	95.4(2.8)	18.1(0.1)	17.3		

Table 2.7. Mössbauer parameters derived from fitting spectra in Figure 2.16.

Sample			<CS>[a] (mm/s)	<QS>[b] (mm/s)	<H>[c] (T)	std(H) (T) or std(QS) (mms^{-1})[d]	Area (%)	χ_v^2
Aged SRNOM-Fh (1.2)	With Fe(II)	Fe(II) Doublet	1.59	2.60	-	0.81	2.92	3.16
		Fe(III) Sextet	0.48	-0.02	43.30	10.71	97.08	
	No Fe(II)	Fe(III) Sextet	0.48	-0.01	39.28	12.54	100	1.71

[a] Center shift.
[b] Quadrupole splitting for doublets and quadrupole shift parameter for sextets.
[c] Hyperfine field.
[d] Standard deviation of the Voigt profile for the hyperfine field or quadrupole splitting parameters.

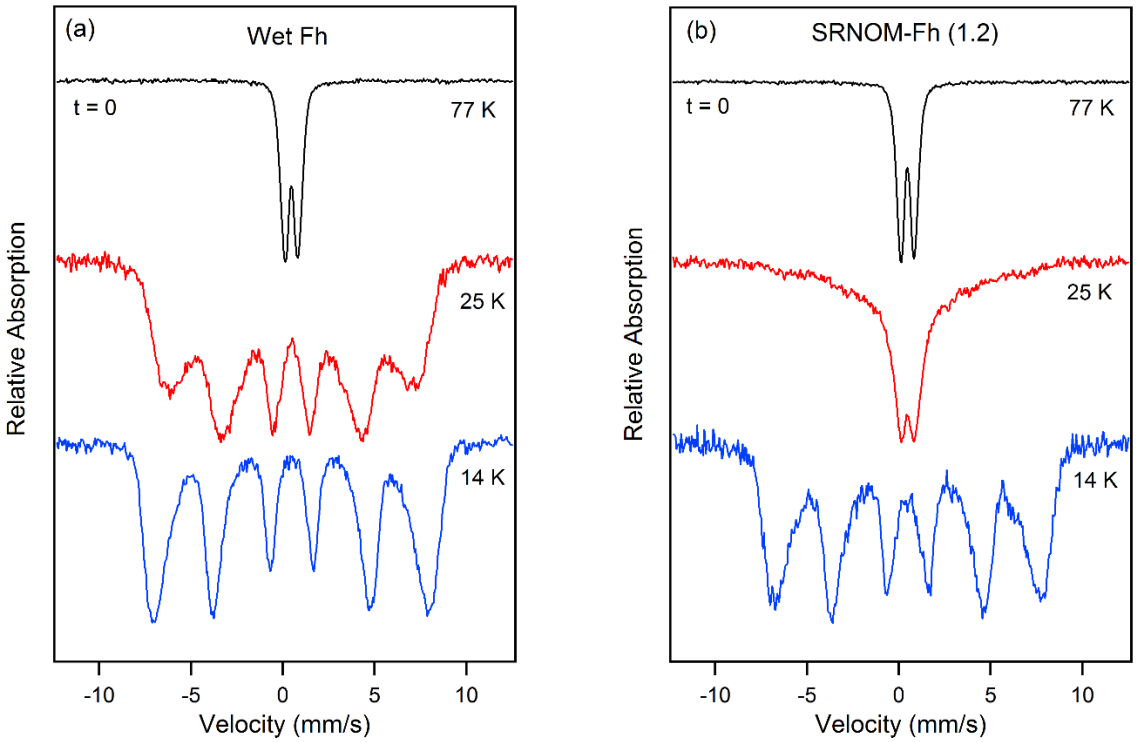

Figure 2.1. Mössbauer temperature profile of (a) wet Fh and (b) SRNOM-Fh (C/Fe = 1.2) coprecipitate.

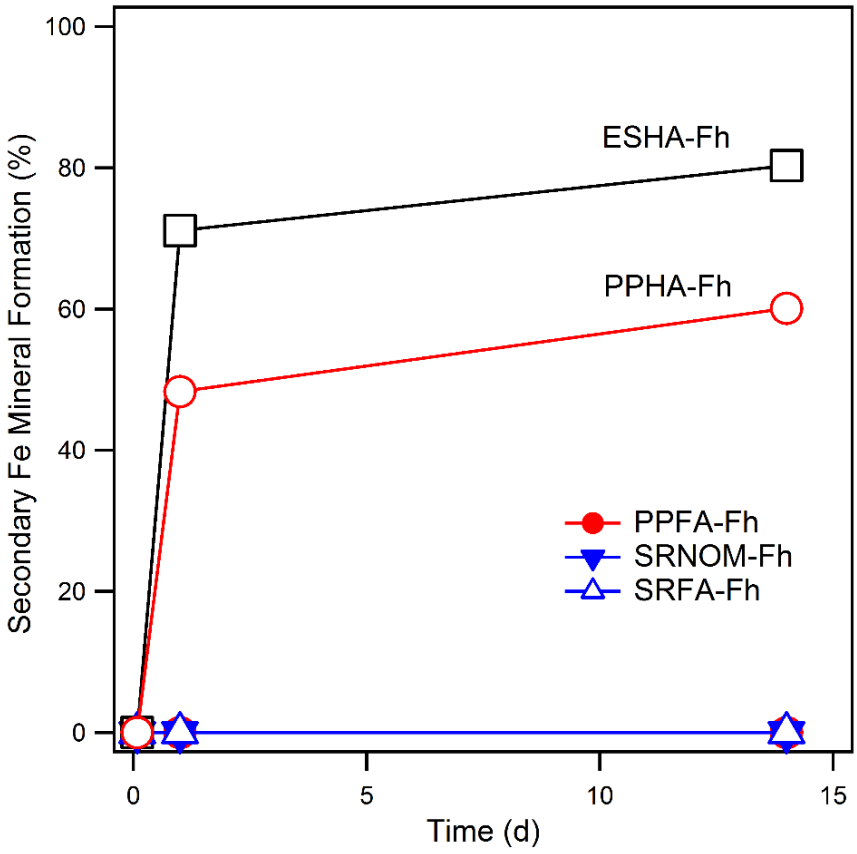

Figure 2.2. Percent of transformation of OM-ferrihydrite coprecipitates to secondary Fe minerals during reaction with 2 mM ^{NA}Fe(II). Percent of secondary Fe minerals formed was determined from relative areas of Mössbauer spectra given in **Table 2-3**. Conditions: 10 mM Fe(III) from OM-Fh, initial C/Fe ratio of 1.6 (see **Table 2-2** for final C/Fe ratio), 10 mM PIPES at pH 7.0.

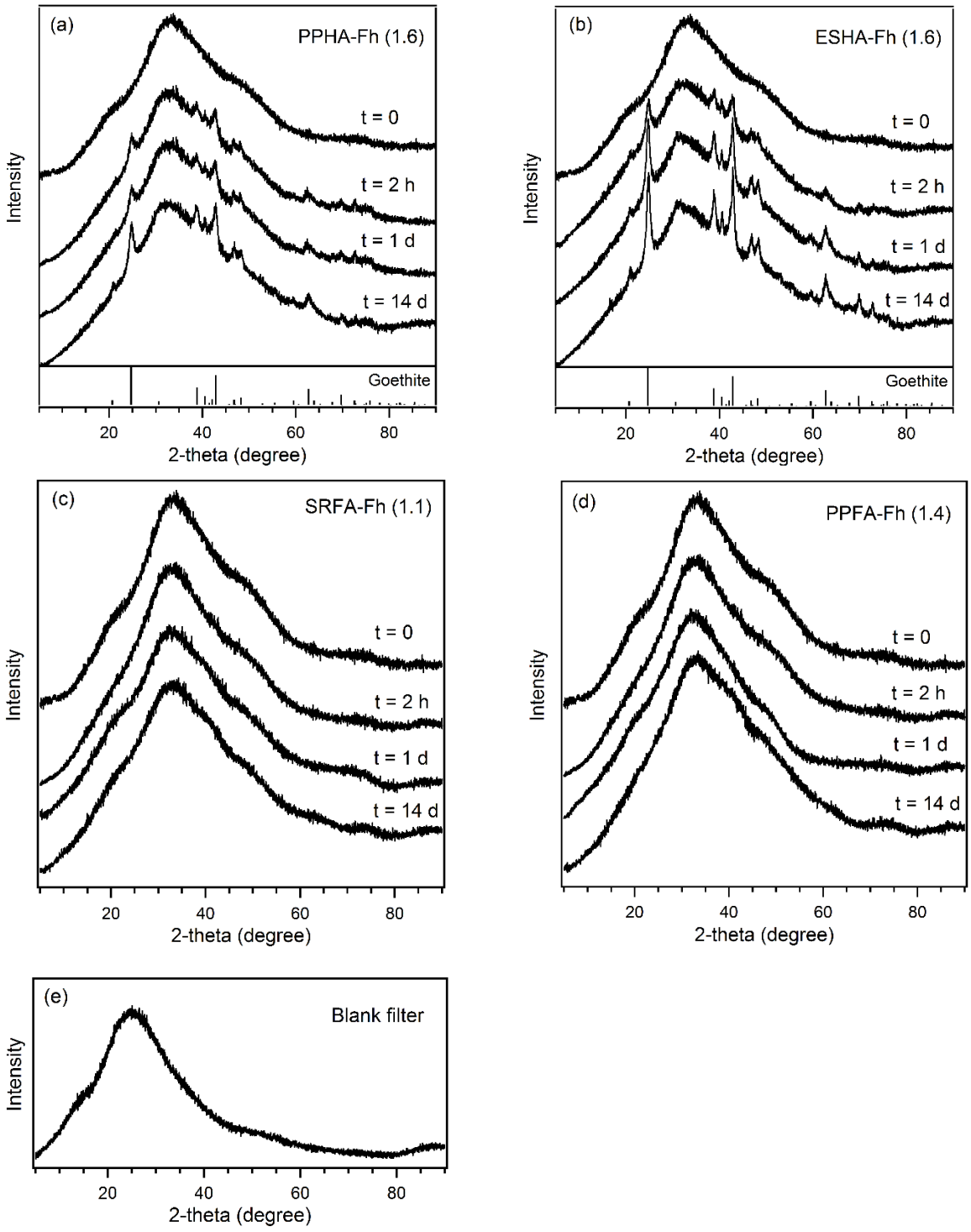

Figure 2.3. X-ray diffraction of (a) PPHA-Fh (C/Fe = 1.6), (b) ESHA-Fh (C/Fe = 1.6), (c) SRFA-Fh (C/Fe = 1.1) and (d) PPFA-Fh (C/Fe = 1.4) reacted with 2 mM Fe(II) in 10 mM PIPES (pH 7.0) over 14 days. Solids were collected and characterized with 0.22 μm glass fiber filter (e). Measurement was conducted at step width 0.02 at 30 kV and 15 mA. The identical peaks of secondary Fe mineral in (a) and (b) are consistent with goethite and the intensity of peaks increased over time.

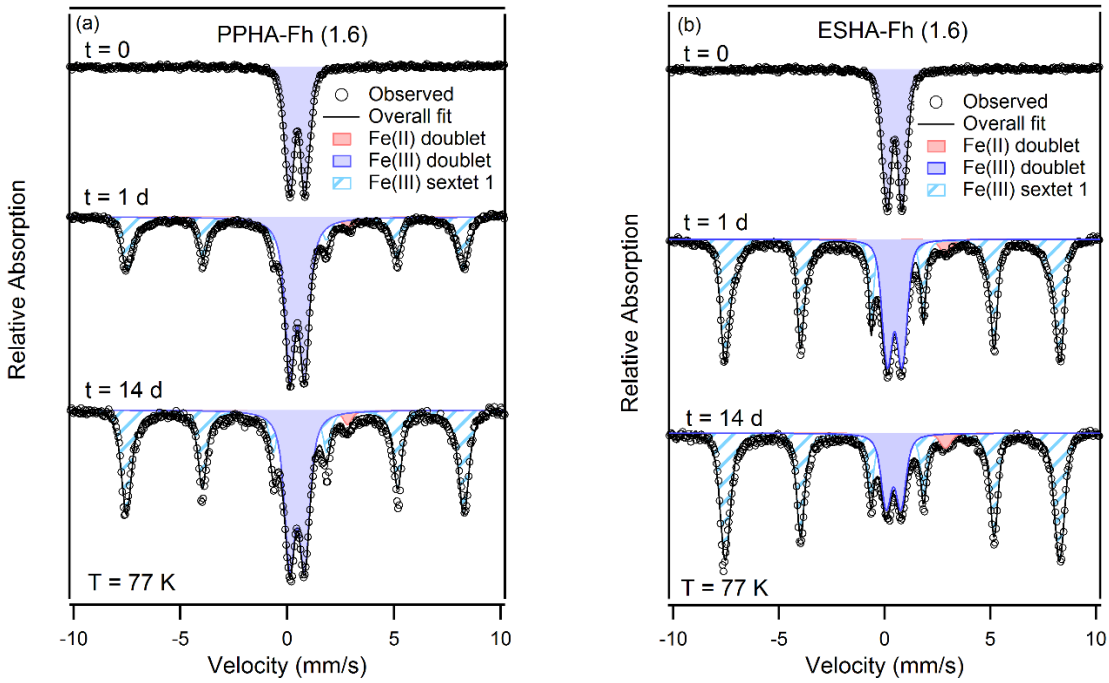

Figure 2.4. Mössbauer spectra and fitting of (a) PPHA-Fh (C/Fe = 1.6) (b) ESHA-Fh (C/Fe = 1.6) reacted with 2 mM ^{NA}Fe(II) over time. The spectra were fitted using one sextet and two doublets with Recoil. Based on XRD result (Figure 2.3) and Recoil fitting report, in PPHA-Fh (C/Fe = 1.6), there are 44.23% of goethite and 51.70% of ferrihydrite in 1 day sample, and 56.52% of goethite and 39.94% of ferrihydrite in 14 days sample; in ESHA-Fh(C/Fe = 1.6), there are 67.33% of goethite and 28.91% of ferrihydrite in 1 day sample, and 72.05% of goethite and 19.69% of ferrihydrite in 14 days sample. Detailed fitting parameters were listed in Table 2.3.

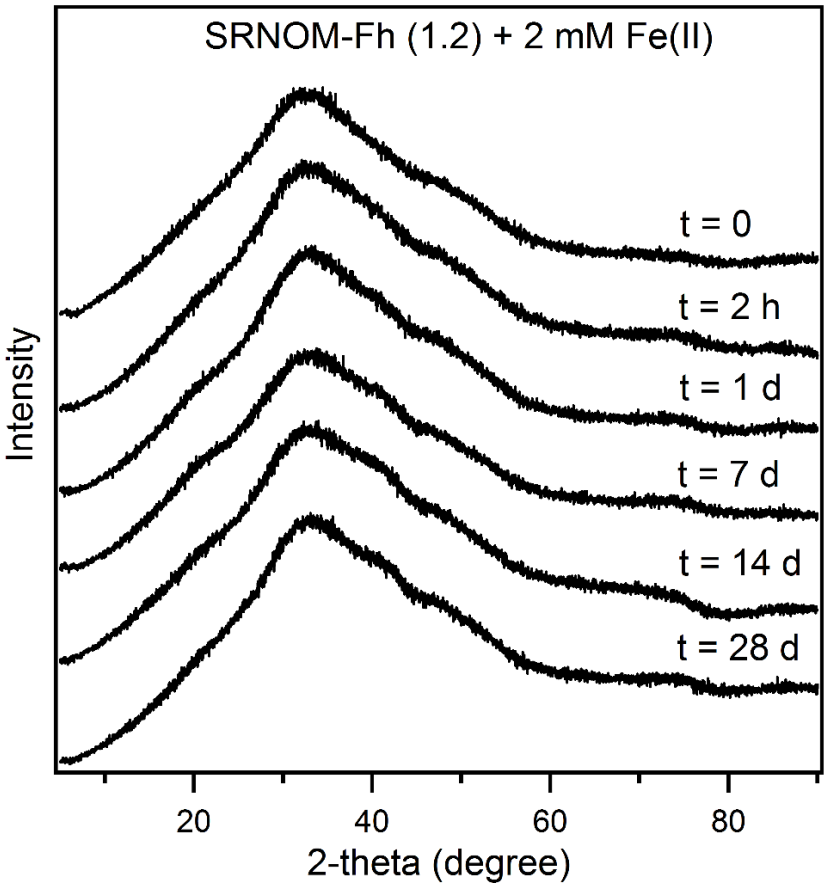

Figure 2.5. X-ray diffraction of SRNOM-Fh (1.2) reacted with 2 mM Fe(II) over time in PIPES buffer, pH 7.0. Solids were collected and characterized on the 0.22 μm glass filter. No mineral transformation was observed over 28 days.

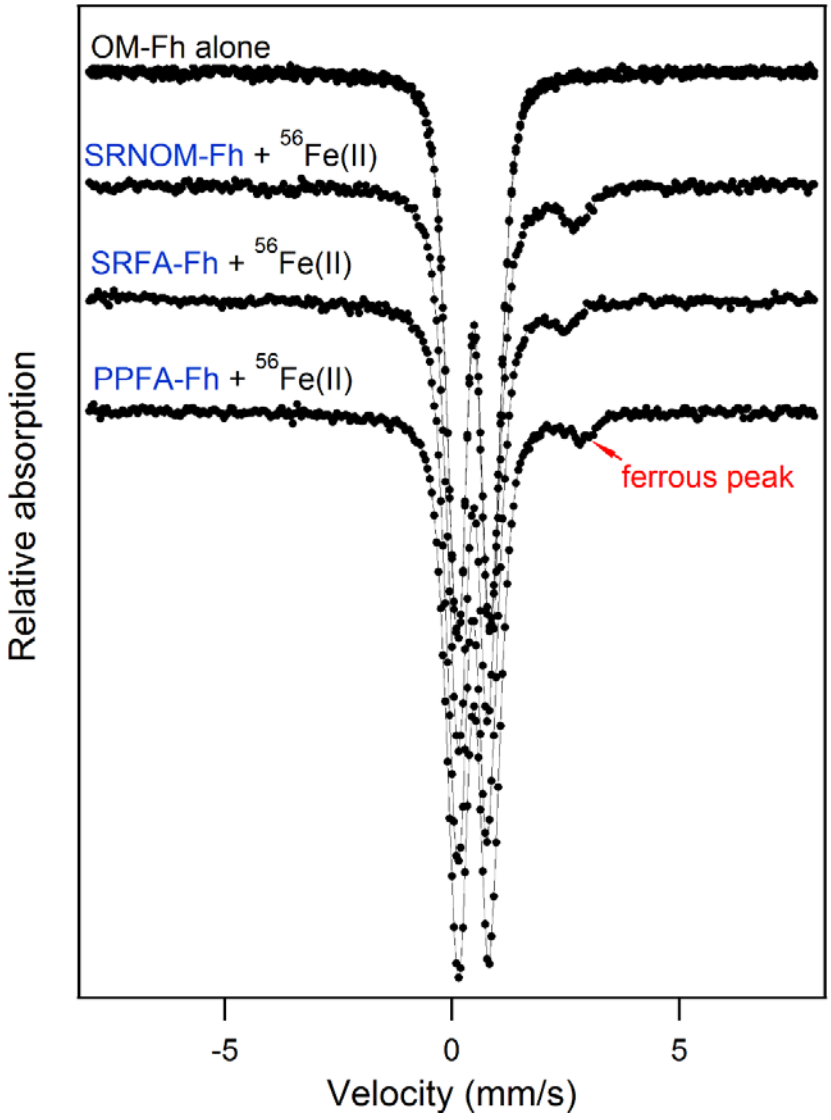

Figure 2.6. ^{57}Fe Mössbauer spectra of various OM-Fh coprecipitates (10 mM Fe(III)) reacted with 2 mM ^{56}Fe(II) in 10 mM PIPES buffer (pH 7.0) over 1 day. Spectra were collected at 77 K. A ferrous peak emerged in reacted OM-Fh coprecipitates.

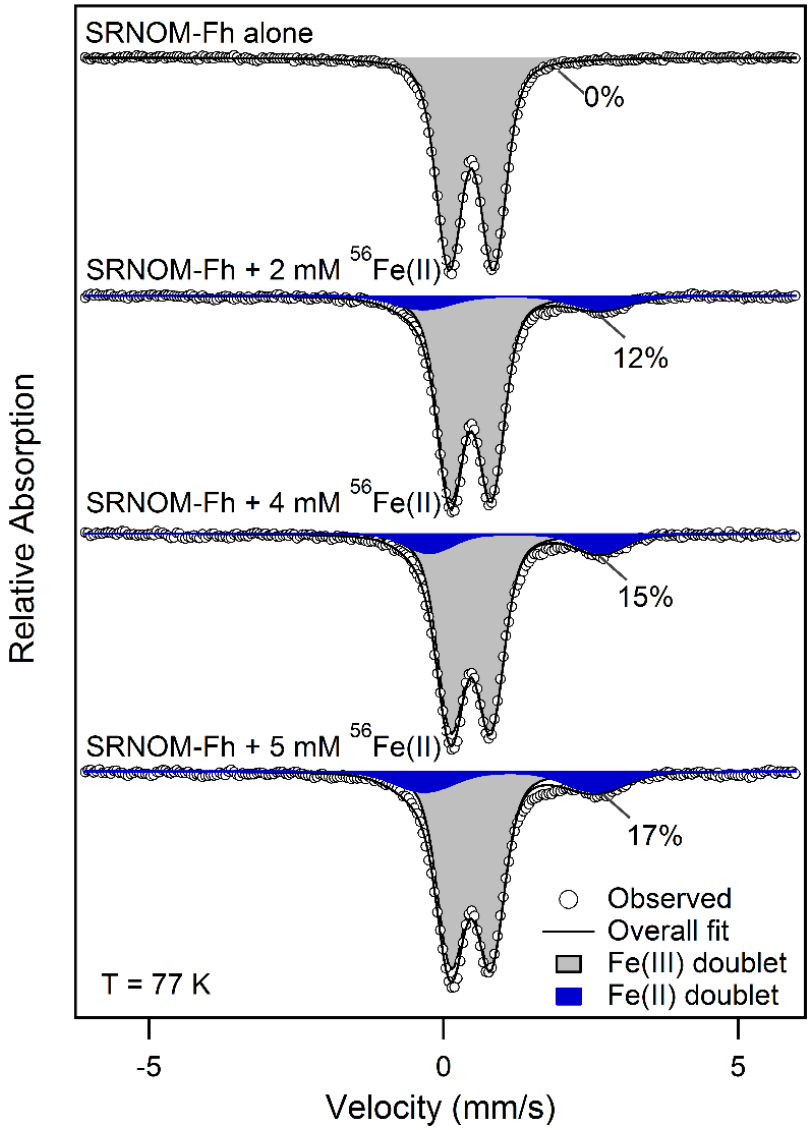

Figure 2.7. Mössbauer spectra of SRNOM-Fh (C/Fe = 1.2) reacted with ^{56}Fe(II) at various concentrations over 7 days. Percent labels are the percent relative area of the Fe(II) doublets (**Table 2.4**). Conditions: 0 to 5 mM ^{56}Fe(II), 10 mM Fe(III) from SRNOM-Fh (C/Fe = 1.2) synthesized with naturally abundant Fe, 10 mM PIPES at pH 7.0.

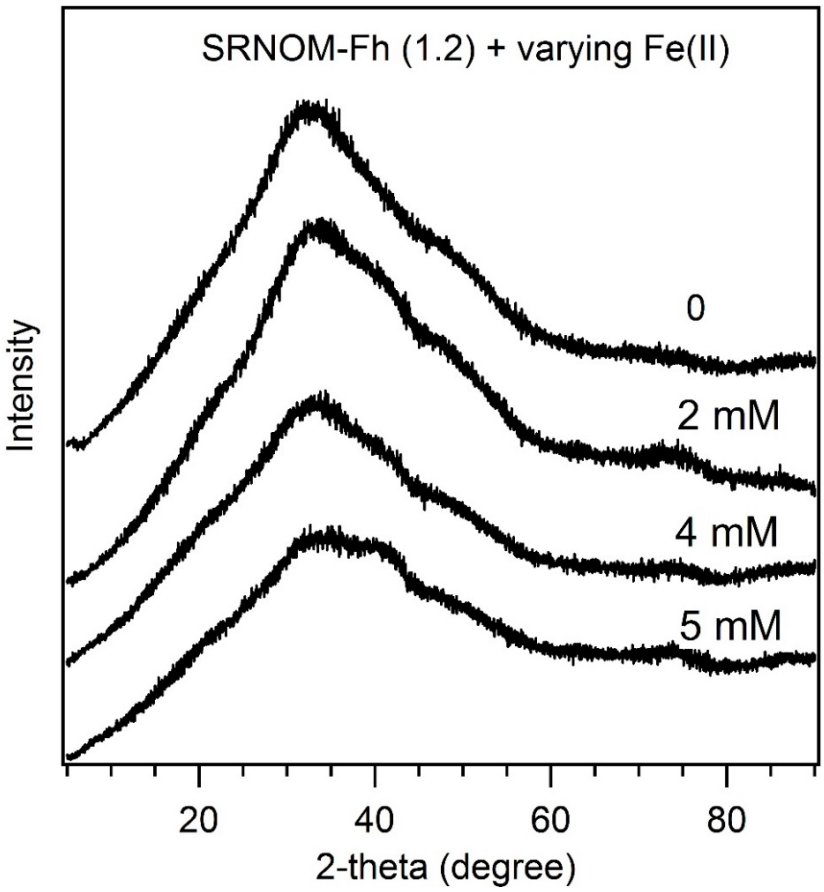

Figure 2.8. X-ray diffraction of reacted SRNOM-Fh (C/Fe = 1.2) with various Fe(II) concentration. Same solids as measured in Figure 2.7.

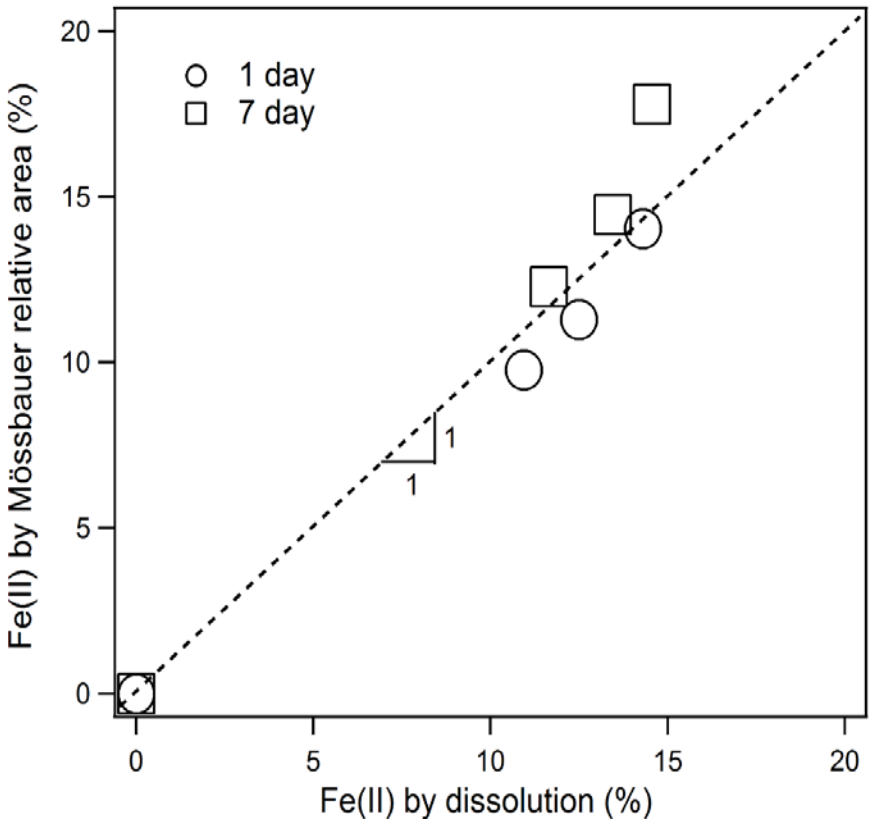

Figure 2.9. A comparison of the percent Fe(II) in SRNOM-Fh (C/Fe = 1.2) coprecipitates reacted with ^{56}Fe(II) as measured by the relative area of the Fe(II) doublet in the Mössbauer spectra and percent of Fe(II) in the dissolved coprecipitates, same condition as Figure 2.7. Table 2.4 contains Mössbauer spectra and fitting parameters from which the relative area of the Fe(II) doublets were determined.

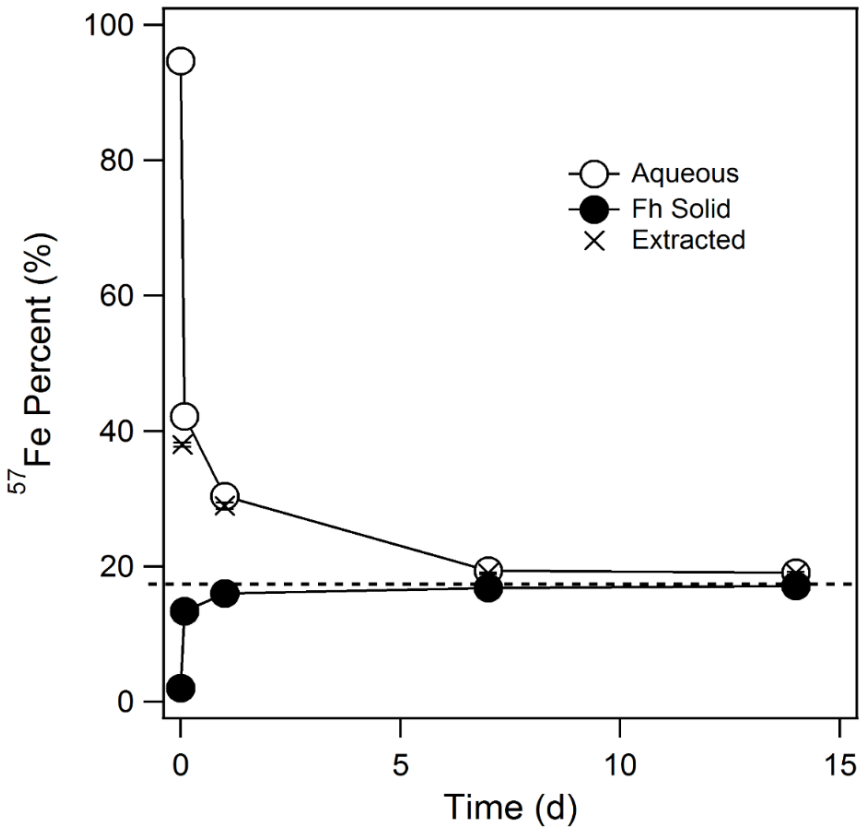

Figure 2.10. Percent 57Fe in aqueous Fe(II), extracted Fe(II) and residual SRNOM-Fh (C/Fe = 1.2) over time. The horizontal dashed line is the calculated 57Fe percent completely mixed value of 17.45%. Conditions: 2 mM 57Fe(II), 10 mM Fe(III) from SRNOM-Fh (C/Fe = 1.2) synthesized with naturally abundant Fe, 10 mM PIPES at pH 7.0. Values for data points represent the mean of triplicate reactors; error bars not visible are smaller than symbols.

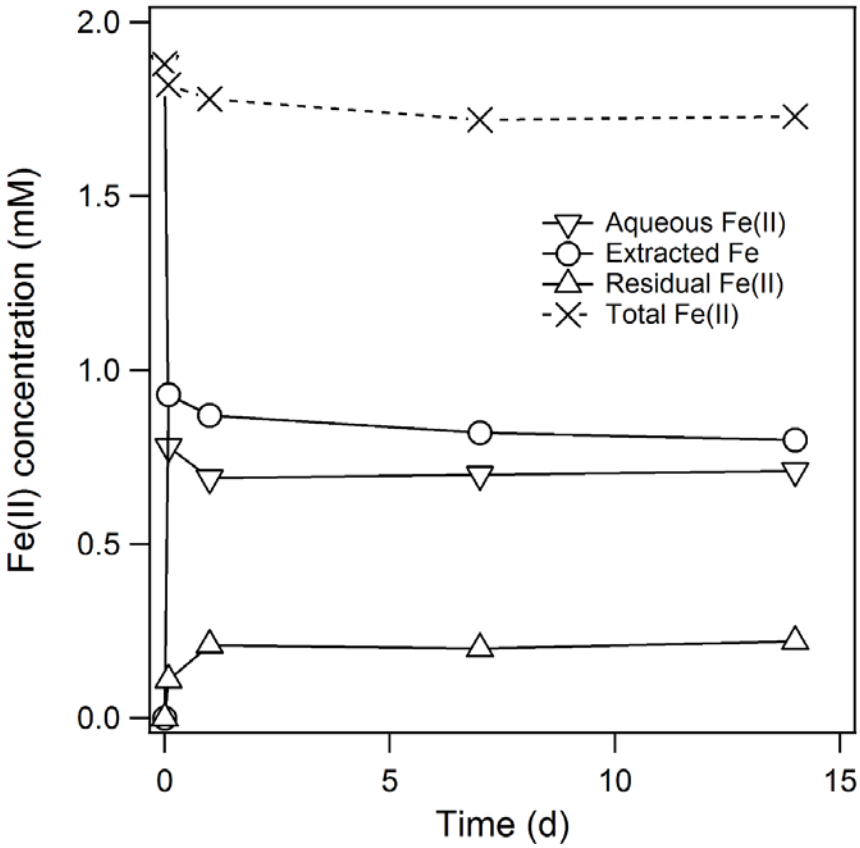

Figure 2.11. Fe(II) distribution in each phase during Fe(II) reaction with SRNOM-Fh (C/Fe = 1.2).

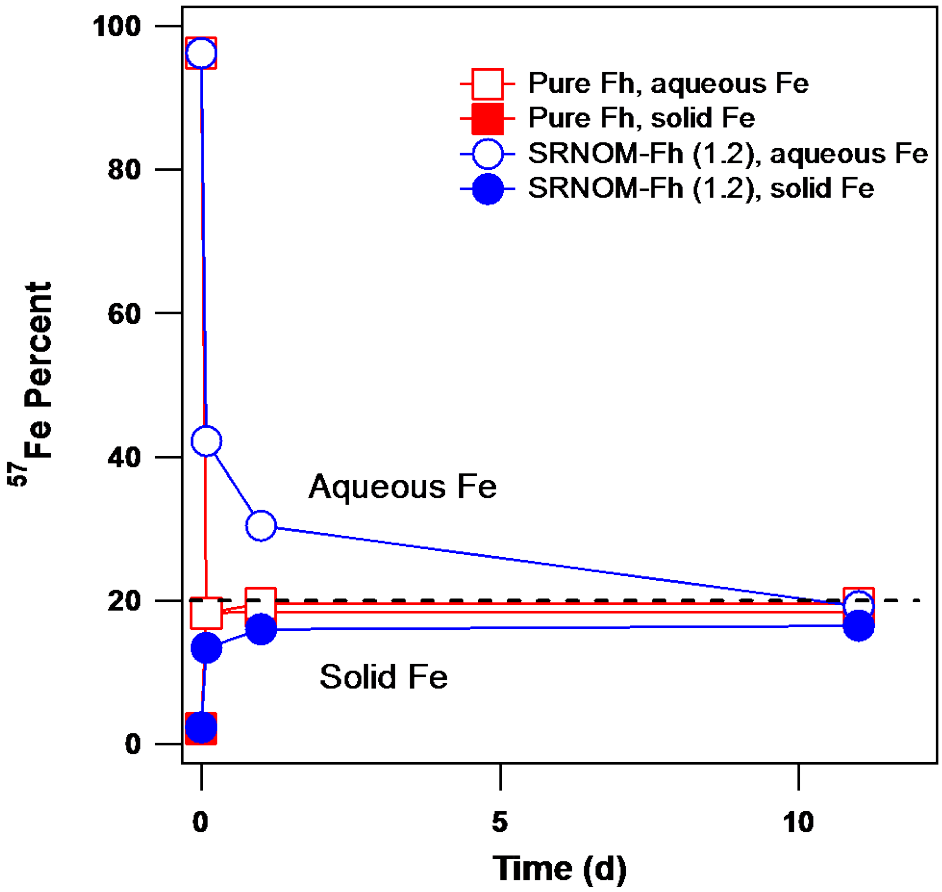

Figure 2.12. Measured ^{57}Fe percentage of aqueous Fe(II) and residual solid Fe over time when 2 mM ^{57}Fe(II) was reacted with wet ferrihydrite and SRNOM-Fh (C/Fe = 1.2) synthesized with naturally abundant Fe. Dash line represents the completely mixed ^{57}Fe percent value in pure Fh reactors.

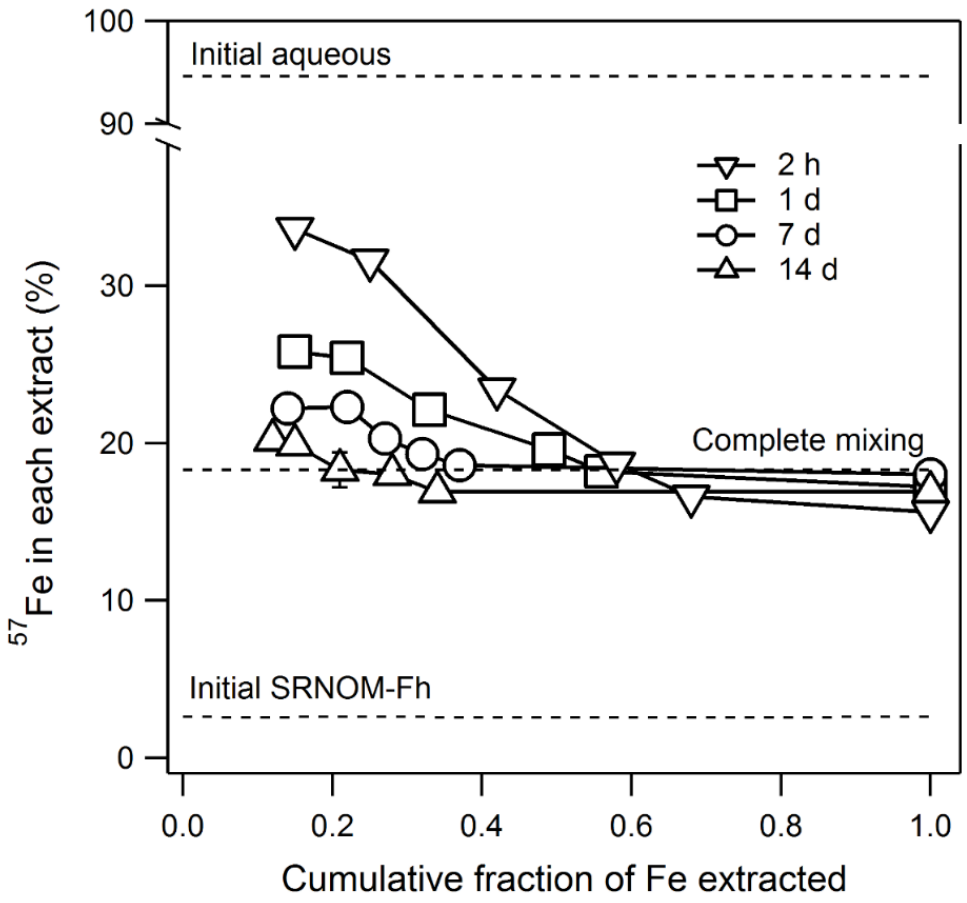

Figure 2.13. Percent of 57Fe isotope in each fraction of sequentially extracted Fe from SRNOM-Fh (C/Fe = 1.2). Data is shown for SRNOM reacted with Fe(II) for vary amounts of time (2 h, 1 d, 7 d, and 14 d) at similar condition as Figure 2.10. The completely mixing line is the calculated mass balance of 57Fe percent (18.3%) in the reactor assuming the isotopes in the solids and aqueous phases have complete mixed (See SI for calculation). Values for data points represent the mean of triplicate experiments.

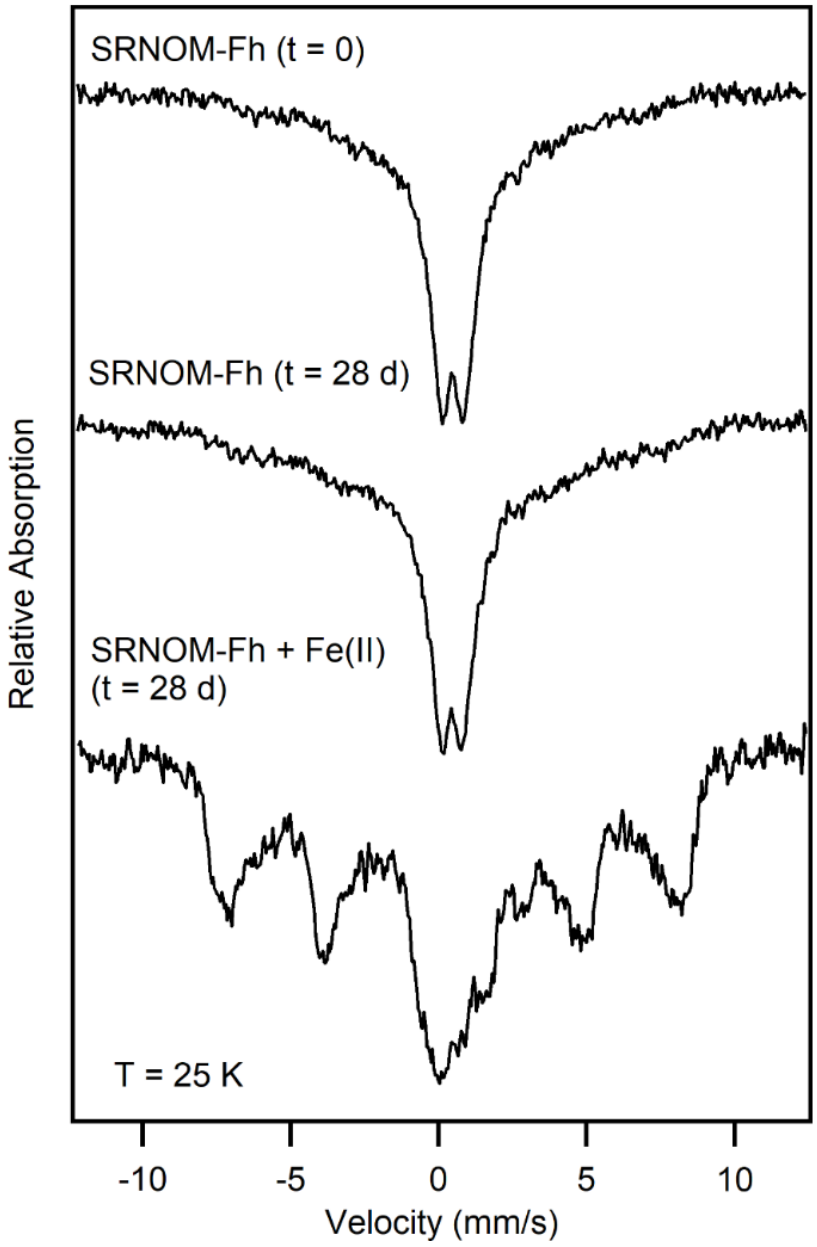

Figure 2.14. Mössbauer spectra of SRNOM-Fh (C/Fe = 1.2) alone and reacted with Fe(II) over 28 days at 25 K.

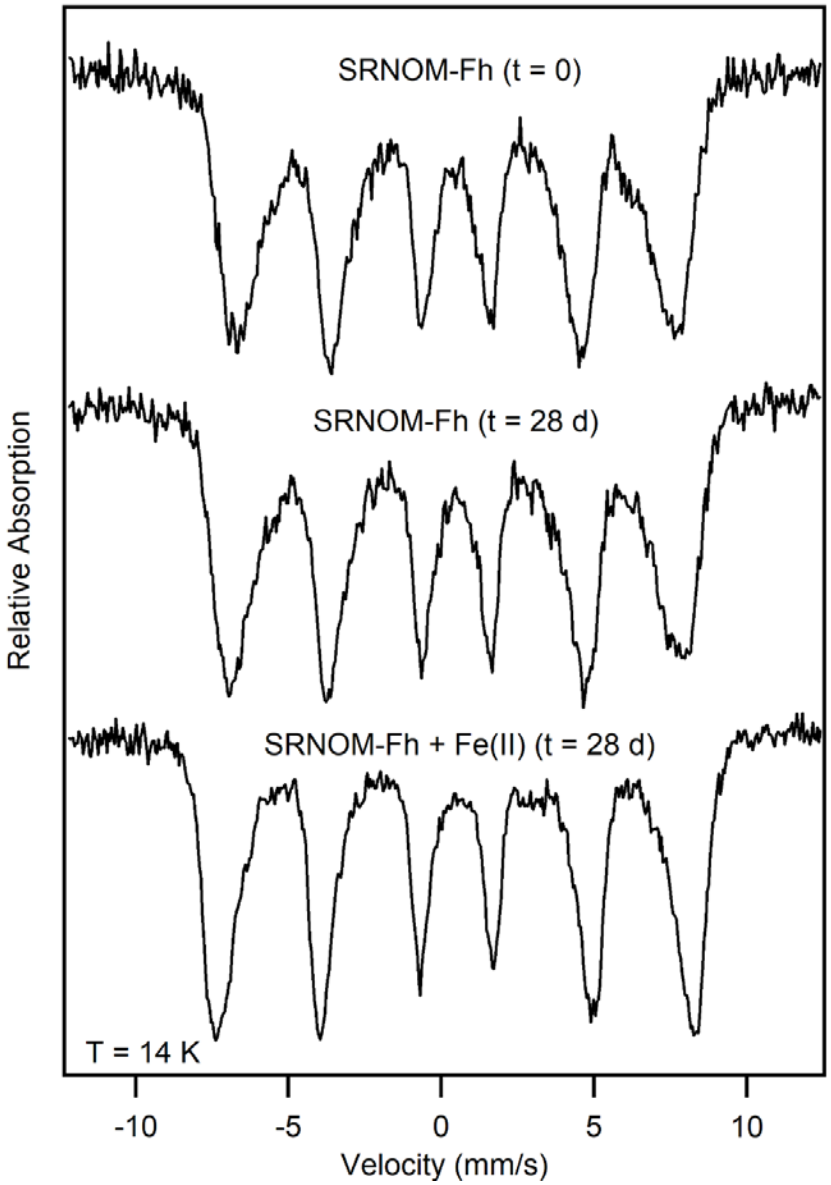

Figure 2.15. Mössbauer spectra of SRNOM-Fh (C/Fe = 1.2) with or without Fe(II) over 28 days at 14 K.

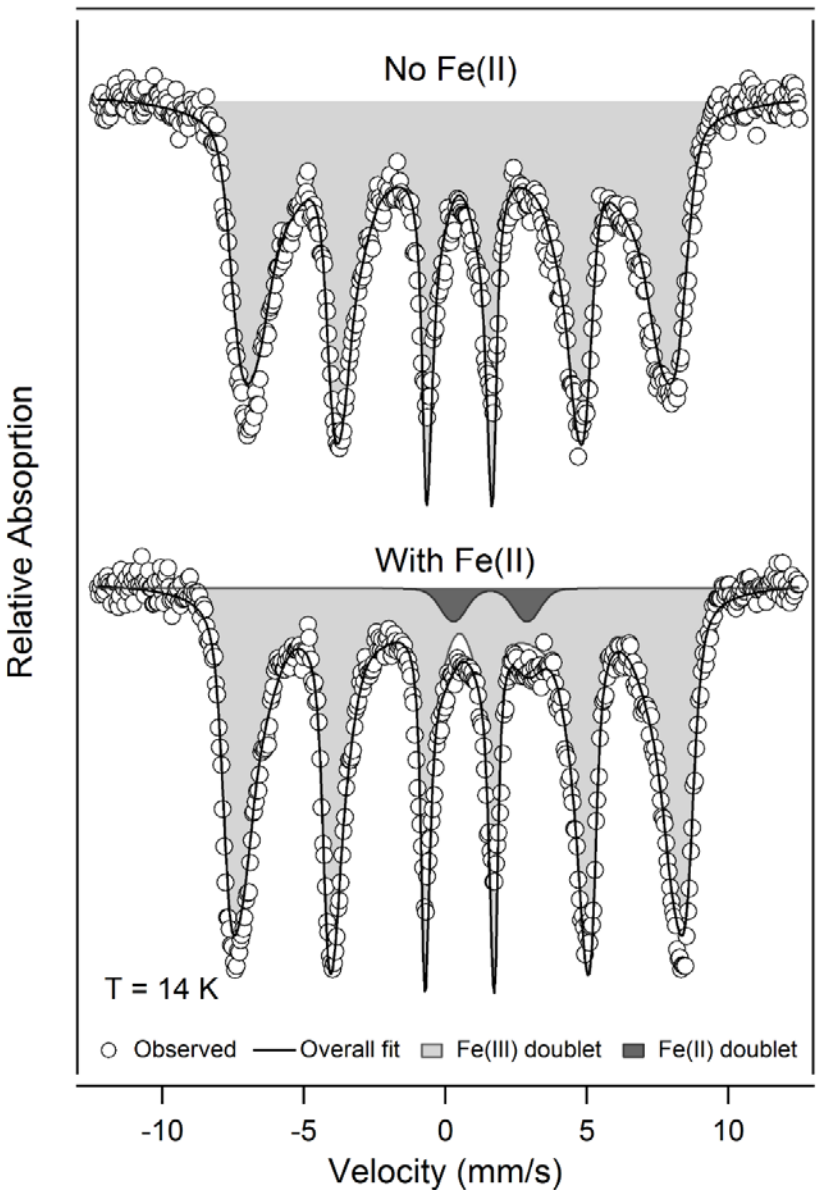

Figure 2.16. Mössbauer spectra fitting of SRNOM-Fh (C/Fe = 1.2) aged with or without Fe(II) over 28 days.

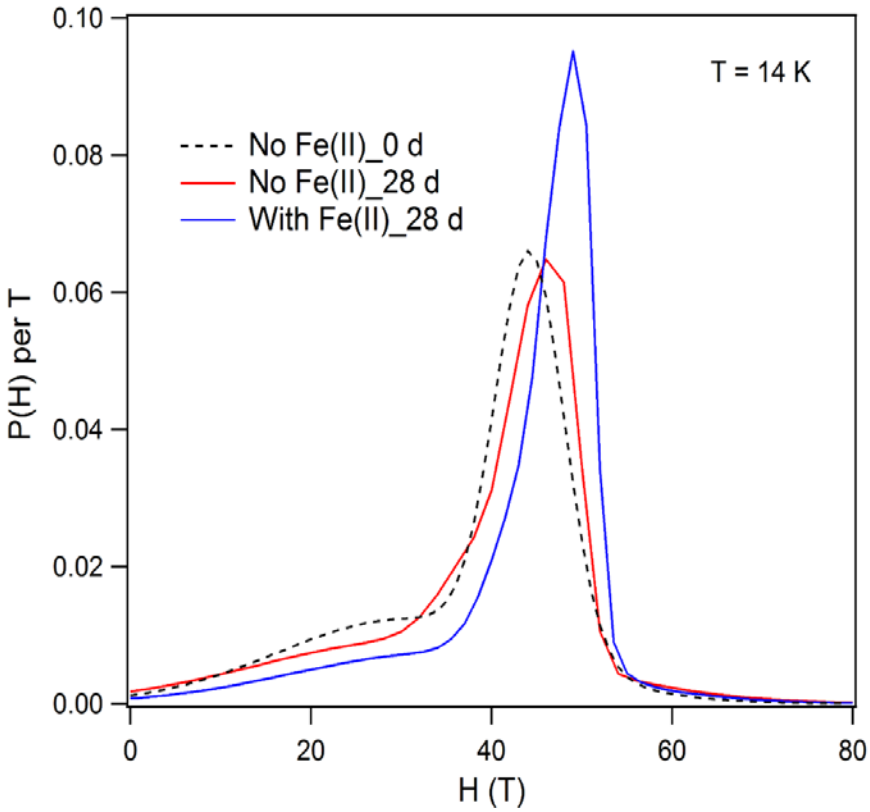

Figure 2.17. Hyperfine field distribution of SRNOM-Fh (C/Fe = 1.2) with or without Fe(II) at 14 K.

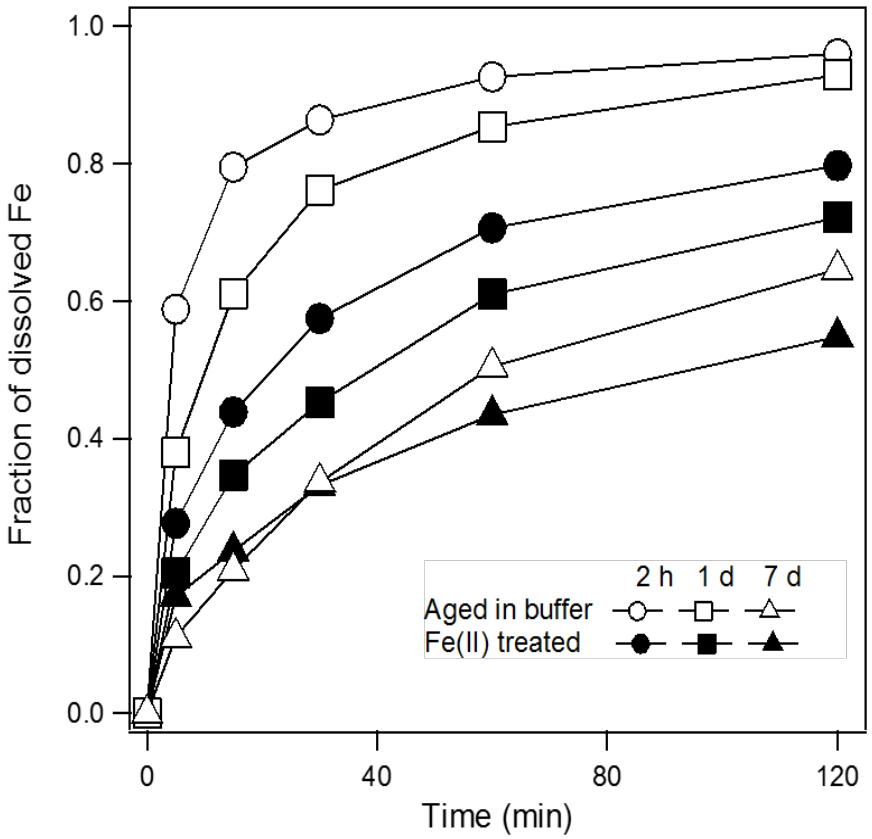

Figure 2.18. Acid dissolution with 0.2 M HCl to (a) SRNOM-Fh (C/Fe = 1.2) treated with Fe(II) in PIPES buffer (pH 7.0) over time; (b) SRNOM-Fh (C/Fe = 1.2) aged in PIPES buffer (pH 7.0) over time.

Figure 2.19. The sedimentation of SRNOM-Fh (C/Fe = 1.2) in PIPES buffer (pH 7.0) with or without 2 mM Fe(II) over 30 minutes.

CHAPTER 3: EFFECT OF C/FE RATIO ON FE(II)-CATALYZED TRANSFORMATION OF FERRIHYDRITE

Abstract

The inhibition of natural organic matter (NOM) on Fe(II)-catalyzed ferrihydrite transformation has been shown in many studies, but yet to be further explored under wider conditions. Here we investigated Fe(II)-catalyzed transformation of ferrihydrite coprecipitated with different species of NOM at various C/Fe ratios. Adsorbed NOM were also used and compared. Both coprecipitated NOM and adsorbed NOM decreased the percent of ferrihydrite transformation to secondary minerals as the C/Fe ratio increased. Further comparison between humic acid and fulvic acid revealed that at low C/Fe ratio ferrihydrite coprecipitated with humic acids transformed primarily to goethite after reaction with Fe(II). In contrast, ferrihydrite coprecipitated with Suwannee River NOM (SRNOM) and fulvic acid transformed primarily to lepidocrocite which has lower crystallinity than goethite. The fulvic content was found to be more inhibitive than humic acids on Fe(II)-catalyzed ferrihydrite transformation at different C/Fe ratios. Adsorbed SRNOM was found to inhibit ferrihydrite transformation at lower C/Fe ratio than coprecipitated SRNOM. The fate of NOM in SRNOM-Fh coprecipitates was also tracked during the reaction with Fe(II). No carbon release was observed regardless of whether ferrihydrite transformed into secondary Fe minerals or not. The thermal stability of carbon, however, was found to increase with the formation of secondary Fe minerals, whereas no change was observed in SRNOM-Fh coprecipitate that underwent extensive Fe atom exchange without formation of secondary Fe minerals.

Introduction

Abundant natural organic matter (NOM) in soil and sediments was directly associated with Fe minerals and this association has been shown deeply affect the fate of Fe minerals (69, 139). Fe(II)-catalyzed ferrihydrite transformation, an important Fe mineral behavior, was found inhibited by with the presence of NOM decades ago (85). Further study about the effect of NOM on Fe(II)-catalyzed ferrihydrite transformation has been carried by us and many others (42, 47, 86, 87). With the help of Fe isotope tracers, the electron transfer and atom exchange between aqueous Fe(II) and ferrihydrite in the presence of NOM was deeply investigated (42, 87). Adsorbed Suwannee River fulvic acid was found to reduce ^{55}Fe release from ferrihydrite and inhibit the formation of goethite (42). With higher C/Fe ratios, less ferrihydrite was transformed until the transformation was totally inhibited (86). While our study found even without the formation of secondary Fe minerals, there still has extensive Fe atom exchanged between aqueous Fe(II) and ferrihydrite, and we suggested the inhibited electron transfer and Fe atom exchange cannot explain the lack of ferrihydrite transformation by NOM. To date, there are lots of studies focused on the impact of NOM on ferrihydrite transformation but the mechanism behind the inhibition of ferrihydrite transformation is still in debate. The use of different NOM and methods of associating them with ferrihydrite in these studies make the comparison and discussion even more challenging.

In Chapter 2, we made some efforts to compare the effect of different NOM on Fe(II)-catalyzed ferrihydrite transformation, and found fulvic acid was more inhibitive than humic acid (87). But note it was only tested under certain C/Fe ratio, we want to see if this conclusion still correct at broader conditions. In addition, only coprecipitated NOM was investigated on Fe(II)-catalyzed ferrihydrite transformation in last chapter. We know adsorption was also a very important way for the combination of NOM and Fe minerals (78, 140). There are some studies

investigating how adsorbed NOM impacts ferrihydrite transformation (42, 141), however, there is no study comparing the effect of coprecipitated OM and adsorbed OM on Fe(II)-catalyzed ferrihydrite transformation. Maybe more importantly, little is known about the fate of NOM during Fe(II)-catalyzed transformation of ferrihydrite, which would be extremely meaningful to understand the stability of carbon in soil and sediments. Here different species of OM were used to synthesize OM-Fh coprecipitates with different C/Fe ratios and reacted with aqueous Fe(II), and the ferrihydrite transformation pathways were compared under different conditions. The Fe(II)-catalyzed transformation of ferrihydrite with adsorbed and coprecipitated SRNOM were also investigated and compared in this study. To understand the fate of NOM during ferrihydrite transformation, we probed the carbon content and thermal stability in SRNOM-Fh coprecipitates before and after reaction with Fe(II).

Materials and Methods

Fe Minerals Preparation and Transformation Experiments

Similar methods as we described in chapter 2 were used to synthesize ferrihydrite and NOM-Fh coprecipitates (87). The amount of OM added at the beginning was adjusted to get coprecipitates with different C/Fe ratios. Ferrihydrite coprecipitated with Leonardite humic acid (LHA) and Suwannee River NOM (SRNOM) were denoted as LHA-Fh coprecipitate and SRNOM-Fh coprecipitate, respectively. The experiments for Fe(II)-catalyzed transformation of ferrihydrite and NOM-Fh coprecipitates were set exactly same as we described in chapter 2. To investigate the effect of adsorbed NOM on Fe(II)-catalyzed ferrihydrite transformation, we reacted wet ferrihydrite with 2 mM aqueous Fe(II) in the presence of dissolved SRNOM. A stock solution of dissolved SRNOM (1 g/L) was used to obtain different initial SRNOM concentrations in each reactors. Wet ferrihydrite was then added to adsorb SRNOM over 24 hours at pH 7.0. Aqueous

Fe(II) enriched with 57Fe (~95% ^{57}Fe) was then added to catalyze ferrihydrite transformation and further probe the Fe atom exchange between Fe(II) and ferrihydrite in the presence of adsorbed NOM. Same methods for sample collection and measurement were applied as we described in chapter 2. Note we tried to measure the amount of adsorbed NOM with TOC analyzer, but the organic buffer (PIPES) used in this experiment had extremely high carbon concentration and compromised the signal of SRNOM in TOC analyzer, and make the data indecipherable.

Carbon Characterization

The carbon content in NOM-Fh coprecipitate before and after reaction with Fe(II) were measured by TOC analyzer and CHN analyzer. The solid was collected through centrifugation and washed with deionized water twice to remove the residual PIPES buffer. Further carbon characterization was carried out in our collaborators' lab in University of Pennsylvania. The thermal stability of the SRNOM-Fh coprecipitates was assessed by thermal analysis using ramped combustion. Samples (~6 mg) were heated to 105 °C at 10°C min^{-1}, held at 105 °C for 15 minutes to dry and equilibrate the sample, then heated at 10°C min^{-1} to 800°C. Experiments were performed in an oxidizing atmosphere of 40 mL min^{-1} of CO_2-free synthetic air (20% O_2 and N_2 balance) using a Netzsch STA 449PC Jupiter simultaneous thermal analyzer equipped with an automatic sample carrier (ASC) and a type-S platinum/ rhodium (Pt/PtRh) sample carrier (Netzsch–Gerätebau GmbH, Selb, Germany). The gas outlet of the thermal analyzer was coupled to a LICOR LI-820 infrared gas analyzer (Licor Biosciences, Lincoln, NE) for evolved gas analysis of CO_2 during the ramped combustion. Thermal stability of the SRNOM-Fh coprecipitates was determined using the temperature at which the peak in CO_2 evolution occurred.

Results and Discussion

Effect of C/Fe Ratio on OM-Fh Coprecipitate Transformation Products

We previously showed that fulvic acids inhibit Fe(II)-catalyzed ferrihydrite transformation more than humic acids at a C/Fe ratio around 1.2 (87). To determine if a similar trend exists over a range of C/Fe ratios, we synthesized OM-Fh coprecipitates with different C/Fe ratios using a humic acid (Leonardite humic acid, LHA) and an NOM similar to fulvic acid (Suwannee River NOM, SRNOM).

For ferrihydrite coprecipitated with LHA at C/Fe ratio 0.8, goethite and small percent of lepidocrocite were formed in the reacted solid and the intensity of XRD peaks increased over time (**Figure 3.1**). Interestingly, lepidocrocite was formed at a later time point than goethite, and the intensity of XRD peaks for both Fe minerals increased over time. At a C/Fe ratio of 1.6, only goethite was found and the intensity of XRD peaks at each time point were weaker compared to C/Fe ratio of 0.8 suggesting that less ferrihydrite was transformed (**Figure 3.2**). At an even higher C/Fe ratio of 3.2, the ferrihydrite transformation was totally inhibited (**Figure 3.3**). Comparing the XRD patterns at 7 days reveals a marked difference in transformation products as a function of C/Fe ratio (**Figure 3.4**). Magnetite was only found in pure ferrihydrite and was inhibited in the presence of NOM, the intensity of goethite XRD peaks decreased as the C/Fe ratio increased and were barely present at C/Fe ratio 3.2. Very limited amount of lepidocrocite was found at a C/Fe ratio of 0.8.

In addition to LHA-Fh coprecipitate, we also synthesized SRNOM-Fh coprecipitate with different C/Fe ratios. In contrast to Leonardite humic acid, ferrihydrite coprecipitated with SRNOM, which has significant fulvic acid, transformed only into lepidocrocite at the lower C/Fe ratio (0.8) (**Figure 3.5)**. We observed a similar result with ferrihydrite coprecipitated with

Suwannee River fulvic acid (SRFA) at C/Fe ratio 0.8, but with lower intensity of XRD peaks (**Figure 3.6**). Compared to the dominance of goethite in LHA-Fh (C/Fe = 0.8) coprecipitate and other HA-Fh (C/Fe = 1.6) coprecipitates (87), lepidocrocite appeared to form more in ferrihydrite coprecipitated with fulvic acid or SRNOM at low C/Fe ratio (**Figure 3.6**). This observation is consistent with a published study where adsorbed SRFA (25 mg/L, C/Fe ratio ~0.4) facilitated the accumulation of lepidocrocite (81.2%) and inhibited goethite formation (42). At low Fe(II)/Fe(III) ratios, it was also observed that coprecipitated OM inhibited the formation of goethite and facilitated lepidocrocite formation (86). Our observation that lepidocrocite is the dominant transformation product from ferrihydrite coprecipitated with fulvic acid and SRNOM is consistent with our earlier conclusion that fulvic acid is more inhibitive than humic acid (87) because lepidocrocite has lower crystallinity than goethite and is normally regarded as the precursor of goethite (55, 142).

Since it has been observed that NOM can facilitate ferrihydrite reduction at high C/Fe ratio by dissimilatory Fe(III)-reducing bacterium (DIRB) (104), we further increased the C/Fe ratio in SRNOM-Fh coprecipitate to test if carbon facilitated ferrihydrite transformation also occurred during aqueous Fe(II)-catalyzed transformation of ferrihydrite. Over 7 days reaction with Fe(II), no secondary Fe mineral was observed in SRNOM-Fh (C/Fe = 2.4) coprecipitate (**Figure 3.7**), consistent with what we observed in LHA-Fh (C/Fe = 3.2) coprecipitate and in contrast to what was observed with DIRB. Our results suggest that other processes must be occurring in DIRB reduction of ferrihydrite other than what we are observing when adding aqueous Fe(II) to induce Fe(II)-catalyzed ferrihydrite transformation as we only observed inhibition of NOM on Fe(II)-catalyzed ferrihydrite transformation (**Figure 3.4** and **3.8**).

Less ferrihydrite transformation at higher C/Fe ratios, however, is consistent with previous work using adsorbed Suwannee River fulvic acid (SRFA) where ferrihydrite transformation was completely inhibited with 150 mg/L SRFA (C/Fe ratio ~2.5) (42). A similar trend was also observed in a study with coprecipitated OM extracted from an Ultisol, but magnetite was not totally inhibited until C/Fe ratio 1.2 in their study (86). In another study, complete inhibition of magnetite was reported in the presence of bicarbonate (55). The inhibition of carbon on ferrihydrite structural conversion and nucleation were proposed to explain the lack of magnetite formation (143). In these studies, different carbon sources were used making it difficult to directly compare the data. We also want to note the characterization method in our study may not be sensitive enough to catch the small amounts of magnetite observed in the previous studies.

To evaluate whether different amounts of Fe(II) sorb on the different C/Fe ratio ferrihydrite coprecipitates, we measured the amount of Fe(II) sorbed by LHA-Fh coprecipitates with different C/Fe ratios (**Figure 3.9**). We observed more Fe(II) sorption with increasing of C/Fe ratio possibly because of additional sorption to NOM (144). However, it was challenging to distinguish whether Fe(II) was sorbed to Fe minerals or NOM. Based on our study and others (87, 145, 146), NOM can be an electron shuttle and may not inhibit the electron transfer between Fe(II) and ferrihydrite. With more Fe(II) sorbed on NOM-Fh coprecipitate with higher C/Fe ratio, there may be more electrons available for ferrihydrite, however, ferrihydrite still not transform. This is consistent with our earlier conclusion that limited electron transfer is not responsible for the lack of ferrihydrite transformation (87). We do not, however, know how the presence of NOM change the redox potential of Fe(II)-Fe(III) which may influence electron transfer and subsequent ferrihydrite transformation. Indeed, Studies have suggested that OM can decrease Fe(II) oxidation rate by preventing formation of the inner-sphere complex between Fe(II) and the oxide surface (33, 114).

Effect of Adsorbed OM on Fe(II)-catalyzed Ferrihydrite Transformation

In addition to coprecipitation, adsorption of NOM on the ferrihydrite surface is another common way for NOM to associate with ferrihydrite in soil and sediments (88, 147, 148), particularly considering the large surface area of ferrihydrite. To evaluate whether adsorbed and coprecipitated OM have a similar influence on Fe(II)-catalyzed ferrihydrite transformation, we reacted ferrihydrite equilibrated with different concentrations of SRNOM with ^{57}Fe(II) for 7 days. Adsorbed OM resulted in a decreased percentage of ferrihydrite transformation with an increase in C/Fe ratios, similar to what we observed with coprecipitated OM (**Figure 3.10**). At an SRNOM concentration of 120 mg/L (C/Fe ratio = 0.5), adsorbed OM inhibited the formation of magnetite and facilitated lepidocrocite formation, with only minor transformation to goethite over 7 days (**Figure 3.10**). As SRNOM concentration further increased, Fe(II)-catalyzed ferrihydrite transformation was completely inhibited. The lowest C/Fe ratio where we saw overall transformation inhibition with adsorbed NOM was around C/Fe ratio 1.0 (120 mg/L SRNOM). But considering only around 70% of SRNOM may adsorb to ferrihydrite estimated from similar study (149), suggesting that the actual C/Fe ratio in the SRNOM-Fh association may be lower and close to 0.7. Note for the SRNOM-Fh coprecipitate with C/Fe ratio 0.8, we observed secondary Fe minerals formed at the same Fe(II) concentration. Based on these estimates, it appears that adsorbed NOM may inhibit Fe(II)-catalyzed ferrihydrite transformation more than coprecipitated NOM but additional work is needed to over a wider range of conditions to evaluate this.

Effect of Adsorbed OM on Fe Atom Exchange

To track the Fe atom movement between aqueous Fe(II) and ferrihydrite in the presence of adsorbed SRNOM, we used a ^{57}Fe(II) tracer and measured aqueous Fe(II) concentration and isotopic composition over time. Aqueous Fe(II) concentration indicates more Fe(II) was sorbed by

ferrihydrite alone (**Figure 3.11**) most likely because the formation of magnetite can incorporate Fe(II) in its octahedral sites (95). In the presence of SRNOM, Fe(II) sorption was slightly increased with higher initial SRNOM concentration, indicating the adsorbed SRNOM on ferrihydrite may provide additional sorption sites for Fe(II). When lepidocrocite and goethite both formed, a slight decrease in Fe(II) sorption was observed over time possibly due to the formation of secondary Fe minerals that have lower surface areas than ferrihydrite (150).

In the absence of SRNOM, ferrihydrite transformed into secondary Fe minerals and the ^{57}Fe percent in the aqueous dropped rapidly to 19.4% over 2 hours which is below the calculated completely mixed isotopic proportion of 21.3% (**Table 3.1**). One explanation for the drop below the completely mixed value may be direct incorporation of aqueous Fe(II) into magnetite (43, 55). The reacted solid was extracted with 0.4 M HCl extraction in an attempt to selectively dissolve ferrihydrite while leaving the newly formed magnetite and goethite. The ^{57}Fe percent in the extractable solid was 17.8% which lower than the ^{57}Fe percent in the aqueous phase suggesting that some of ferrihydrite had not exchanged or completely mixed with the aqueous Fe(II) (**Table 3.1**). The residual solid after extraction was totally dissolved by 5 M HCl and the ^{57}Fe percent in it was 24.8% which is higher than extracted ferrihydrite phase. Our results confirmed that there was a heterogeneous distribution of Fe isotope in the solids. Over 7 days, the ^{57}Fe percent in aqueous phase increased to 21.7% and became closer to the extracted ferrihydrite (20.5%). The ^{57}Fe percent in secondary Fe minerals decreased to 21% over 7 days, which may be resulted by its further exchange with aqueous phase or the formation of new secondary Fe minerals with lower ^{57}Fe percent. Our selective extractions and quantifying isotope distributions suggest a promising approach for evaluating the Fe isotope distributions in solids with secondary Fe minerals, which will help overcome the challenge of interpreting isotope data in a heterogeneous system.

In the presence of 120 mg/L SRNOM, lepidocrocite and goethite were formed in the presence of Fe(II). The initial C/Fe ratio in the presence of 120 mg/L was around 0.5, but the amount of carbon adsorbed on ferrihydrite maybe even lower (149). The percent of ^{57}Fe in aqueous Fe(II) phase decreased from 95% to 32.1% over 2 hours, not as much as it decreased with pure ferrihydrite (19.4%). It further dropped to 19.5% and exceeded the calculated isotope equilibrium value over 1 day reaction, but didn't increased over longer reaction time as we observed in pure ferrihydrite (**Figure 3.10**). The ^{57}Fe percent in secondary Fe minerals after 7 days was 21.8% which was higher than aqueous phase. Clearly there is a heterogeneous Fe isotope distribution in the reacted solids when secondary Fe minerals are formed which makes it challenging to interpret the isotope data and estimate the percent of Fe atom exchange (52).

With even higher initial SRNOM concentration (240 mg/L, C/Fe ratio ~1.0), ferrihydrite transformation was totally inhibited and a higher ^{57}Fe percent in the aqueous phase was observed, suggesting less atom exchange occurred between aqueous Fe(II) and ferrihydrite. The extent of ^{57}Fe percent change was consistent with what we observed in SRNOM-Fh coprecipitate that with C/Fe ratio 1.2 (**Figure 2.10**). Note lower C/Fe ratio was used with adsorbed SRNOM to achieve this similar inhibition as observed with coprecipitated SRNOM. In addition, considering not all SRNOM was adsorbed by ferrihydrite, the C/Fe ratio in solid phase would be even lower than 1.0 (estimated to be 0.7) (149). Further increasing the SRNOM concentration (480 mg/L, C/Fe ratio ~2.0), we saw less ^{57}Fe percent change in aqueous Fe(II) especially at early time point, but it is not proportional to the amount of SRNOM added. If we look at the results after 7 days reaction, it is a somewhat surprising to see similar Fe isotope compositions in aqueous Fe(II) under such varied SRNOM concentrations. Our results are, however, consistent with our speculation that

coprecipitated SRNOM that organic matter may work as electron shuttle, and there still has extensive Fe atom exchange occurred in the lack of ferrihydrite transformation.

Comparison Between Coprecipitated and Aadsorbed OM

Our limited data shows preliminary evidence that adsorbed SRNOM may be more inhibitive than coprecipitated SRNOM on Fe(II)-catalyzed ferrihydrite transformation and Fe atom exchange. This is consistent with another study that found ferrihydrite with adsorbed OM was less susceptible to reduction comparing to the one with coprecipitated OM (101). A possible reason for the different effects between adsorbed and coprecipitated NOM observed is that coprecipitated NOM decreased edge-sharing FeO_6 octahedra and resulted smaller crystal size in ferrihydrite (73, 74). Our study also showed the crystallinity of ferrihydrite decreased in the presence of coprecipitated NOM (87). These observations indicate ferrihydrite coprecipitated with NOM might be more susceptible to Fe atom exchange or recrystallization due to its lower stability than ferrihydrite. The adsorbed NOM, however, would not change the crystallinity of ferrihydrite as its interaction mostly occurred at the surface of minerals (112, 148). In addition, adsorption to ferrihydrite can fractionate NOM and make it has different composition with coprecipitated NOM (151). The preference of aromatic carbon and larger size NOM moieties during the adsorption to Fe mineral surface may also better inhibit the reactivity of ferrihydrite (75, 77).

Fate of NOM during Ferrihydrite Transformation.

To investigate the fate of NOM during Fe(II)-catalyzed ferrihydrite transformation, we measured the carbon content in SRNOM-Fh coprecipitates before and after reaction with Fe(II) (**Table 3.2**). In SRNOM-Fh (C/Fe = 1.2) coprecipitate, we found no secondary Fe mineral formed after reaction with Fe(II) and the carbon content in the coprecipitate was also not changed, even though we observed extensive Fe atom exchanged (87). Ferrihydrite transformation occurred in

SRNOM-Fh (C/Fe = 0.8) coprecipitate after reaction with Fe(II), there is still no evidence showing carbon release during the process. Chen et al. also found carbon content remained unchanged in OM-Fh coprecipitate after reaction with Fe(II), but they suggested the bound OM was less stable (86).

To further characterize the stability of carbon in SRNOM-Fh coprecipitates after reaction with Fe(II), we characterized SRNOM-Fh coprecipitates before and after Fe(II) treatment using thermal analysis during ramped combustion. We used the temperature where we saw the max CO_2 peaks as a guide for carbon thermal stability, and found there is no carbon thermal stability change in SRNOM-Fh (C/Fe = 1.2) before and after Fe(II) treatment **(Table 3.3)**. In this SRNOM-Fh (1.2) coprecipitate, we observed no Fe mineral transformation. We further compared the carbon thermal stability in SRNOM-Fh (C/Fe = 0.8) where Fe(II) can start the mineral transformation. The temperature where we observed max CO_2 peak increased after mineral transformation occurred, indicating the carbon thermal stability in SRNOM-Fh (C/Fe = 0.8) coprecipitate increased by ferrihydrite transformation.

Conclusion

In this study, we found the increasing of C/Fe ratio, regardless of whether it is humic acid or fulvic acid, results in less ferrihydrite transformation in the presence of aqueous Fe(II). Comparing our data with other studies suggests the effects of NOM are different between Fe(II)-catalyzed transformation and the dissimilatory Fe(III) reducing bacterium induced transformation. The comparison between adsorbed NOM and coprecipitated NOM showed some preliminary evidence that adsorbed NOM may be more inhibitive than coprecipitated NOM on Fe(II)-catalyzed ferrihydrite transformation. Adsorbed SRNOM slows down the Fe isotope composition change in aqueous Fe(II), but extensive Fe isotope mixing still appears to occur between aqueous Fe(II) and

ferrihydrite. The NOM associated through different pathways is likely to have different implications for stability of ferrihydrite in reducing environments. In environments that have more fluctuate pH or redox potential, the coprecipitation of ferrihydrite and NOM can be a common process which would form a more dynamic NOM-Fh phase (152, 153).

We also found fulvic acid and humic acid would lead to different ferrihydrite transformation pathways at low C/Fe ratio. With humic acid, goethite was predominant in the secondary Fe minerals. Whereas lepidocrocite formed more when ferrihydrite coprecipitated or adsorbed with fulvic acid and NOM that was enriched with fulvic content. As expected, ferrihydrite transformation to more stable minerals is strongly influenced by the nature of the organic matter present during ferrihydrite formation. Based on our results and those of others (42, 86), we speculate that higher percentage of ferrihydrite and lepidocrocite were expected in Fe minerals associated with highly decomposed OM than those newly formed OM.

As an important sink for the storage of carbon in soil and sediments, ferrihydrite was found associate with NOM during Fe(II)-catalyzed transformation. No carbon release or change in thermal stability was observed in SRNOM-Fh coprecipitate after reaction with Fe(II) in the lack of ferrihydrite transformation. The formation of secondary Fe minerals was found to improve the thermal stability of NOM. However, this was only tested under a very limited condition. More work is needed to test the carbon distribution or stability during Fe mineral transformation or recrystallization.

Table 3.1. The ^{57}Fe percent in different phases during Fe(II)-catalyzed ferrihydrite transformation.

Time (d)	^{57}Fe Percent (%)		
	Aqueous Fe	**0.4 M HCl extracted**	**Residual solid**
0	95.0 (0.2)	-	-
0.08	19.4 (0.3)	17.8 (0.2)	24.8 (0.5)
1	21.6 (0.1)	-	-
7	21.7 (0.2)	20.5 (0.2)	21.0 (0.4)

Table 3.2. The carbon percent in SRNOM-Fh coprecipitate before and after reaction with Fe(II).

Sample Information	Percent in sample	
	N (%)	**C (%)**
SRNOM-Fh (C/Fe =1.2) in PIPES buffer	0.198	**9.712**
SRNOM-Fh (C/Fe = 1.2) +2mM Fe(II) in PIPES buffer	0.212	**9.620**
SRNOM-Fh (C/Fe = 0.8) in PIPES buffer	0.000	**6.878**
SRNOM-Fh (C/Fe = 0.8) +2mM Fe(II) in PIPES buffer	0.000	**7.393**

Table 3.3. The temperature at which max CO_2 peak was measured in SRNOM-Fh coprecipitates.

Sample Information	Max CO_2 peak (℃)
SRNOM-Fh (C/Fe = 1.2) alone	289
SRNOM-Fh (C/Fe = 1.2) with Fe^{2+}	287
SRNOM-Fh (C/Fe = 0.8) alone	289
SRNOM-Fh (C/Fe = 0.8) with Fe^{2+}	295

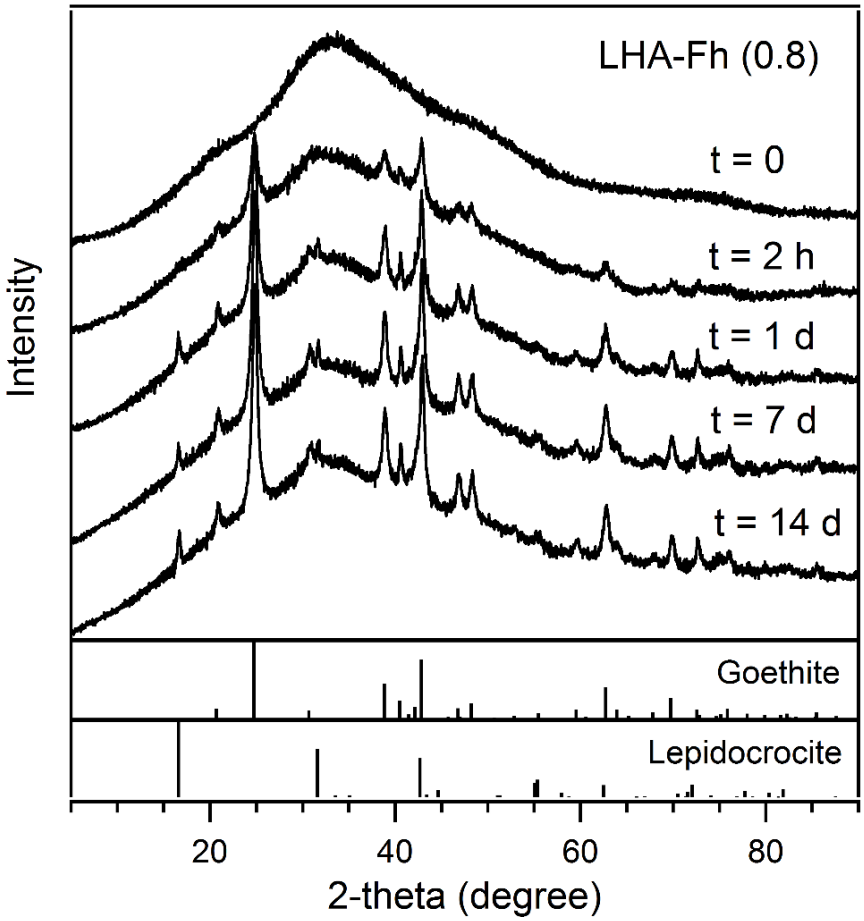

Figure 3.1. X-ray diffraction pattern of LHA-Fh (C/Fe = 0.8) reacted with 2 mM Fe(II) in 10 mM PIPES (pH 7.0) over 14 days. Solids were collected and characterized with 0.22 μm glass filter. The identical peaks of secondary Fe mineral are consistent with goethite and lepidocrocite.

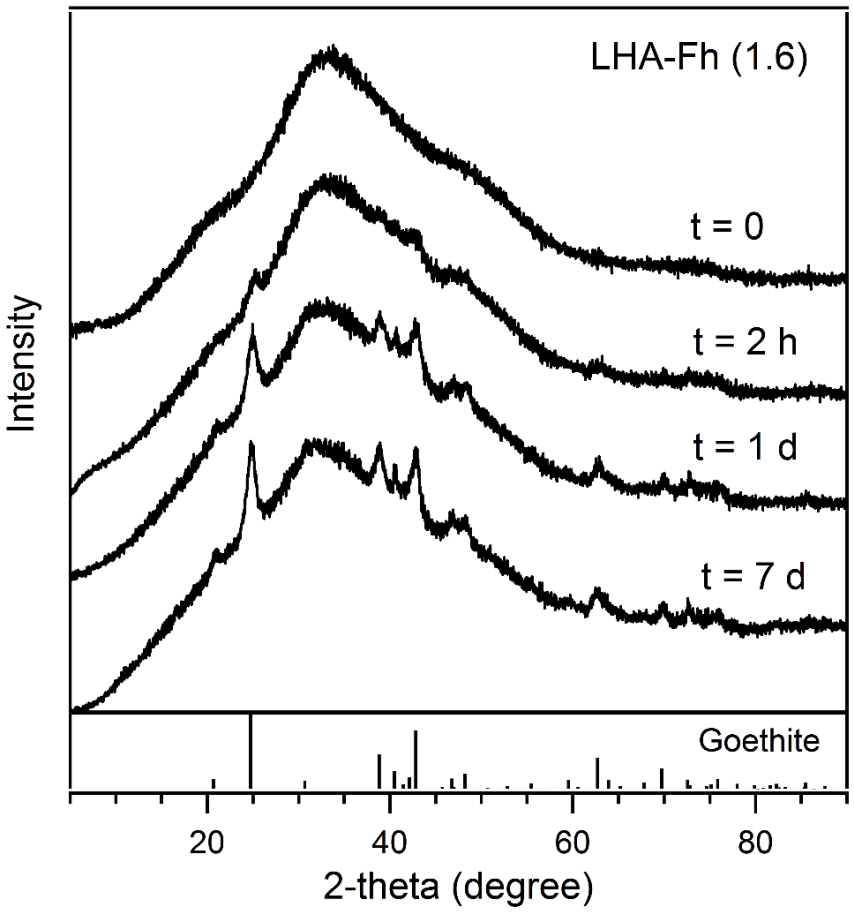

Figure 3.2. X-ray diffraction pattern of LHA-Fh (C/Fe = 1.6) reacted with 2 mM Fe(II) in 10 mM PIPES (pH 7.0) over 7 days. Solids were collected and characterized with 0.22 μm glass filter. The identical peaks of secondary Fe mineral are consistent with goethite.

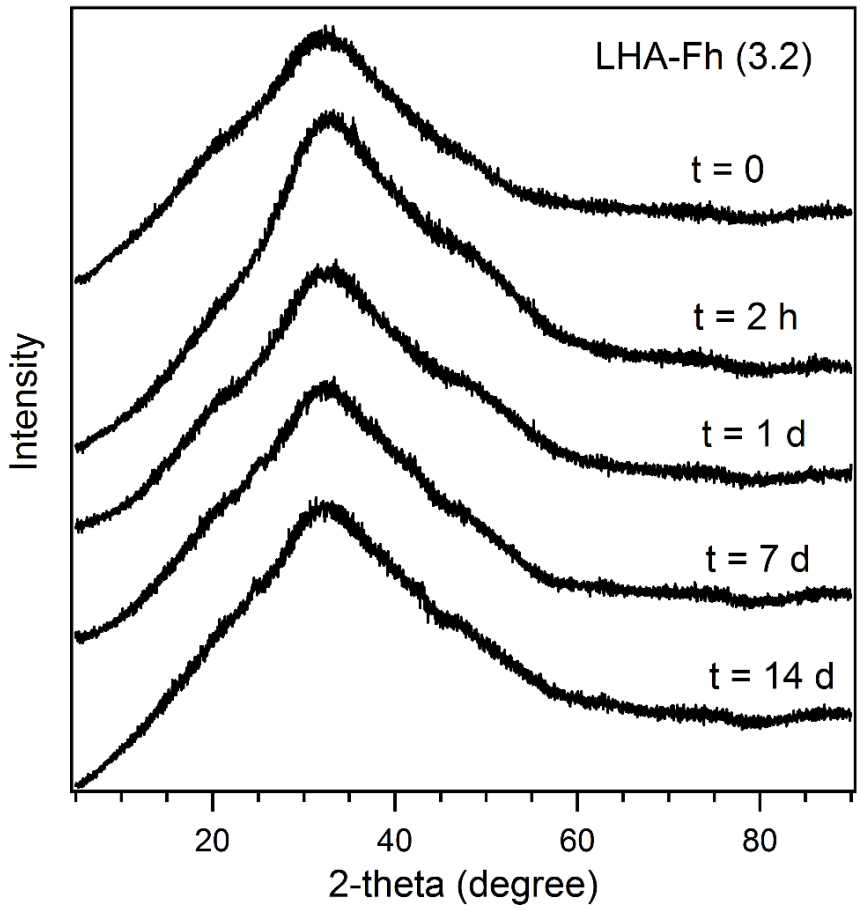

Figure 3.3. X-ray diffraction of LHA-Fh (C/Fe = 3.2) reacted with 2 mM Fe(II) in 10 mM PIPES (pH 7.0) over 14 days. Solids were collected and characterized with 0.22 μm glass filter. No secondary Fe mineral was observed.

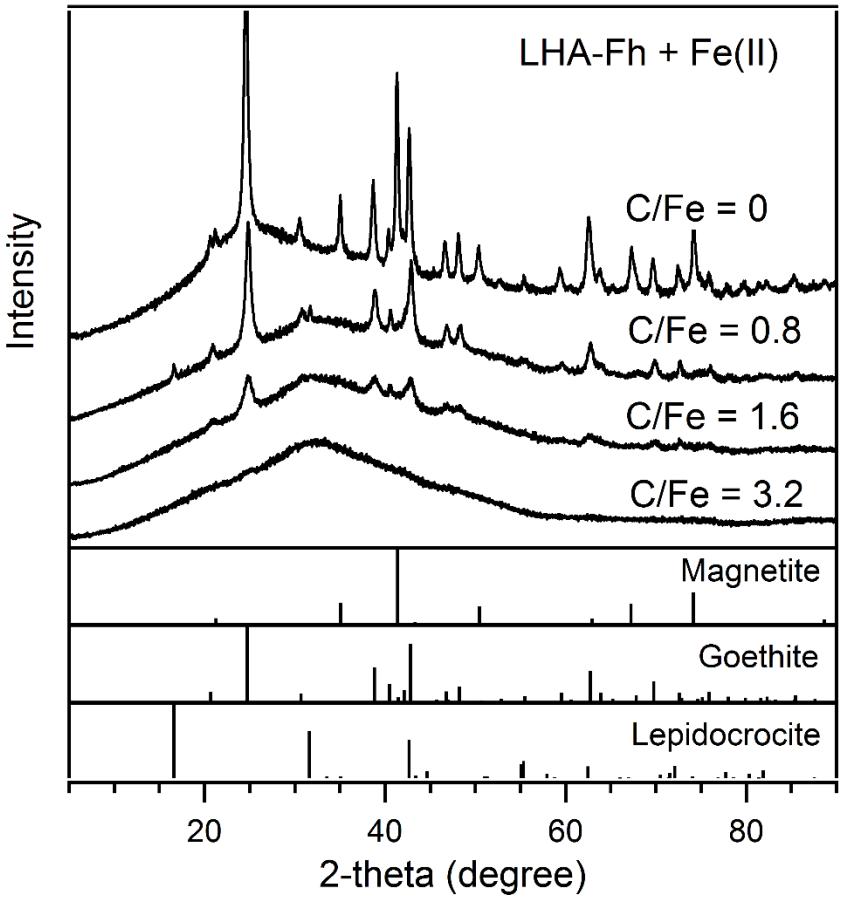

Figure 3.4. X-ray diffraction patter of LHA-Fh coprecipitate with different initial C/Fe ratio reacted with aqueous Fe(II) over 7 days.

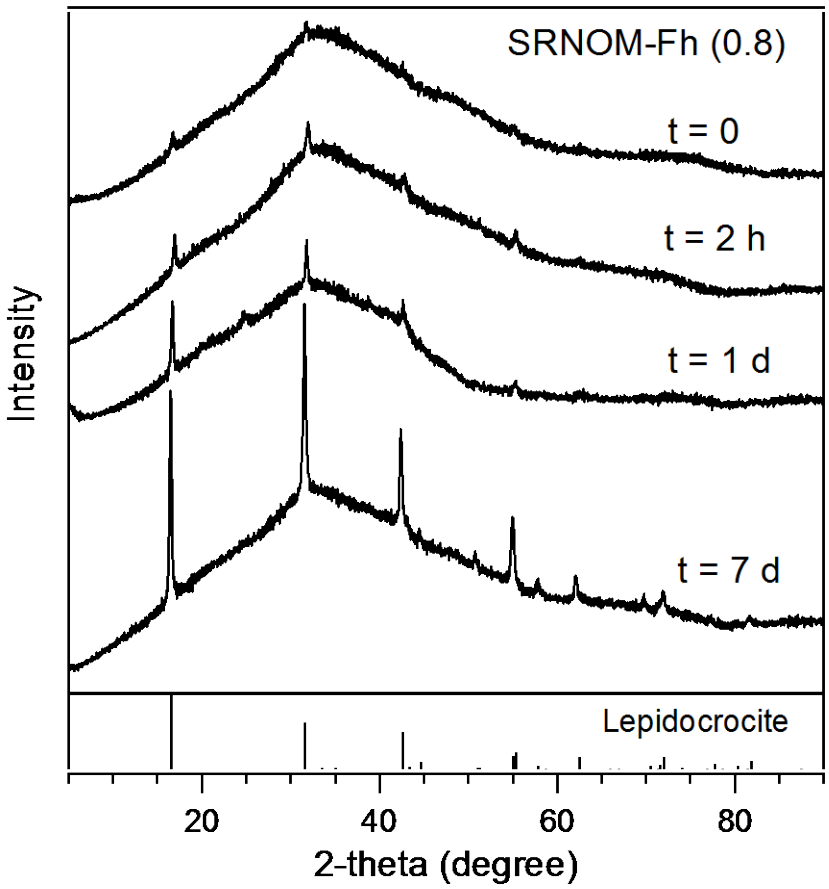

Figure 3.5. X-ray diffraction pattern of SRNOM-Fh (C/Fe = 0.8) coprecipitate reacted with 2 mM Fe(II) in 10 mM PIPES (pH 7.0) over 7 days. Solids were collected and characterized with 0.22 μm glass filter. The identical peaks of secondary Fe mineral are consistent with lepidocrocite.

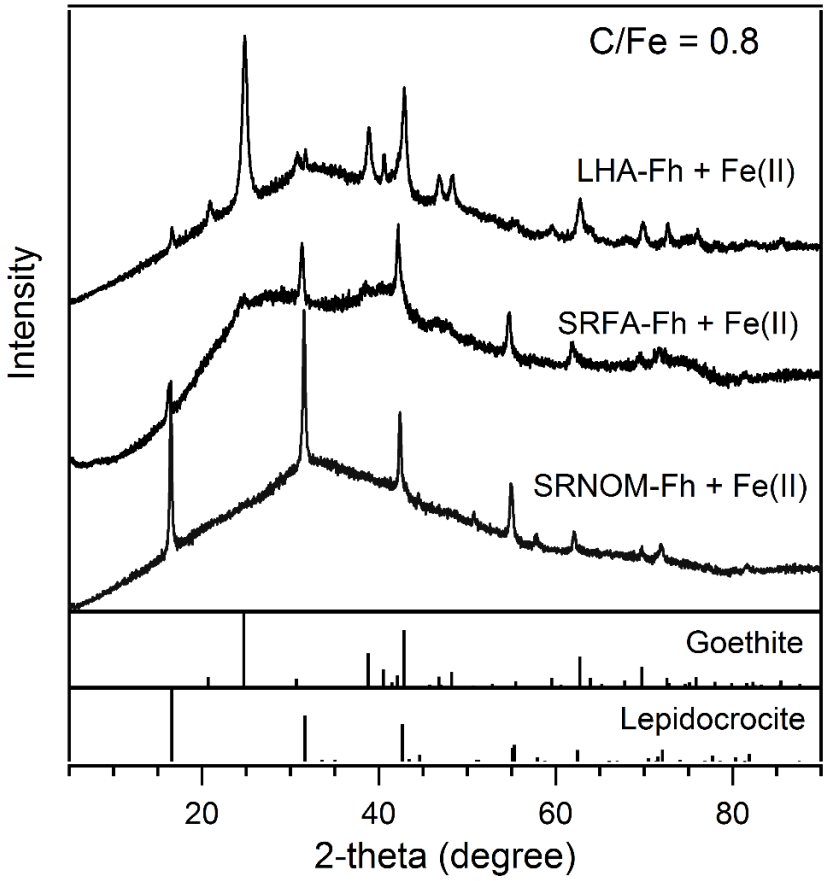

Figure 3.6. The X-ray diffraction pattern of different OM-Fh coprecipitates (C/Fe = 0.8) reacted with 2 mM Fe(II) over 7 days.

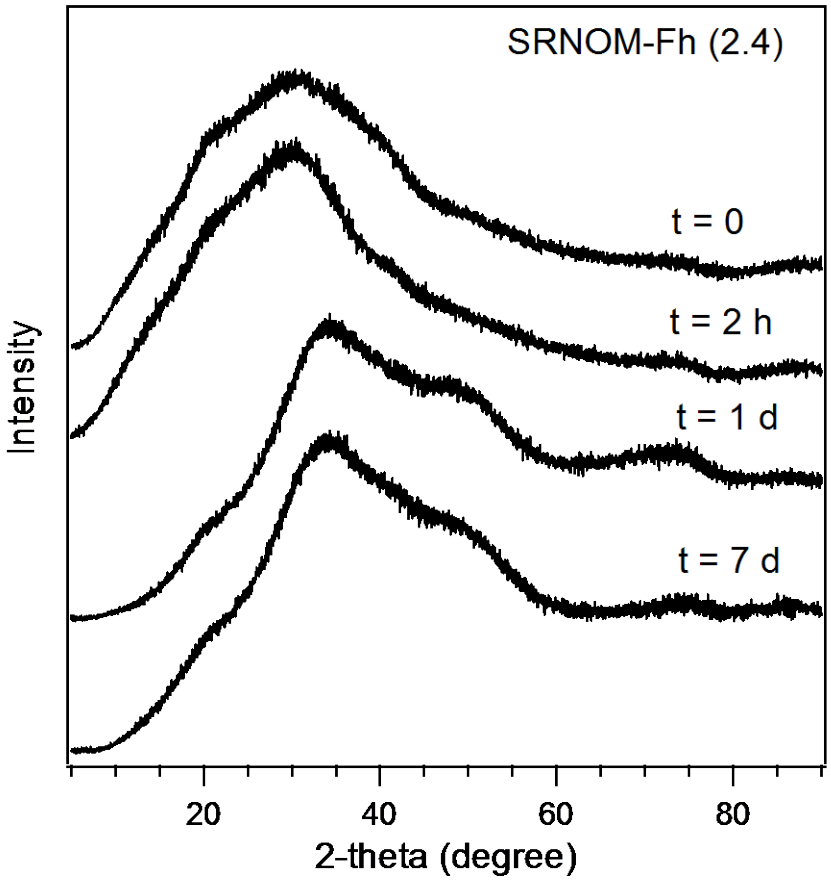

Figure 3.7. X-ray diffraction pattern of SRNOM-Fh (C/Fe = 2.4) coprecipitate reacted with 2 mM Fe(II) in 10 mM PIPES (pH 7.0) over 7 days. Solids were collected and characterized with 0.22 μm glass filter. No secondary Fe mineral was observed.

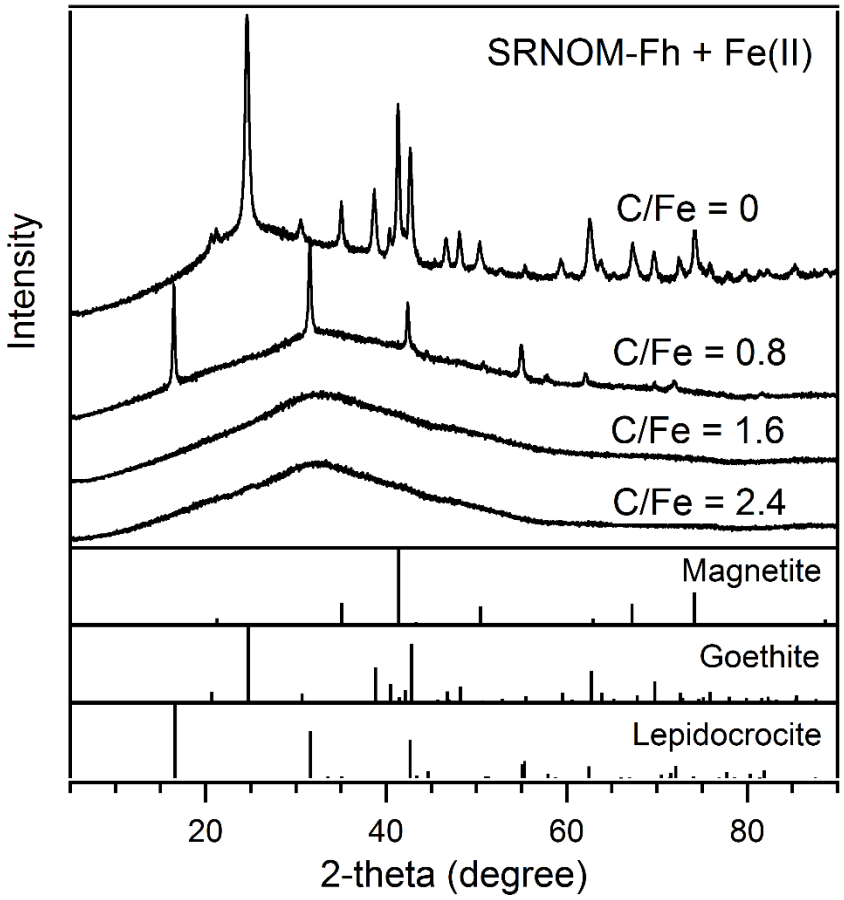

Figure 3.8. X-ray diffraction patter of LHA-Fh coprecipitate with different initial C/Fe ratio reacted with aqueous Fe(II) over 7 days.

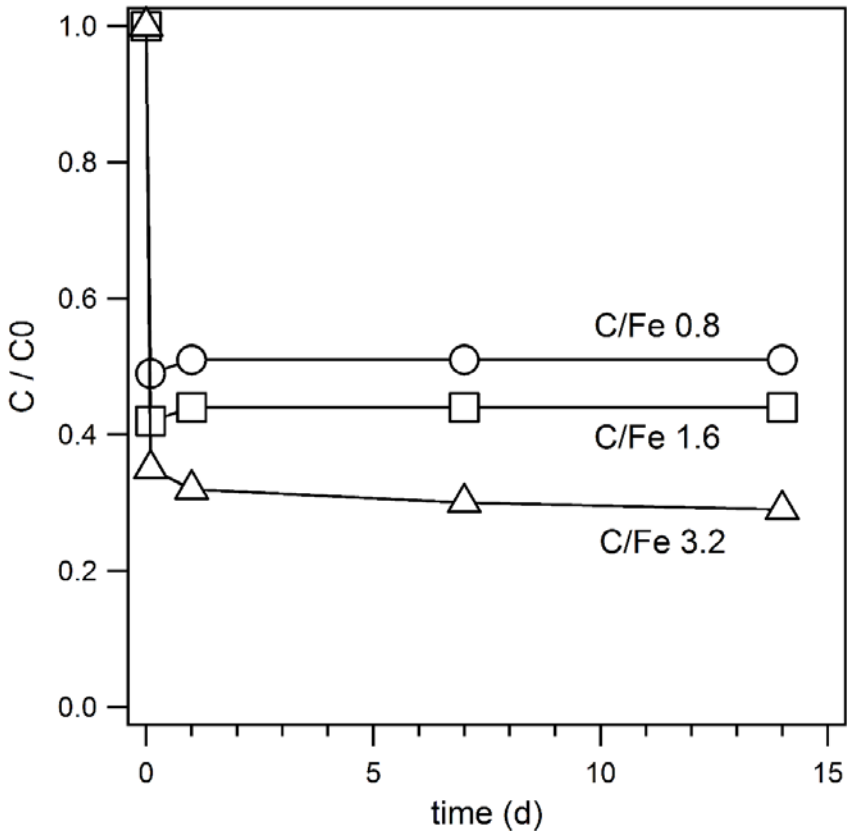

Figure 3.9. Fe(II) sorption by LHA-Fh coprecipitates with different C/Fe ratios. Condition: 2 mM Fe(II), 10 mM Fe(III) in the coprecipitates, 10 mM PIPES buffer, pH 7.0.

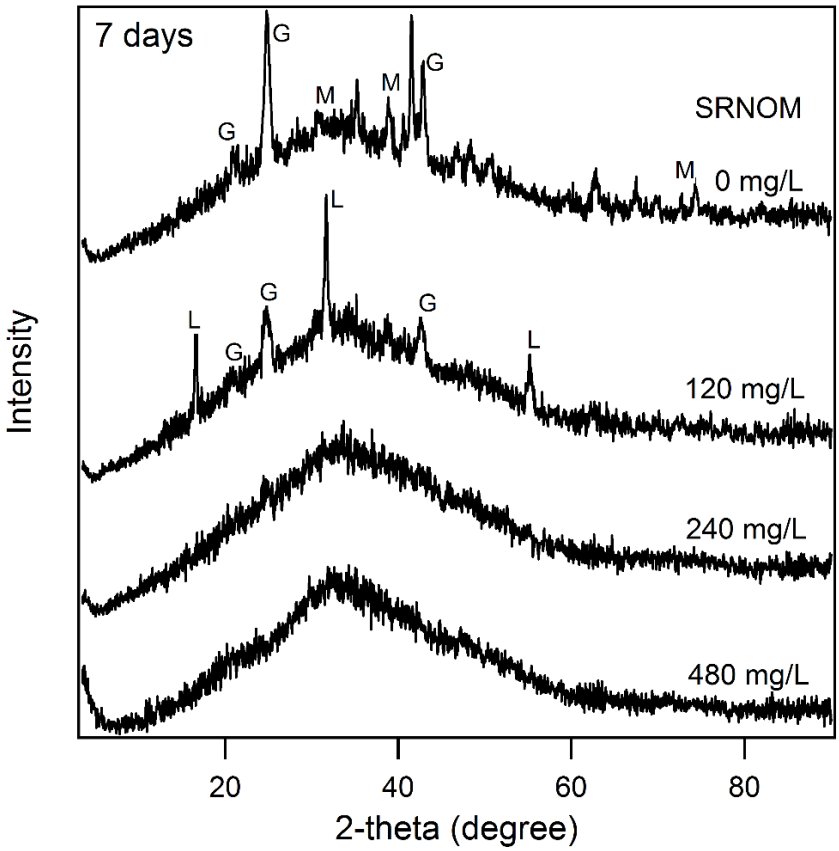

Figure 3.10. X-ray diffraction patter of wet ferrihydrite reacted with Fe(II) in the presence of adsorbed SRNOM. The ferrihydrite and dissolved SRNOM was equilibrated in solution (pH 7.0) overnight before the adding of aqueous Fe(II).

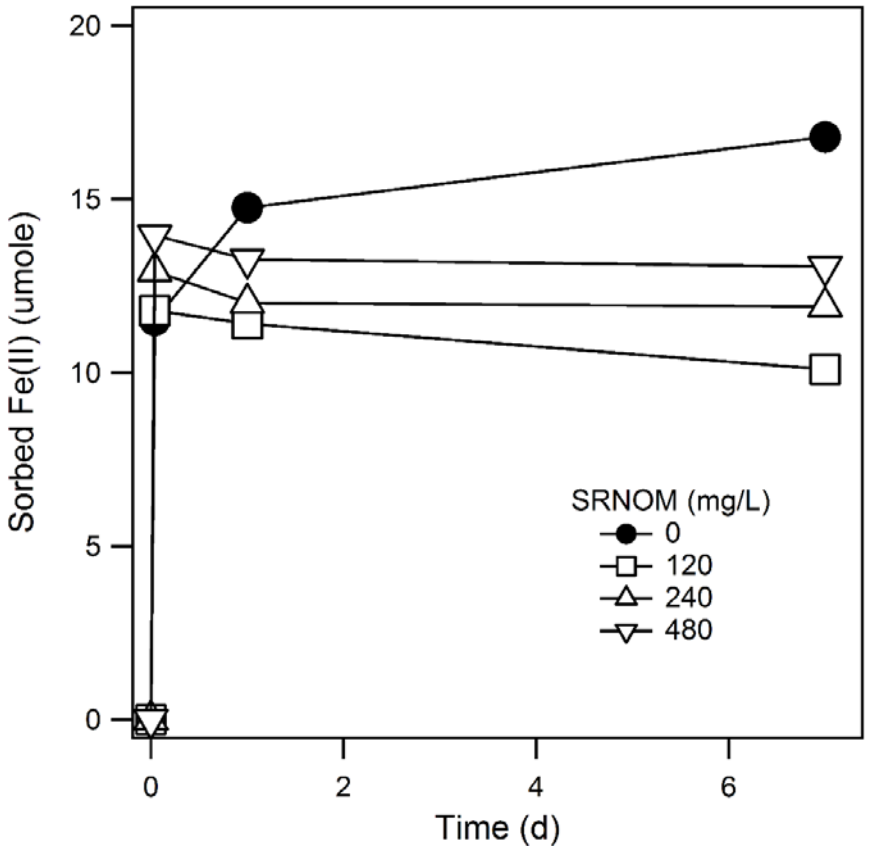

Figure 3.11. The amount of Fe(II) sorption by wet ferrihydrite in the presence of different concentrations of SRNOM. Sorbed Fe(II) was calculated with the initial Fe(II) concentration deducted by aqueous Fe(II) concentration at different time point.

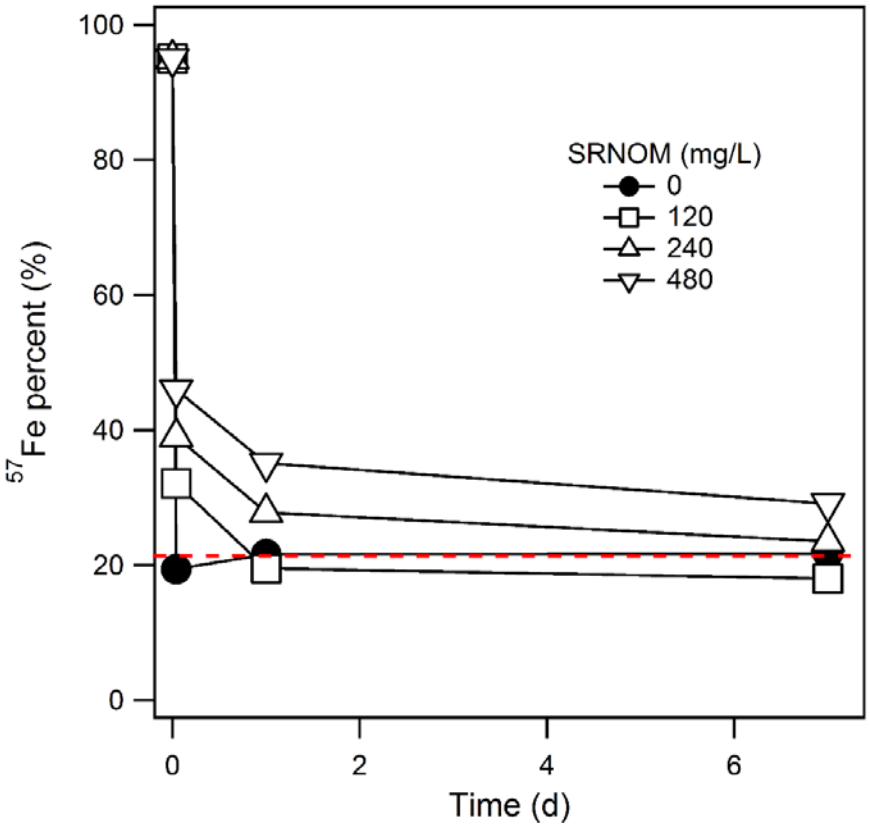

Figure 3.12. The ^{57}Fe percentage in aqueous Fe(II) during the reaction of wet ferrihydrite and Fe(II) in the presence of different amount of SRNOM. The red line indicates the equilibrium of ^{57}Fe percent calculated from initial Fe mass and isotope composition.

CHAPTER 4: NI DISTRIBUTION DURING FE(II)-CATALYZED FERRIHYDRITE TRANSFORMATION: INFLUENCE OF NATURAL ORGANIC MATTER

Abstract

Trace metals associated with iron (Fe) minerals have been shown to redistribute between the aqueous phase, mineral surface, and bulk minerals when reacted with Fe(II). Natural organic matter (NOM), often found with Fe minerals in soil, has been shown to impact Fe mineral transformations, especially Fe(II)-catalyzed ferrihydrite transformation. Little, however, is known about the effect of NOM on trace metal redistribution during Fe(II)-catalyzed ferrihydrite transformation. Here I investigated Ni redistribution during Fe(II)-catalyzed transformation of ferrihydrite associated with NOM. The acid extractable portion of Ni adsorbed on ferrihydrite decreased from 51% to 17% in the presence of Fe(II), potentially caused by incorporation of Ni into the structure of secondary Fe minerals formed during ferrihydrite transformation. Ferrihydrite coprecipitated with Suwannee River natural organic matter (SRNOM-Fh) did not transform but extensive Fe atom exchange between aqueous Fe(II) and structural Fe(III) in SRNOM-Fh coprecipitate still occurred. The acid extractable portion of Ni adsorbed on SRNOM-Fh coprecipitate decreased 5-9% in the presence of Fe(II), suggesting there was little change to Ni stability or Ni distribution. To evaluate the release of Ni, Ni pre-coprecipitated with ferrihydrite and Ni pre-coprecipitated with ferrihydrite and SRNOM were made. Increased Ni release was observed in the presence of Fe(II) during the beginning of reaction, but released Ni appeared to resorb as secondary Fe minerals formed. No significant Ni resorption or mineral transformation was observed in Ni-SRNOM-Fh coprecipitate where no secondary Fe minerals formed. Acid dissolution experiments indicate the residual Ni did not redistribute in Ni-SRNOM-Fh

coprecipitate after reaction with aqueous Fe(II), even though extensive Fe atom exchange between aqueous Fe(II) and structural Fe(III) in Ni-SRNOM-Fh coprecipitate was measured.

Introduction

In soils and sediments, aqueous Fe(II) and Fe(III) minerals often coexist (11, 154). The redox cycle between Fe(II) and Fe(III) is linked to cycling of other important elements, such as C, N, and P (51, 155-157). Fe isotope tracer studies have provided compelling evidence that Fe atom exchange occurs between aqueous Fe(II) and Fe minerals (26, 44, 124) and includes Fe(II) adsorption, electron injection into Fe(III) minerals, and Fe(III) reduction and release (44). The Fe mineral dissolution and reprecipitation during Fe atom exchange induces, in some cases, recrystallization of Fe minerals (52, 53).

Natural Fe minerals are normally formed under complex environments and often associated with trace metals either through coprecipitation or adsorption (158-161). Metal association with Fe minerals can alter the transport and fate of trace metals (162, 163) and the Fe redox cycle. Fe mineral recrystallization has been shown to impact the distribution and availability of associated trace metals (161, 164, 165). When aqueous Fe(II) is present it can increase Ni^{2+}, Cu^{2+} and Co^{2+} uptake by goethite and the incorporation of trace metals into goethite was proposed (28). XAS evidence of Ni incorporation into goethite and hematite during Fe(II)-catalyzed recrystallization was also reported by Frierdich et al. (134). Fe(II)-catalyzed recrystallization was also shown to result in the release of pre-incorporated Ni and Zn in goethite and hematite (161, 166). The amount of trace metal released from the Fe mineral is correlated with the extent of Fe atom exchange between aqueous Fe(II) and Fe mineral (167). More recently, some natural ligands and anions were found to inhibit the metal redistribution during Fe mineral recrystallization, but the extent of Fe atom exchange under these situations was not tracked (168, 169).

Unlike hematite and goethite, Fe(II)-catalyzed recrystallization of ferrihydrite results in transformation to secondary minerals (61, 170). The redistribution of associated metals during ferrihydrite transformation has been investigated (135, 150, 171, 172) and incorporation of metals into secondary Fe minerals has been suggested for Cu^{2+}, Zn^{2+}, Mn^{2+}, Co^{2+}, Sb^{5+}, As^{5+} and U^{6+} (172-177). Some studies have shown spectroscopic evidence that As^{5+} and Sb^{5+} that were adsorbed to ferrihydrite were structurally incorporated into goethite and hematite formed during the ferrihydrite transformation (173-175). The stability of metals significantly increased after incorporation and may have also altered the properties of the secondary Fe minerals (150, 172). For ferrihydrite, most of metal redistribution studies focused on the role of mineral transformation but have not investigated the role of Fe atom exchange as was explored in the goethite and hematite studies.

Similar to trace metals, NOM is frequently found associated with Fe minerals in soil and sediments (69, 148, 178). The associated NOM has been shown to inhibit ferrihydrite transformation (85, 86), but our recent study found that even without secondary Fe mineral, there is still extensive Fe atom exchange between aqueous Fe(II) and Fe(III) in NOM-Fh coprecipitate (87). The "hidden" Fe atom exchange (i.e., hidden in the sense that no secondary minerals form) raises the interesting question of how OM affects metal redistribution during ferrihydrite recrystallization. Currently, little is known about the fate of metals during the recrystallization of OM-Fh coprecipitate when secondary Fe minerals do not form. Here I investigate the effect of coprecipitate NOM on Ni redistribution during Fe(II)-catalyzed ferrihydrite transformation. Specifically, I investigated (i) Ni adsorption by pure ferrihydrite and SRNOM-Fh (C/Fe = 1.2) in the absence and presence of Fe(II); (ii) the release of pre-incorporated Ni in Ni-Fh coprecipitate and Ni-SRNOM-Fh coprecipitate in the absence and presence of Fe(II).

Materials and Methods

Synthesis and Characterization of Ferrihydrite Minerals

Pure 2-line ferrihydrite and SRNOM-Fh (C/Fe = 1.2) coprecipitate were synthesized as described in Chapter 2 and 3. Ferrihydrite and SRNOM-Fh (C/Fe = 1.2) with pre-incorporated Ni were also prepared following the method modified from the procedures described by Schwertmann and Cornell (95). Ferrihydrite with pre-incorporated Ni (denoted as Ni-Fh coprecipitate) was synthesized by slowly adding 1 M KOH into a 200 mL solution containing 25 mM ferric nitrate and 1.5 mM Ni(II) chloride (Ni/Fe ratio 0.06) until pH 7.5 was achieved in the solution. Vigorous stirring was applied during the whole process. The coprecipitate was washed with deionized water for 3 times and stored in glovebox as wet. Similar synthesis method was used to prepare Ni-SRNOM-Fh coprecipitate but with extra 188 mg SRNOM dissolved (C/Fe ratio 1.6) prior to the adding of 1 M KOH. All solids were used as wet and within 7 days after synthesis.

Ni Adsorption Experiments

Ni adsorption onto pure ferrihydrite and SRNOM-Fh (C/Fe = 1.2) coprecipitate were investigated in triplicate reactors. Each reactor consisted of 1 mM Ni(II), 10 mM PIPES buffer, and 10 mM NaCl (for ionic strength). In some reactors, 1 mM ^{57}Fe labelled Fe(II) (~97% of ^{57}Fe) was added. Pure ferrihydrite and SRNOM-Fh (C/Fe =1.2) were then added to achieve 10 mM Fe(III) in each reactor. The pH was adjusted back to pH 7.0 ± 0.05 using 1 M KOH. The reactors were rotated on end-over-end rotators while wrapped in aluminum foil. One mL aliquots at each time point were collected and centrifuged. The supernatant was filtered through 0.22 μm filters to collect aqueous samples. Solids were resuspended in 10 mM PIPPS at pH 3.0 for 20 minutes as a mild Ni extraction. After mild extraction, the residual solids were totally dissolved in 5 M HCl. Fe(II) and Ni concentration in each sample were measured separately with Phenanthroline method

and ICP-MS (87). One reactor at each time point was sacrificed and filtered through an 0.22 μm glass filter to prepare XRD samples.

Ni Release Experiments

The effect of Fe(II) on pre-incorporated Ni in Ni-Fh and Ni-SRNOM-Fh coprecipitate were probed by macroscopic Ni release, mild extraction and acid dissolution. The coprecipitates were set in 10 mM PIPES buffer at pH 7.0 with or without 1 mM Fe(II) labelled with ^{57}Fe. Similar methods as we used in Ni adsorption experiments were applied to collect and measure aqueous Ni(II), extracted Ni(II) and residual Ni(II). The reacted Ni-SRNOM-Fh coprecipitate was leached with 0.1 M HCl. The reacted solids under different conditions were collected by centrifugation and resuspended in 10 mL of 0.1 M HCl. One mL aliquots reacted over 2 min, 5 min, 15 min, 30 min, 60 min and overnight were collected and the concentration of dissolved Ni and Fe were measured as described above.

Results and Discussion

Ni(II) Adsorption by Ferrihydrite With and Without NOM

To explore the influence of NOM on Ni adsorption by ferrihydrite, I measured Ni adsorption to ferrihydrite and SRNOM-Fh coprecipitate with and without Fe(II) present. In the absence of Fe(II), around 80% of Ni(II) was sorbed to ferrihydrite within 1 day followed by a slower rate of removal plateauing about 85% Ni(II) adsorbed over 14 days (**Figure 4.1**). This behavior of initial rapid adsorption of Ni(II) at pH 7.0 followed by a slower adsorption is consistent with other studies investigating trace metals sorption by ferrihydrite (106, 179) where the formation of inner-sphere sorption complex is typically invoked to explain the fast removal and surface diffusion was invoked to explain the slow sorption process. In the presence of aqueous

Fe(II), a similar trend in Ni(II) sorption was observed with slightly more Ni sorbed (~5%) (**Figure 4.1**). The small effect of Fe(II) on Ni(II) adsorption to ferrihydrite is somewhat surprising as a significant amount of ferrihydrite was transformed to magnetite and goethite in the presence of Fe(II) (**Figure 4.2**).

Even more surprisingly, I found the presence of SRNOM in the SRNOM-Fh coprecipitates (C/Fe=1.2) also had minimal effect on the amount of Ni(II) adsorbed with between 85 and 88% Ni(II) adsorbed (**Figure 4.1**). Coprecipitated NOM extensively altered ferrihydrite properties as reported by us (87) and others (75, 96), and NOM itself may interact with metal cations (180, 181). Despite this, SRNOM had little effect on Ni adsorption to ferrihydrite. Note that no secondary Fe minerals were observed in SRNOM-Fh coprecipitate (C/Fe = 1.2) over 14 days which may explain why slightly less Ni(II) sorption occurred in the presence of Fe(II) on SRNOM-Fh as Fe(II) may have blocked Ni(II) sorption sites (**Figure 4.2**).

To further characterize Ni(II) associated with the ferrihydrite and SRNOM-Fh coprecipitate, a mild extraction at pH 3.0 was applied. No Fe(III) was detected in the extraction. The amount of residual Ni in the extracted solid was also measured by completely dissolving the solids. Ni distribution in ferrihydrite reactors with or without Fe(II) is shown in **Figure 4.3**. In the absence of Fe(II), the amount of extracted Ni(II) was constant but with an increase in residual Ni and a decrease in aqueous Ni. The presence of Fe(II) significantly decreased the amount of extracted Ni(II) (< 20% over 14 days) and increased the residual Ni(II) (> 60%), which is consistent with the formation of secondary Fe minerals. Around 90% of the initial added Ni was recovered during the sequential extraction. In SRNOM-Fh (C/Fe = 1.2) coprecipitate, the residual Ni was all around 40% with or without the presence of Fe(II) (**Figure 4.4**), suggesting that there was no significant change of Ni stability in SRNOM-Fh coprecipitate.

To better compare the effect of coprecipitated OM on the stability of associated Ni, the percent of extractable Ni in solid-bound Ni (extracted + residual) was calculated and compared in **Figure 4.5**. For both ferrihydrite and SRNOM-Fh with and without Fe(II), a decrease of extractable Ni over time was observed, which may cause by the diffusion of adsorbed Ni(II) into the inner structure of the ferrihydrite (182). In addition, aggregation of ferrihydrite and SRNOM-Fh coprecipitate in 10 mM PIPES buffer may also contribute to the increased stability of Ni(II) to some extent (183). While the amount of extractable Ni(II) decreased over time for both ferrihydrite and SRNOM-Fh, there were other marked differences in the effect of Fe(II) (**Figure 4.5**). With ferrihydrite alone, there was a large effect of Fe(II) with significantly smaller fraction of the solid Ni(II) extracted in the presence of Fe(II) (17% compared to 51% without Fe(II)). The obviously improved stability of Ni was related to the structural incorporation of Ni into secondary Fe minerals during ferrihydrite transformation (150, 184, 185).

Whereas with SRNOM-Fh (C/Fe = 1.2), the transformation of ferrihydrite was inhibited by coprecipitated SRNOM, but the presence of Fe(II) still decreased the fraction of Ni extracted from the solid (5-9%), indicates increased Ni stability in the solids by the presence of Fe(II). It is consistent with what Flynn et al. observed in goethite and hematite, where 9-10 % of Ni incorporated by the Fe(II)-catalyzed recrystallization of Fe minerals (134, 167-169). Based on our earlier study (87), Fe atom exchange between aqueous Fe(II) and ferrihydrite may still occur in the absence of secondary Fe minerals, and may redistribute Ni during Fe dissolution and reprecipitation process (or recrystallization, similar to the situation in goethite or hematite).

To confirm that Fe atom exchange between aqueous Fe(II) and SRNOM-Fh (C/Fe=1.2) still occurred in the presence of Ni(II), the same ^{57}Fe(II) tracer was used to track Fe atom movement during the reaction. The Fe(II) mass in aqueous phase, extractable pool and the residual

solid phase was tracked over time, around 90-105% of initial added Fe(II) was recovered (**Figure 4.6**). The percentage of ^{57}Fe in aqueous Fe(II) dropped from 97% to 25% over one hour accompanied by a rapid increase in solid Fe (from 2.3% to 10%). The initial rapid Fe isotope mixing was followed by a further mixing over 14 days reaction, and the Fe isotope composition in the aqueous and solid Fe phase was finally approached the complete isotopic mixing (**Figure 4.7**). Since we don't known if Fe isotope was homogeneously distributed in the solid phase, we chose not to estimate the percent of atom exchange based on the homogenous model (53, 54, 87), but certainly there was extensive Fe isotope mixing between aqueous Fe and solid Fe in the presence of Ni. Our data here showed SRNOM-Fh (C/Fe = 1.2) coprecipitated was recrystallized and would redistribute the adsorbed Ni as others suggested (161, 167). That will explain the increased Ni stability we observed through acid extraction method. But note that the redistribution of Ni caused by Fe atom exchange in SRNOM-Fh coprecipitate (no secondary mineral) was less significant than the situation in ferrihydrite where mineral transformation occurred.

In SRNOM-Fh coprecipitate, SRNOM itself may associate with Ni and impact its fate. Unfortunately, we do not have any data to explore on the distribution of Ni between SRNOM and ferrihydrite. A study has reported more than 70% of Pb(II) in OM-Fh coprecipitate bonded with ferrihydrite(186), but we do not know if it applies to our experiment as Ni and Pb behave quite differently during their interaction with Fe minerals (28, 172). More efforts are needed to figure out the Ni distribution between SRNOM and ferrihydrite, then we can better discuss the effect of NOM on the fate of Ni.

Ni(II) Release From Ni-Fh and Ni-SRNOM-Fh Coprecipitate With and Without Fe(II)

Trace metals can associate with Fe minerals not only through adsorption but also coprecipitation. To explore the fate of pre-incorporated Ni in ferrihydrite with or without NOM

under reducing environment, ferrihydrite coprecipitated with Ni(II) (denoted as Ni-Fh) and ferrihydrite coprecipitated with Ni(II) and SRNOM (denoted as Ni-SRNOM-Fh) were synthesized and reacted with aqueous Fe(II). Same initial Ni/Fe was set to synthesis two coprecipitates, but higher final Ni/Fe ratio was measured in Ni-SRNOM-Fh coprecipitate (0.061) than Ni-Fh coprecipitate (0.046). The presence of SRNOM increased Ni uptake by coprecipitation, indicating part of Ni in the coprecipitate may associate with SRNOM. XRD pattern and Mössbauer spectroscopy showed ferrihydrite is the only Fe mineral in Ni-Fh and Ni-SRNOM-Fh coprecipitates. At 25 K and 14 K, ferrihydrite was better magnetically ordered than Ni-Fh coprecipitate, implying the pre-incorporated Ni decreased Fe-Fe interaction (**Figure 4.8**). But its influence was less obvious compared to SRNOM. The Mössbauer spectroscopy of different solids at 14 K were fitted with Recoil and got the hyperfine field distribution. The pre-incorporated Ni slightly changed the hyperfine field distribution in ferrihydrite, and it was negligible compared to the influence of coprecipitated SRNOM (**Figure 4.9**).

In the absence of Fe(II), there was around 2.2% Ni(II) released from Ni-Fh coprecipitate and 2.4% from Ni-SRNOM-Fh coprecipitate (**Figure 4.10**). After the adding of Fe(II) over 2 hours, increased Ni(II) release was observed in both Ni-Fh and Ni-SRNOM-Fh coprecipitates. After a longer reaction time, a quick drop of aqueous Ni(II) concentration was observed in Ni-Fh coprecipitate, while the aqueous Ni(II) in Ni-SRNOM-Fh reactor was stabilized around 45 μM. Note the released Ni(II) only account 6-8% of pre-incorporated Ni in the Ni-SRNOM-Fh coprecipitate, which is very consistent with the observation in goethite with pre-incorporated Ni (~8% Ni release was reported) (166). In the presence of Fe(II), the situation in Ni-Fh system and Ni-SRNOM-Fh system were quite different. Goethite and magnetite was identified in Ni-Fh coprecipitate after reaction with Fe(II), while no secondary Fe mineral was found in Ni-SRNOM-

Fh coprecipitate (**Figure 4.11)**. The Fe(II)-catalyzed Ni-Fh transformation was trigger by the Fe(III) dissolution and reprecipitation process, during which the pre-incorporated Ni can be released by Fe dissolution (62, 135, 187). But with the precipitation of new Fe minerals, part of the released Ni would be incorporated into the structure or resorbed to the surface of secondary Fe minerals (150, 188, 189).

To better understand the Ni distribution in the solid, a mild extraction at pH 3.0 was applied to all solids reacted with or without Fe(II), and residual Ni in the extracted solid was also measured. For Ni-Fh coprecipitate, not surprisingly, the presence of Fe(II) decreased the amount of extracted Ni accompanied with increasing in residual Ni (**Figure 4.12**). For better comparing, the extractable portion of pre-incorporated Ni was calculated and plotted in **Figure 4.13**. The extraction method used here can extract around 50% of pre-incorporated Ni from the Ni-Fh coprecipitate aged in buffer over 2 hours and further decrease to around 40%. The improvement of Ni stability by aging may due to the aggregation of Ni-Fh coprecipitate in buffer or the further Ni diffusion as we discussed before. The presence of Fe(II) induced the transformation of ferrihydrite and significantly decreased the fraction of extractable Ni in the solid phase, which is consistent with structural incorporation of heavy metals during the formation of secondary Fe minerals (150, 185, 189).

While in Ni-SRNOM-Fh coprecipitate, the presence of Fe(II) did not transform ferrihydrite into secondary Fe minerals. Significant Fe atom exchanged between aqueous Fe(II) and the structural Fe(III) in Ni-SRNOM-Fh coprecipitate still occurred based on our ^{57}Fe(II) tracer experiment (**Figure 4.14**). This extensive Fe atom exchange may explain the partial release of pre-incorporated Ni from Ni-SRNOM-Fh coprecipitate (167, 169). The amount of extractable and residual Ni, however, was not changed measurably, implies the residual Ni was not redistributed

(**Figure 4.15**). To further investigate the Ni distribution in Ni-SRNOM-Fh with or without Fe(II) treatment, acid dissolution was applied to dissolve the whole solids while measuring the Ni release. After aging in PIPES buffer with or without Fe(II) over 14 days, there is no measurable difference of Ni distribution in the reacted solids (**Figure 4.16**). The extensive Fe atom exchange between aqueous Fe(II) and Fe(III) in Ni-SRNOM-Fh coprecipitate can partially release pre-incorporated Ni but will not redistribute the residual Ni in the solid. It is challenging to explain this observation without known the binding of Ni between SRNOM and ferrihydrite, the characterization of X-ray absorption spectroscopy would be extremely beneficial to interpret our macroscopy observations.

Environmental Implications

This study shows some interesting results about Ni sorption by ferrihydrite in the presence of NOM and Fe(II) and has important implications to predict the stability of trace metals under complex environment. During ferrihydrite transformation, adsorbed trace metal can incorporate into the structural of secondary Fe minerals. The presence of NOM inhibited ferrihydrite transformation and limited the incorporation of adsorbed trace metal. Even though we observed the Fe atom exchange between aqueous Fe(II) and Fe minerals in the presence of NOM may partially incorporate adsorbed metals, but it is less significant compared to mineral transformation. When NOM, trace metal and Fe mineral coprecipitate together, the presence of Fe(II) can partially release the pre-incorporated Ni, while the residual Ni was not measurably redistributed. Under redox dynamic environments, this study indicates the presence of NOM will compromise the stability of heavy metals associated with poor crystalized Fe minerals by inhibiting Fe mineral transformation and structural metal incorporation during the process.

Table 4.1. Ni mass distribution in ferrihydrite reactors with or without Fe(II) over time.

Time (d)	Aqueous Ni (mM)		Extracted Ni (mM)		Residual Ni (mM)		Sum (mM)		Recovery Percent (%)	
	no Fe(II)	with Fe(II)	no Fe(II)	with Fe(II)	no Fe(II)	with Fe(II)	no Fe(II)	with Fe(II)	no Fe(II)	with Fe(II)
0	1.01(0.004)	1.01(0.004)	-	-	-	-	1.01	1.01	100	100
0.08	0.368(0.022)	0.295(0.018)	0.462(0.013)	0.350(0.002)	0.082(0.001)	0.233(0.009)	0.912	0.878	90.3	86.5
1	0.205(0.01)	0.161(0.014)	0.468(0.013)	0.248(0.003)	0.217(0.005)	0.487(0.007)	0.889	0.895	88.0	88.2
7	0.170(0.012)	0.119(0.006)	0.456(0.005)	0.140(0.008)	0.350(0.007)	0.663(0.042	0.975	0.923	96.6	90.9
14	0.149(0.01)	0.107(0.008)	0.419(0.004)	0.141(0.019)	0.398(0.003)	0.677(0.013)	0.966	0.924	95.6	91.1

Table 4.2. Ni mass distribution in SRNOM-Fh coprecipitate reactors with or without Fe(II) over time.

Time (d)	Aqueous Ni (mM)		Extracted Ni (mM)		Residual Ni (mM)		Sum (mM)		Recovery Percent (%)	
	no Fe(II)	with Fe(II)	no Fe(II)	with Fe(II)	no Fe(II)	with Fe(II)	no Fe(II)	with Fe(II)	no Fe(II)	with Fe(II)
0	1.02(0.008)	0.99(0.019)	-	-	-	-	1.02	0.99	100	100
0.08	0.333(0.025)	0.316(0.021)	0.508(0.011)	0.464(0.014)	0.086(0.005)	0.128(0.009)	0.927	0.908	90.9	91.7
1	0.178(0.013)	0.201(0.019)	0.482(0.003)	0.407(0.014)	0.214(0.004)	0.270(0.014)	0.874	0.878	85.7	88.7
7	0.128(0.012)	0.167(0.013)	0.351(0.003)	0.302(0.058)	0.370(0.021)	0.417(0.082)	0.849	0.886	83.2	89.5
14	0.119(0.008)	0.161(0.012)	0.390(0.005)	0.337(0.014)	0.367(0.006)	0.380(0.011)	0.876	0.878	85.9	88.7

Table 4.3. Ni mass distribution in Ni-Fh coprecipitate reactors with or without Fe(II) over time.

Time (d)	Aqueous Ni (mM)		Extracted Ni (mM)		Residual Ni (mM)		Sum (mM)		Recovery Percent (%)	
	no Fe(II)	with Fe(II)	no Fe(II)	with Fe(II)	no Fe(II)	with Fe(II)	no Fe(II)	with Fe(II)	no Fe(II)	with Fe(II)
0	0	0	-	-	-	-	0.460	0.460	100	100
0.08	0.011(0.001)	0.055(0.006)	0.219(0.002)	0.146(0.002)	0.189(0.004)	0.184(0.001)	0.419	0.385	89.6	83.8
1	0.009(0.001)	0.020(0.006)	0.148(0.001)	0.051(0.002)	0.258(0.004)	0.355(0.002)	0.416	0.425	90.4	92.5
7	0.01(0.002)	0.009(0.002)	0.153(0.003)	0.026(0.003)	0.276(0.005)	0.373(0.005)	0.439	0.408	95.5	88.6
14	0.01(0.001)	0.007(0.001)	0.147(0.001)	0.018(0.003)	0.271(0.01)	0.367(0.031)	0.428	0.392	93.1	85.2

Table 4.4. Ni mass distribution in Ni-SRNOM-Fh coprecipitate reactors with or without Fe(II) over time.

Time (d)	Aqueous Ni (mM)		Extracted Ni (mM)		Residual Ni (mM)		Sum (mM)		Recovery Percent (%)	
	no Fe(II)	with Fe(II)	no Fe(II)	with Fe(II)	no Fe(II)	with Fe(II)	no Fe(II)	with Fe(II)	no Fe(II)	with Fe(II)
0	0	0	-	-	-	-	0.62	0.62	100	100
0.08	0.015(0.006)	0.045(0.003)	0.29(0.004)	0.273(0.007)	0.263(0.014)	0.258(0.004)	0.567	0.575	91.5	92.8
1	0.015(0.002)	0.042(0.002)	0.283(0.002)	0.264(0.002)	0.268(0.005)	0.268(0.005)	0.566	0.574	91.3	92.5
7	0.015(0.001)	0.036(0.002)	0.250(0.002)	0.235(0.002)	0.283(0.013)	0.282(0.003)	0.548	0.552	88.4	89.0
14	0.016(0.001)	0.038(0.002)	0.257(0.003)	0.240(0.002)	0.309(0.010)	0.305(0.000)	0.584	0.583	94.2	94.0

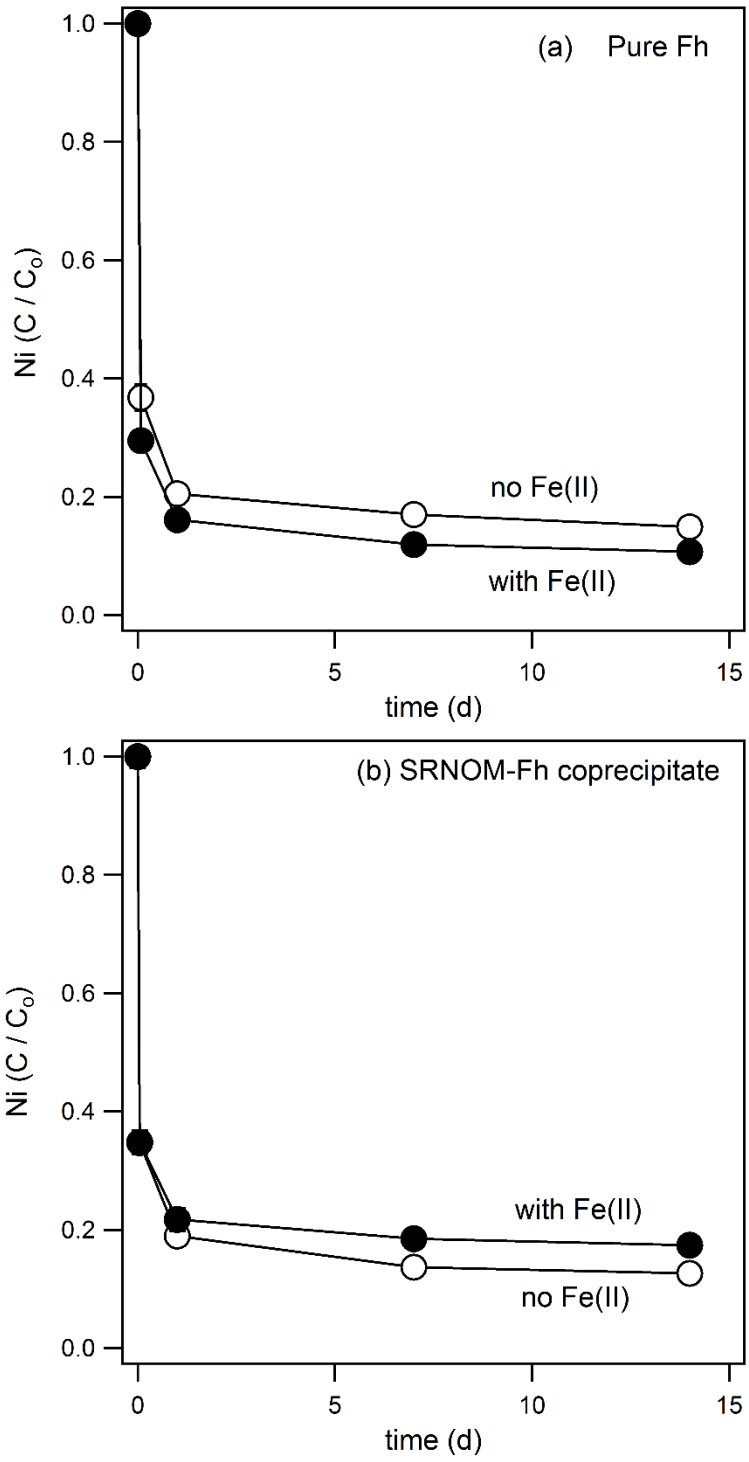

Figure 4.1. Ni(II) adsorption by (a) pure ferrihydrite and (b) SRNOM-Fh (C/Fe =1.2) with or without Fe(II) overtime. Experimental conditions: 1 mM Ni(II), 10 mM Fe(III) from Fh, 10 mM PIPES (pH 7.0), 1 mM Fe(II). Each point represents the average of triplicate samples.

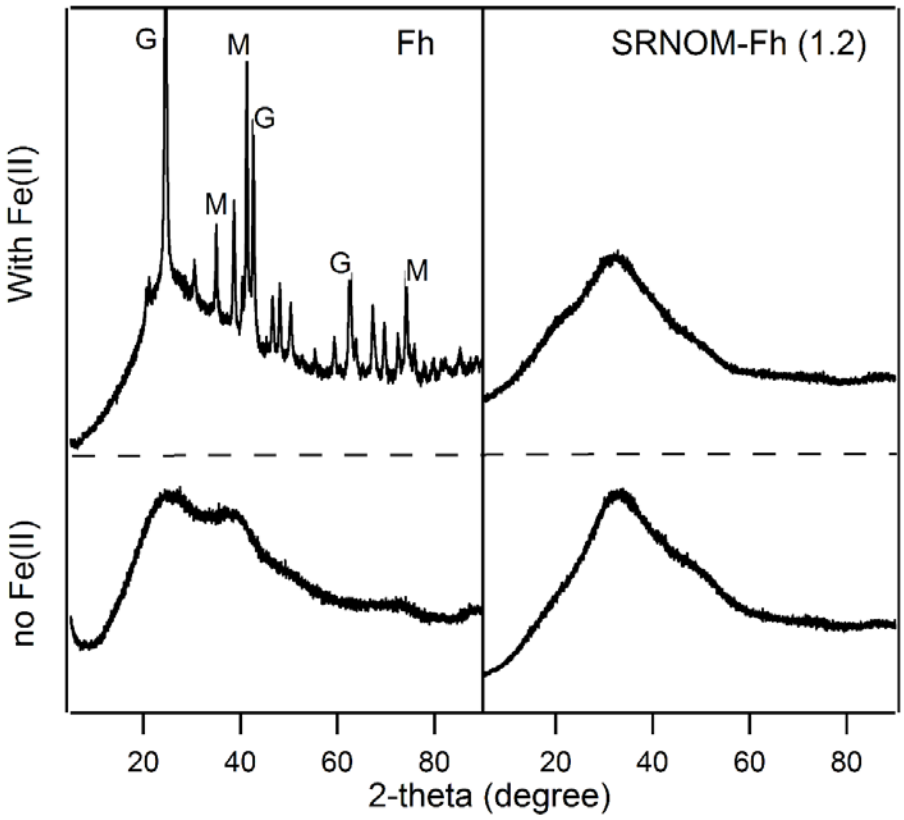

Figure 4.2. X-ray diffraction pattern of ferrihydrite and SRNOM-Fh (C/Fe=1.2) reacted with or without Fe(II) in the presence of adsorbed Ni after 14 days. Note: G = goethite, M = magnetite.

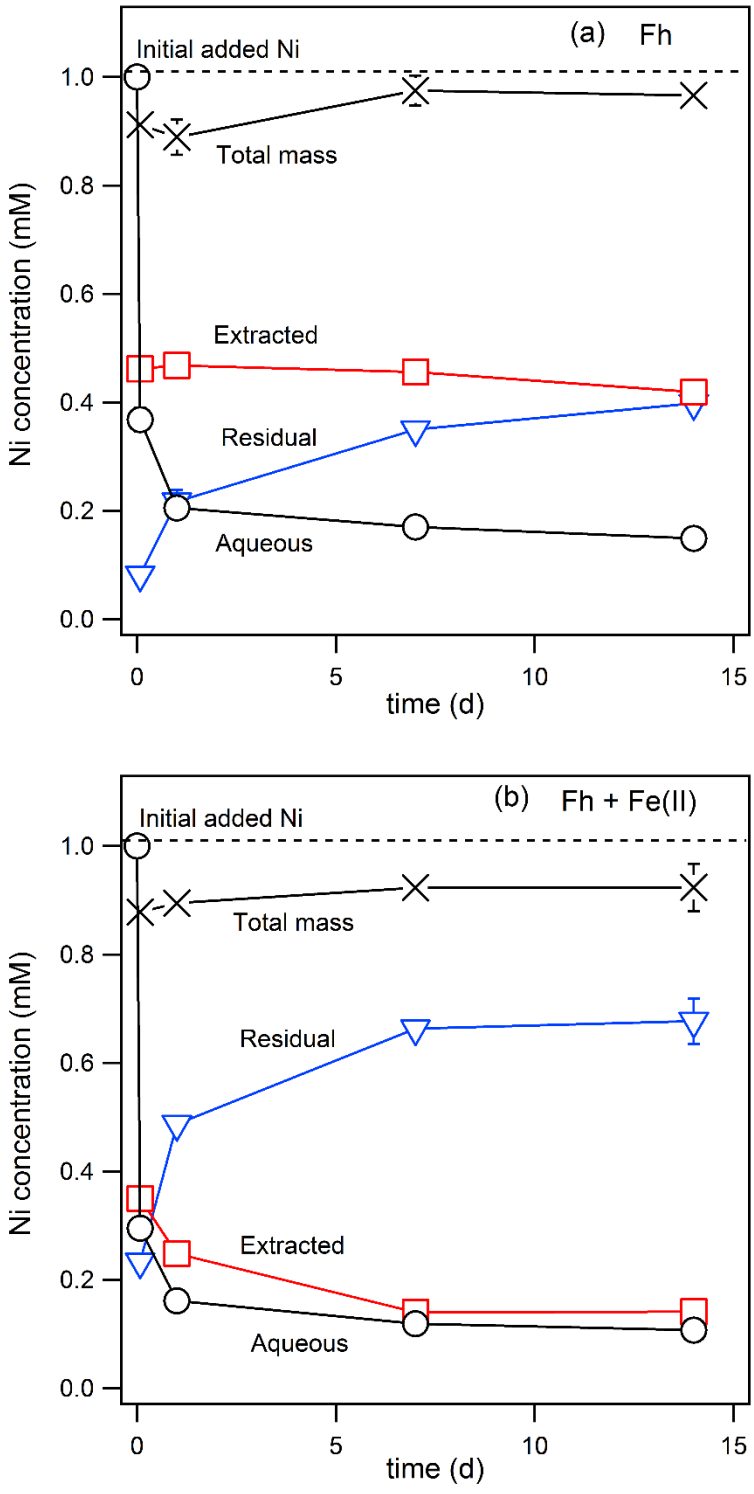

Figure 4.3. Sequential extraction of Ni in ferrihydrite reactors (a) without Fe(II) and (b) with Fe(II) over time. Same experimental conditions as listed in Figure 4.1. Data are listed in Table 4.1.

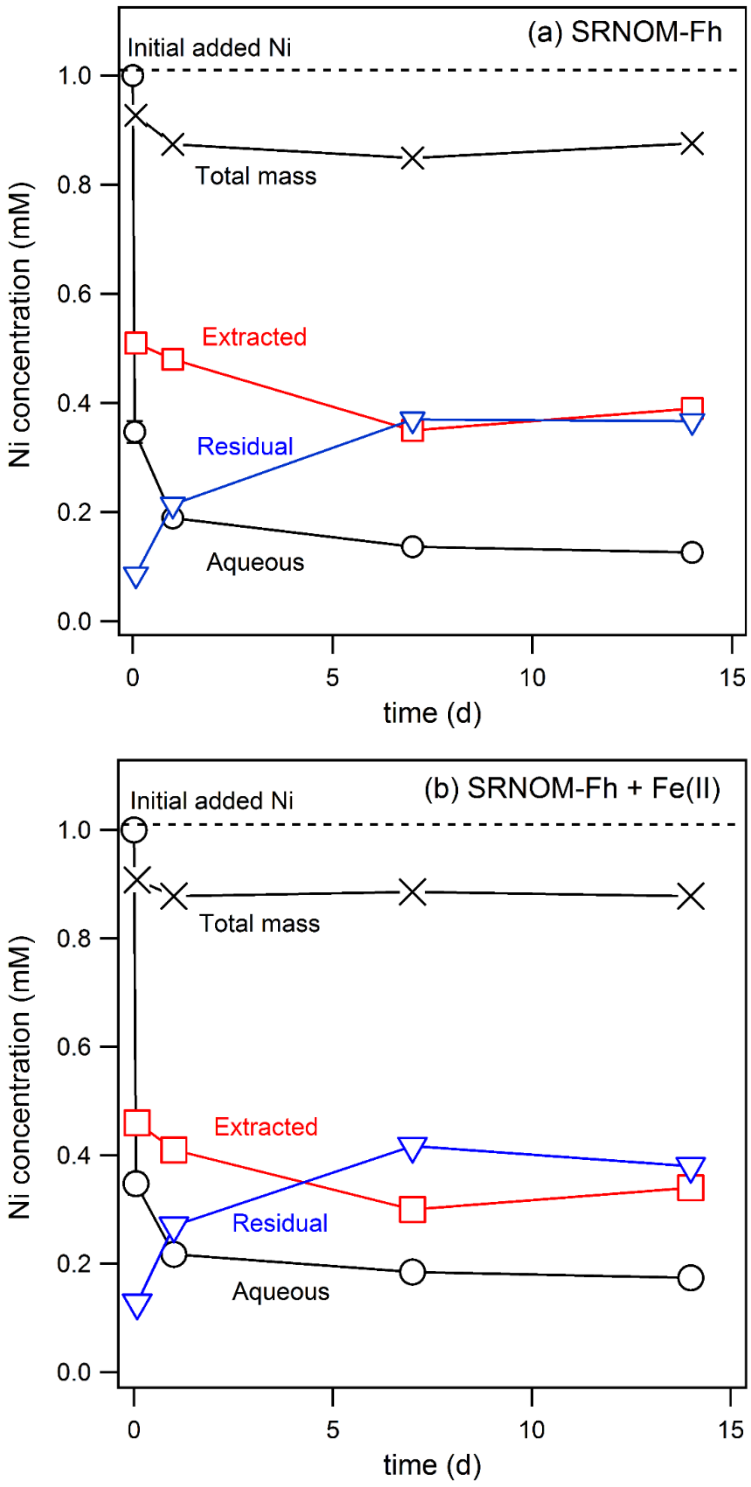

Figure 4.4. Sequential extraction of Ni in SRNOM-Fh (C/Fe=1.2) coprecipitate reactors (a) without Fe(II) and (b) with Fe(II) over time. Same experimental conditions as listed in Figure 4.1. Data are listed in Table 4.2.

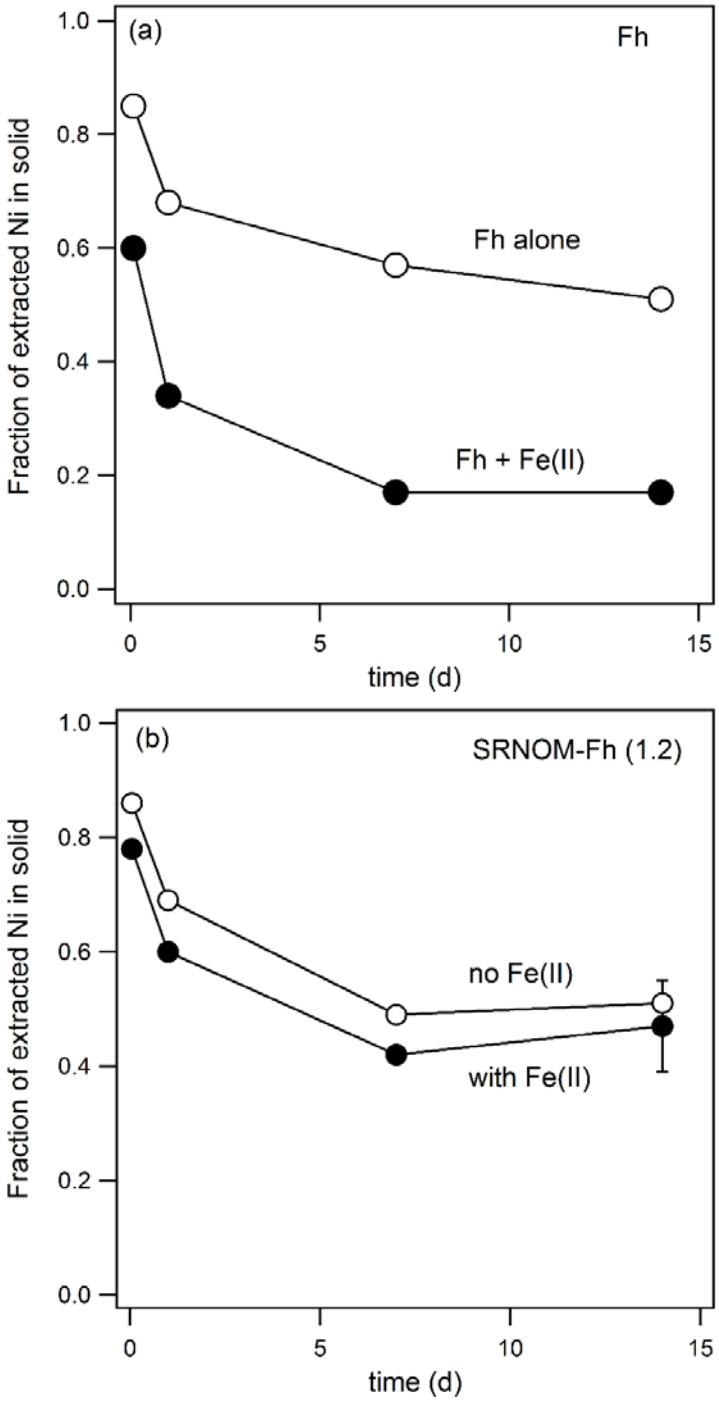

Figure 4.5. Fraction of extracted Ni in overall Ni associated in solid phase. (a) Ferrihydrite with or without Fe(II) over time; (b) SRNOM-Fh (C/Fe = 1.2) with or without Fe(II) over time. I measured the extracted Ni by PIPPS solution at pH 3.0 over 20 minutes, and the residual Ni in the extracted solid. The fraction was calculated with extracted Ni divided by the sum of extracted Ni and residual Ni.

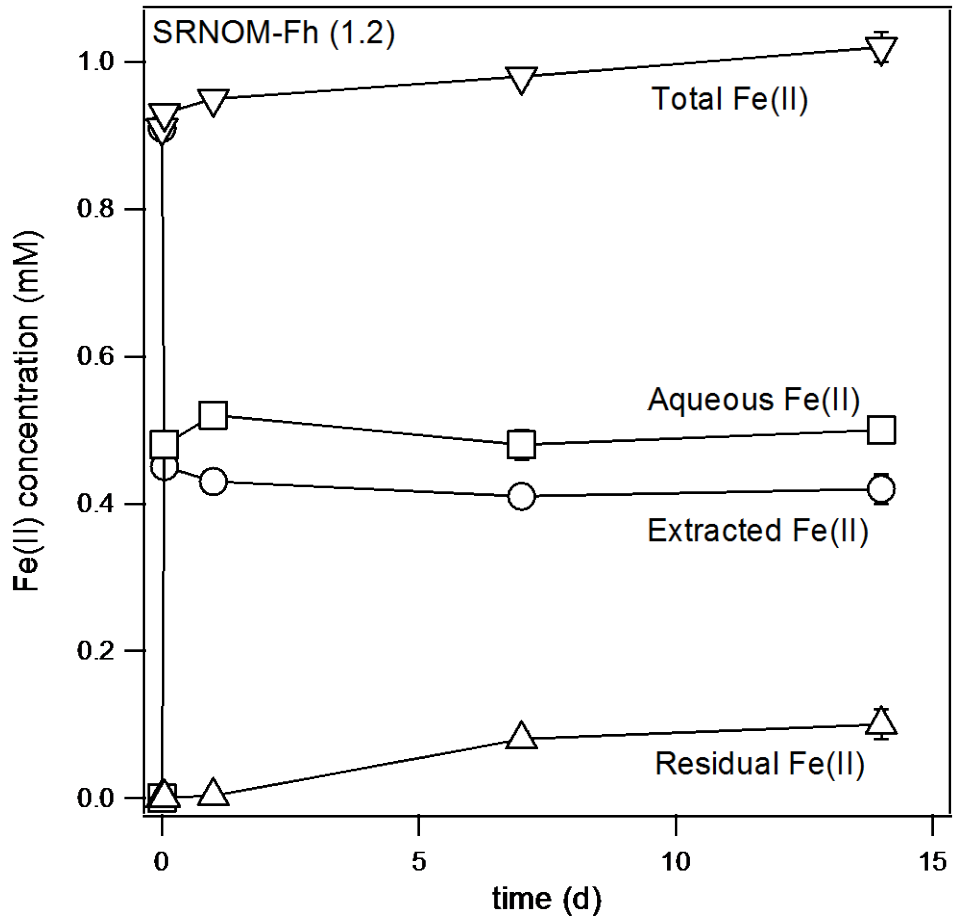

Figure 4.6. Fe mass distribution between different phase in the reactor of SRNOM-Fh (C/Fe = 1.2) with 1 mM ^{57}Fe(II). Extracted Fe(II) indicates the amount of Fe(II) extracted at 10 mM PIPPS solution (pH 3.0).

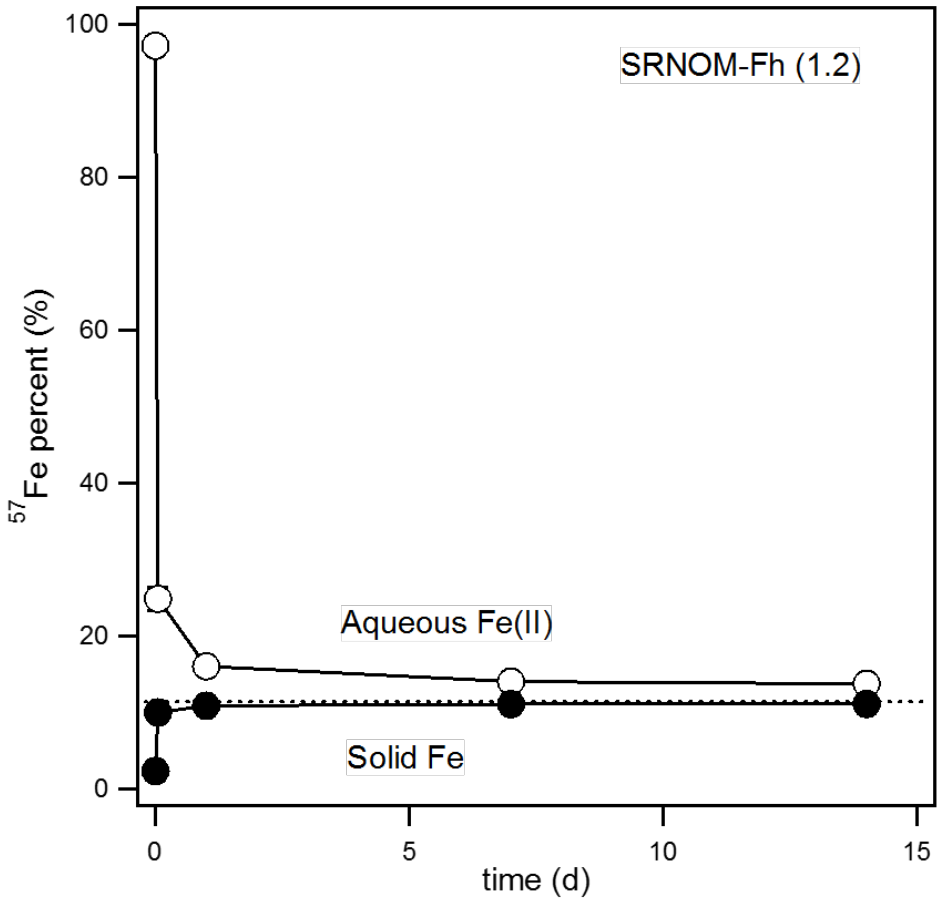

Figure 4.7. Fe isotope mixing process between aqueous Fe(II) and SRNOM-Fh in the presence of Ni(II), same condition as Figure 4.1.

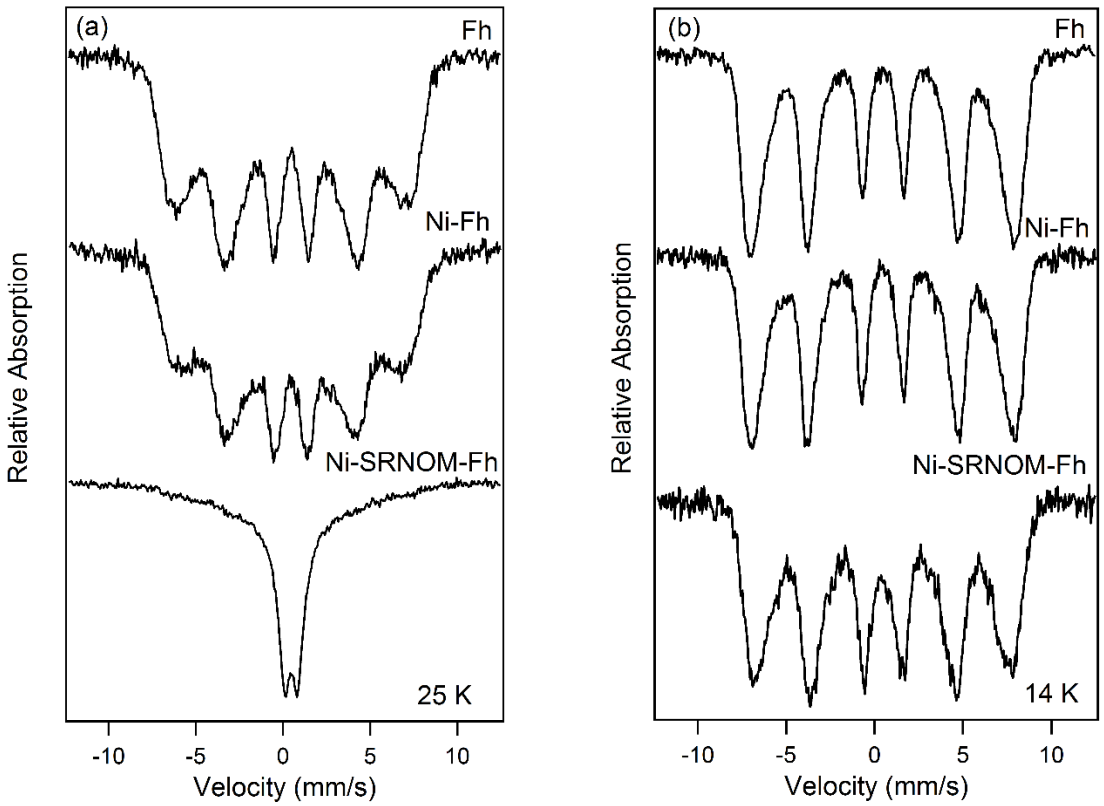

Figure 4.8. The Mössbauer spectroscopy of ferrihydrite, Ni-Fh coprecipitate and Ni-SRNOM-Fh coprecipitate at (a) 25 K; (b) 14 K.

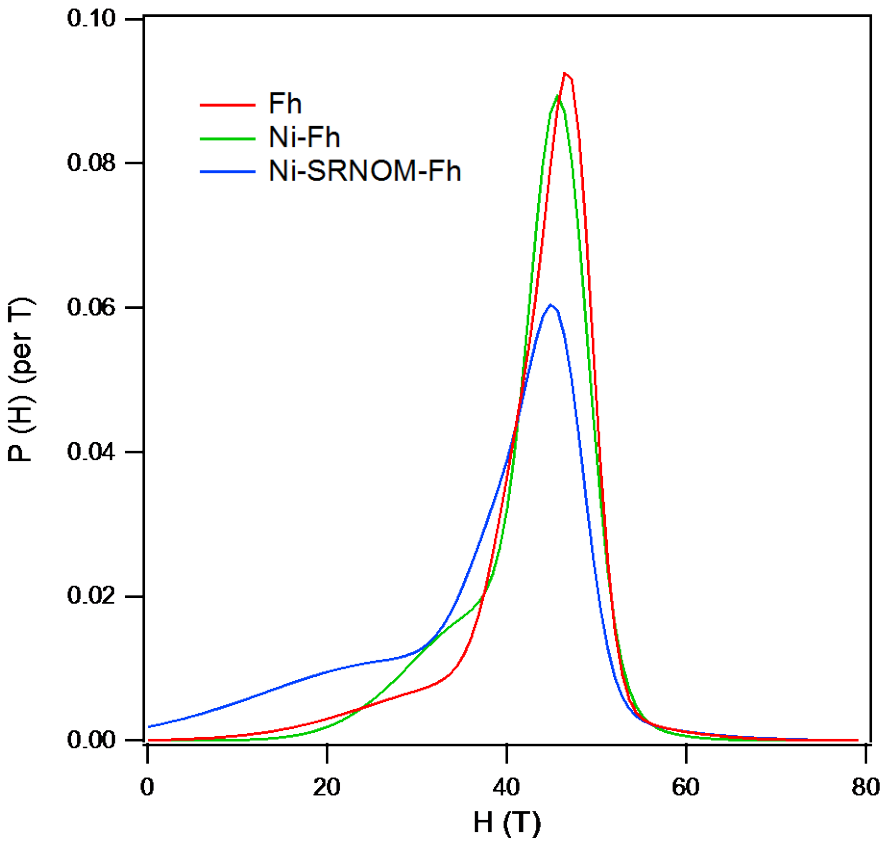

Figure 4.9. Hyper-fine field distribution in wet ferrihydrite, Ni-Fh coprecipitate and Ni-SRNOM-Fh coprecipitate at 14 K.

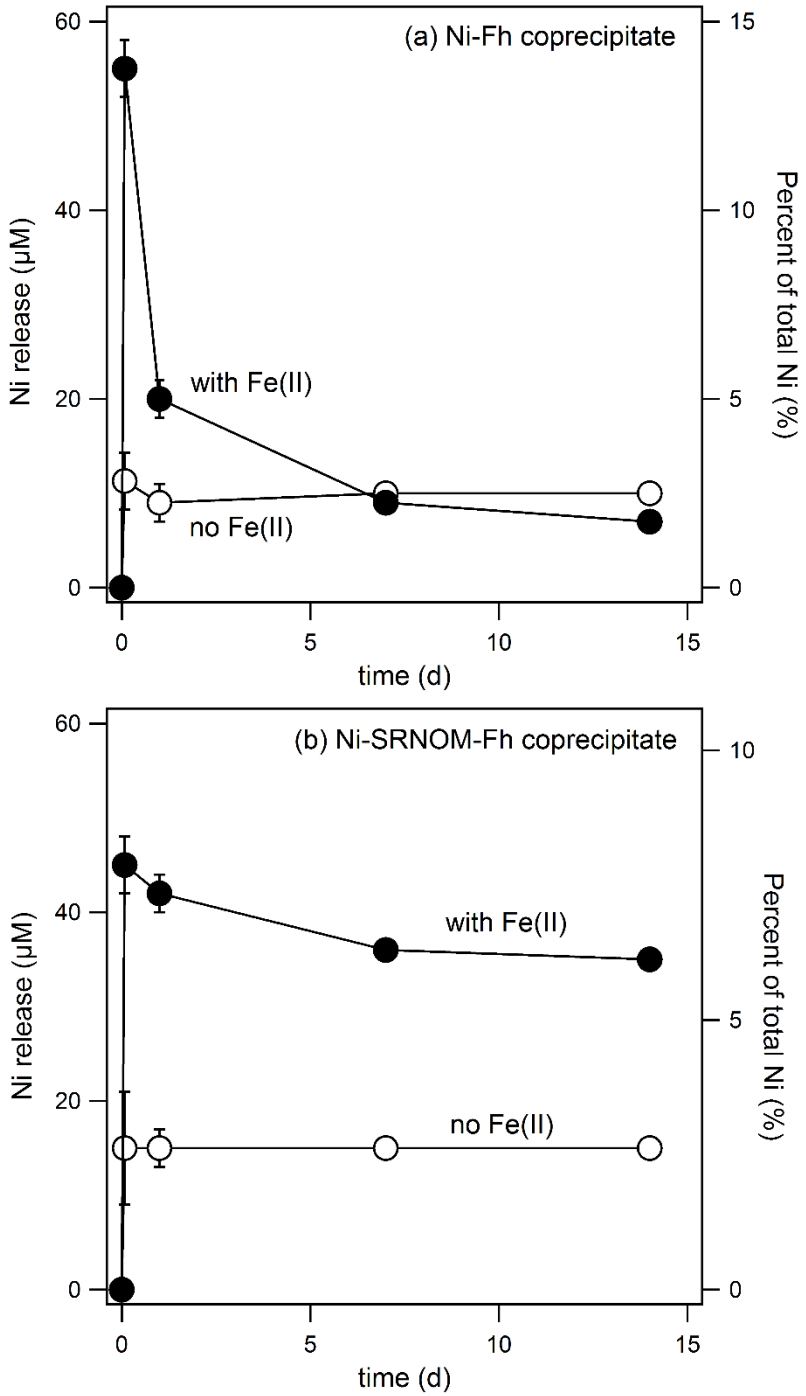

Figure 4.10. The Ni released from (a) Ni-Fh coprecipitate and (b) Ni-SRNOM-Fh coprecipitate with or without 1 mM Fe(II) at 10 mM PIPES buffer (pH 7.0). The overall Ni concentration are 460 μM in Ni-Fh system and 620 μM in Ni-SRNOM-Fh system.

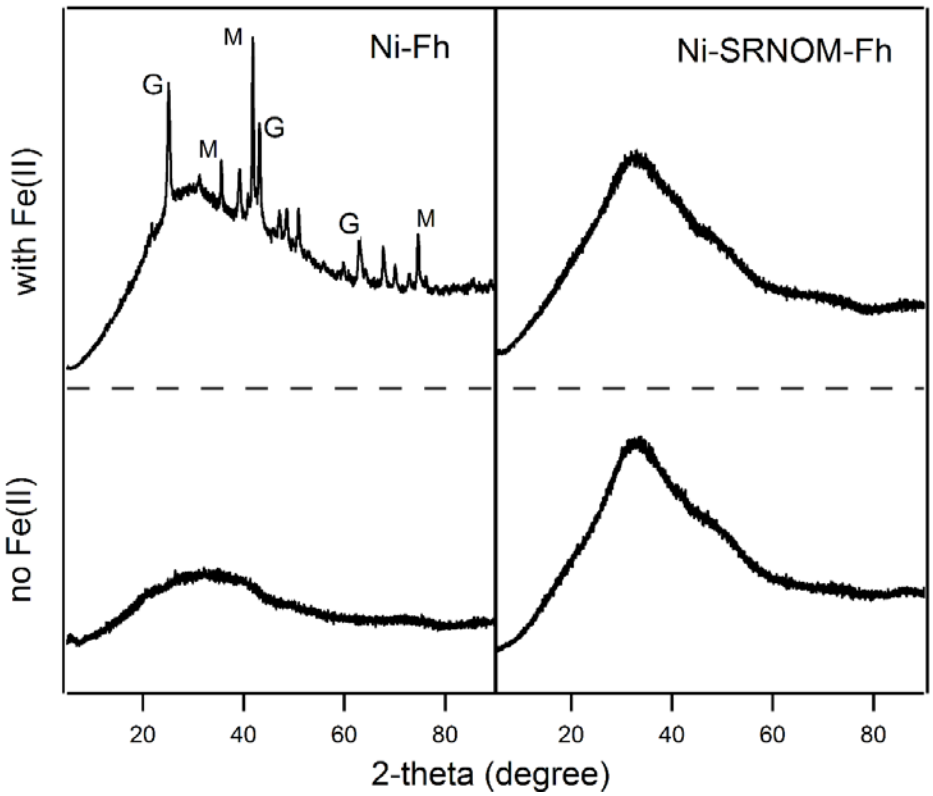

Figure 4.11. X-ray diffraction pattern of ferrihydrite and SRNOM-Fh (C/Fe=1.2) reacted with or without Fe(II) in the presence of adsorbed Ni after 14 days. Note: G = goethite, M = magnetite.

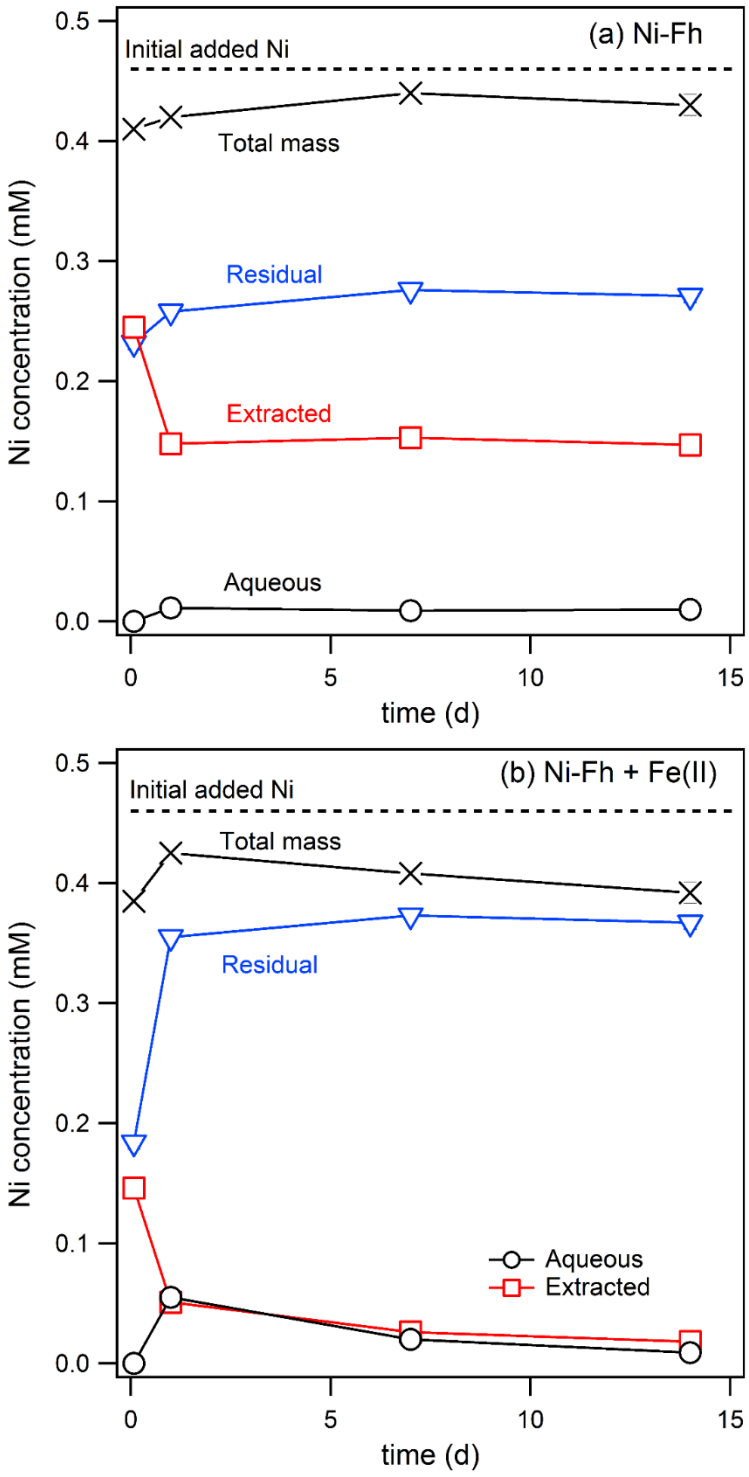

Figure 4.12. Ni distribution in Ni-Fh coprecipitate reactors (a) without Fe(II) and (b) with Fe(II) over time. The extracted Ni indicated the amount of Ni released during mild extraction at pH 3.0. The residual Ni was measured by dissolving the extracted solid with 5 M HCl. All the data were listed in Table 4.3.

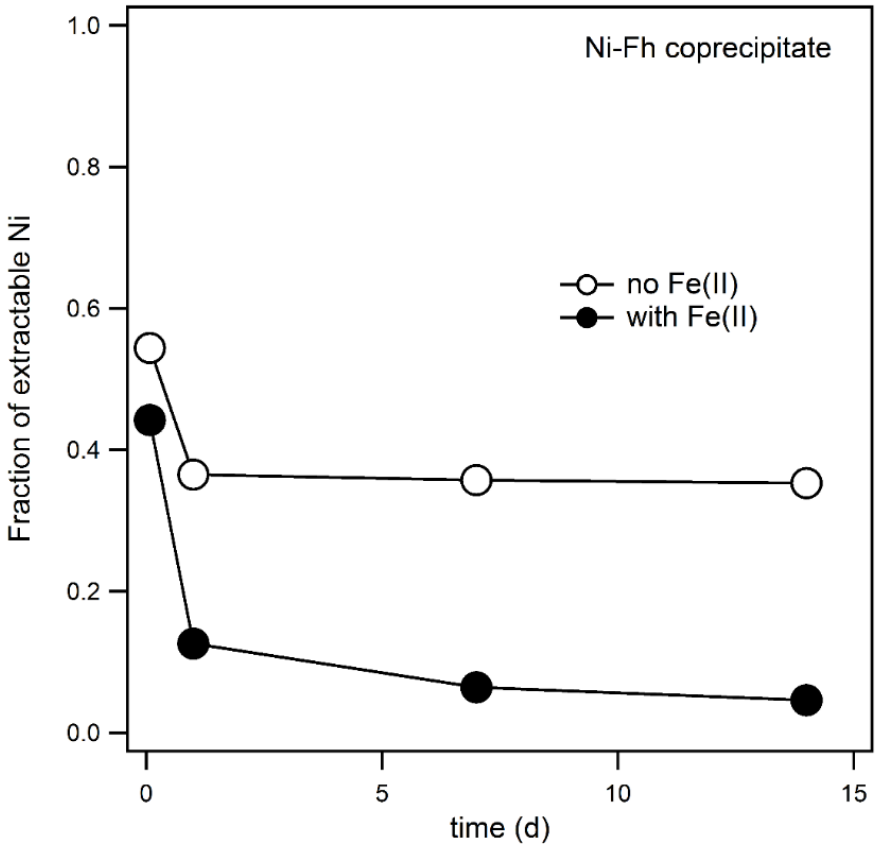

Figure 4.13. The fraction of Ni extractable under pH 3.0 from the reacted Ni-Fh coprecipitates with or without Fe(II).

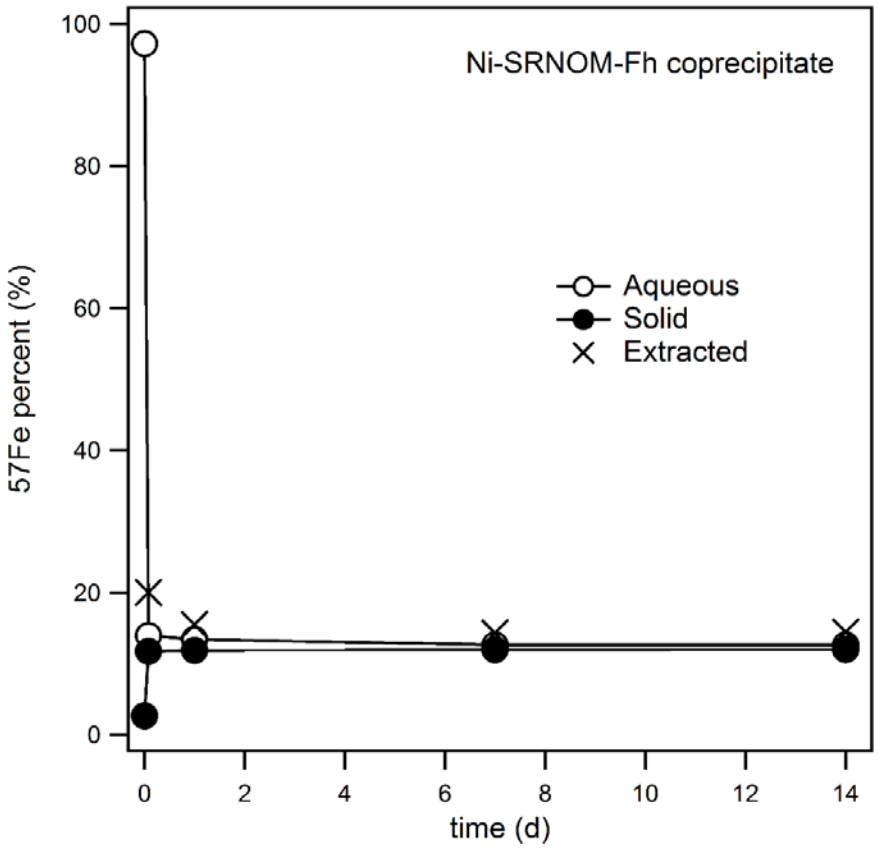

Figure 4.14. The ^{57}Fe percent in aqueous Fe(II), extracted Fe and the residual Fe after reacting 1 mM 57Fe(II) with Ni-SRNOM-Fh coprecipitate at pH 7.0.

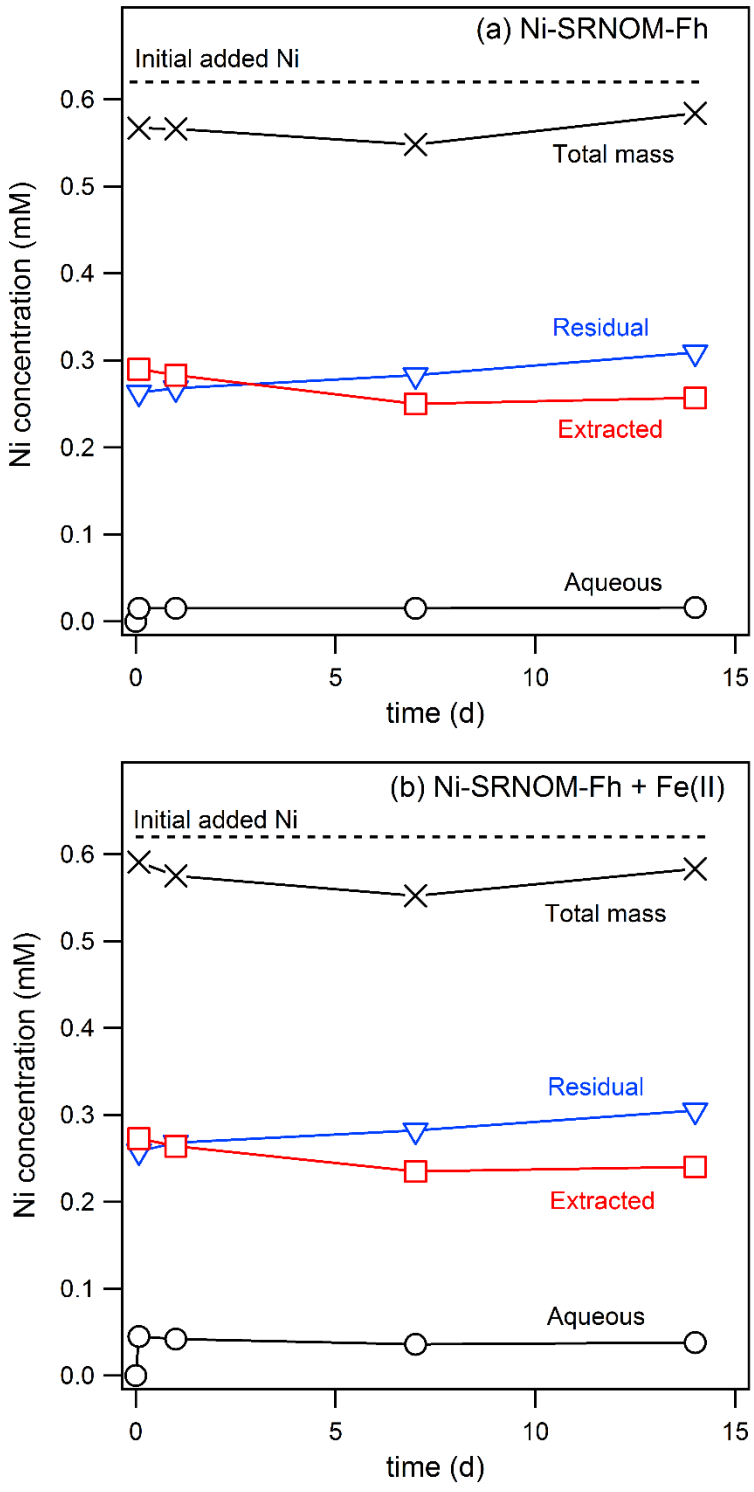

Figure 4.15. Sequential extraction of Ni in Ni-SRNOM-Fh coprecipitate reactors (a) without Fe(II) and (b) with Fe(II) over time. All the data were listed in Table 4.4.

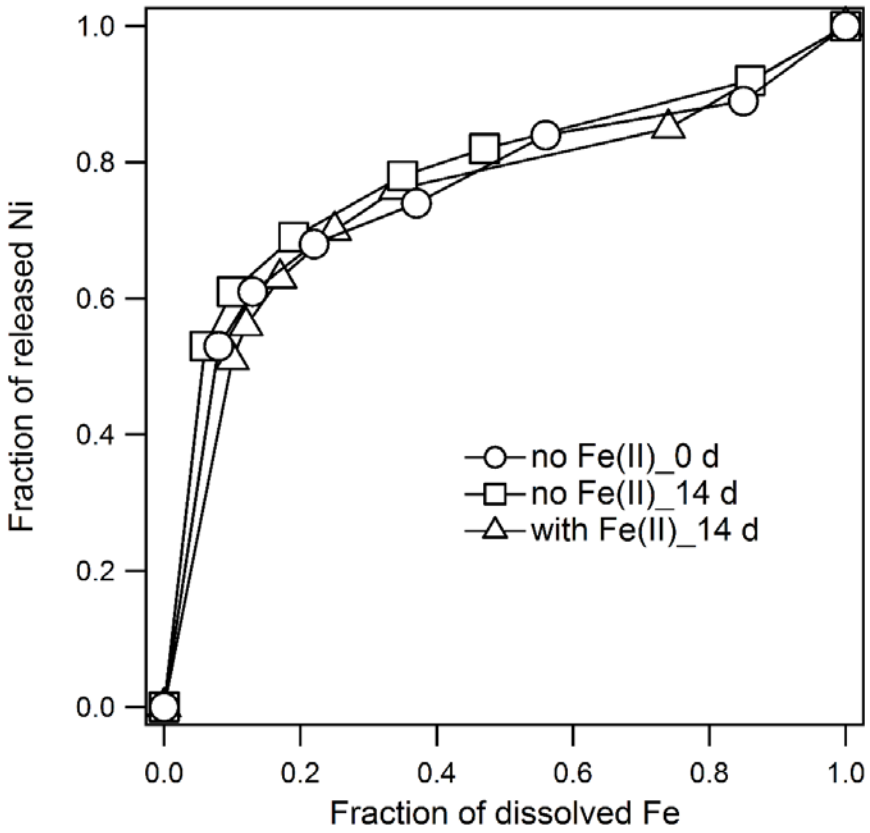

Figure 4.16. The release of Ni during the dissolution of solid Ni-SRNOM-Fh coprecipitates treated with or without 1 mM Fe(II) over 14 days.

CHAPTER 5: ENVIRONMENTAL SIGNIFICANCE

Summary

This work shows new evidence about the reactivity of Fe mineral associated with NOM under reducing environment and explores the implications for the fate of trace metals. The association of NOM with Fe minerals is of significant interest because they are often found together in soil and sediments and previous studies found the NOM inhibits Fe(II)-catalyzed ferrihydrite transformation. In this study, we showed that the species of NOM play an important role in Fe(II)-catalyzed ferrihydrite transformation with fulvic acids inhibiting transformation to a much greater extent than humic acids. NOM associated through adsorption and coprecipitation were also found have different extent inhibition on Fe(II)-catalyzed transformation of ferrihydrite. Using stable Fe isotopes and Mössbauer spectroscopy, we collected direct evidence to show that electron transfer inhibition was not responsible for NOM inhibition of ferrihydrite transformation, and that Fe atom exchange between aqueous Fe(II) and ferrihydrite occurs even in the lack of ferrihydrite transformation. My findings reveal that significant mixing between the ferrihydrite mineral structures and surrounding fluid can occur even when no ferrihydrite transformation is observed. My work has significant implications for how other elements, such as carbon and trace metals often found associated with ferrihydrite, cycle in the environment.

The study of different NOM-Fh coprecipitates with similar C/Fe ratio shows fulvic acids and Suwannee River NOM that has abundant fulvic content required lower C/Fe ratio than humic acids to inhibit Fe(II)-catalyzed ferrihydrite transformation. This indicates that fulvic content has higher inhibition capacity than humic acids on ferrihydrite transformation. Under conditions where secondary Fe minerals formed, we found goethite was predominant in ferrihydrite coprecipitated with humic acids, whereas lepidocrocite formation was favored in ferrihydrite coprecipitated with

fulvic acids. Different inhibition behavior between fulvic acid and humic acid was found across a wide range of conditions. My work demonstrates that nature of the organic matter present during ferrihydrite transformation can strongly influence the fate of ferrihydrite. Based on our result, we speculate that ferrihydrite formed in the environment with further decomposed NOM (i.e., more fulvic content) may be more resistant to Fe(II)-catalyzed transformation than those with newly formed NOM (i.e., more humic content). We also found adsorbed NOM needed a lower C/Fe ratio than coprecipitated NOM to inhibit Fe(II)-catalyzed ferrihydrite transformation suggesting that adsorbed NOM may be more inhibitive than coprecipitated NOM on ferrihydrite reactivity. In nature, the stability of NOM-Fe association would likely be impacted not only by the properties of NOM but also the natural process to form the association (i.e., through coprecipitation or adsorption).

Using stable Fe isotopes and Mössbauer spectroscopy, we tracked the electron transfer and Fe atom exchange between aqueous Fe(II) and ferrihydrite associated with NOM. We found the electron transfer was not inhibited by coprecipitated NOM suggesting that NOM may work as electron shuttles between aqueous Fe(II) and ferrihydrite. By increasing the initial Fe(II) concentration, we observed more electron transferred into ferrihydrite, but still no ferrihydrite transformation occurred. These findings provide direct evidence that extent of electron transfer into the ferrihydrite NOM coprecipitate does not explain the lack of ferrihydrite transformation in the presence of coprecipitated NOM. In the absence of ferrihydrite transformation, the additional ^{57}Fe(II) tracer experiments showed extensive Fe isotope mixing occurred between aqueous Fe(II) and SRNOM-Fh coprecipitate and reached a homogenous Fe isotope distribution over 14 days. This observation indicates the Fe mineral dissolution and reprecipitation, or Fe mineral recrystallization, still occurred even without the formation of secondary Fe minerals. The

ferrihydrite in NOM-Fh coprecipitate remains active and can exchange with aqueous Fe(II). Our finding of hidden mixing raises important questions about the fate of associated NOM in the coprecipitate and other elements that may associate with ferrihydrite, such as some trace metals. The goal of this thesis was to shed some lights on these important questions.

As an important way to stabilize NOM in soil and sediments, the coprecipitated NOM in ferrihydrite was not released after reaction with Fe(II), even in the situation ferrihydrite transformed to secondary Fe minerals. The further characterization shows the thermal stability of carbon in NOM-Fh coprecipitate increased after ferrihydrite transformation occurred. Our observations indicate NOM associated with ferrihydrite was stable under reducing environment and its stability may even be improved with the formation of secondary Fe minerals. Ni was also introduced to our system to test the implication of "active" NOM-Fh coprecipitate to the stability of associated metal. Even though we observed partial incorporation of adsorbed Ni into recrystallized NOM-Fh coprecipitate (with no secondary Fe mineral formation), it is less significant compared to the formation of secondary Fe minerals, during which big amount of Ni incorporated into secondary Fe minerals. The Fe(II)-catalyzed recrystallization of ferrihydrite with or without NOM partially released pre-incorporated Ni, but those released Ni was resorbed with the formation of secondary Fe minerals. No similar resorption process was observed in the absence of ferrihydrite transformation. In general, the presence of coprecipitate NOM did not significantly change the amount of Ni associated with ferrihydrite, but it compromised the stability of associated Ni by preventing the formation of secondary Fe minerals and extensive metal incorporation during the process. Our findings suggest that, at least for Ni and SRNOM, Fe(II)-catalyzed ferrihydrite transformation may be increase the stability of associated OM and metals.

Recommendations for Future Work

Despite the efforts of us and many others on Fe(II)-catalyzed transformation of ferrihydrite associated with NOM, there remain many questions about this NOM-Fe association and its interaction with surrounding environment. In our study, ^{57}Fe enriched aqueous Fe(II) was used to investigate the Fe atom exchange between aqueous Fe(II) and ferrihydrite with or without NOM. The interpretation of the Fe isotope data, however, is challenging and over the last few years multiple models have been introduced and debated in the literature. To address the complexity of these models, we developed an approach to estimate the isotope distribution in the solids by wet chemical extractions before choosing a model to apply. When secondary Fe minerals formed, however, the heterogeneous isotope distribution between secondary Fe minerals and ferrihydrite we found in chapter 3 contains abundant information about the mineral transformation process, but has not yet been fully explored. Since only preliminary data was obtained, we did not give the isotope data further discussion. A more systematic experiment to track the Fe isotope and mass change in aqueous Fe(II) phase, sorbed Fe(II) phase, residual ferrihydrite and secondary Fe minerals over time would be an interesting avenue to explore. Considering the isotope mixing between aqueous Fe(II) and ferrihydrite is, we think, a fast process, more data points at earlier reaction time would be needed which could give us more information about the relationship between Fe atom exchange and ferrihydrite transformation. Data on isotope changes in the different secondary minerals would help us better understand Fe(II)-catalyzed ferrihydrite transformation from a different perspective.

As concerns about atmospheric CO_2 concentration increase, the stability of carbon in the NOM-Fh association will get more and more attention. Thus far, very limited studies explored the stability of associated carbon during Fe mineral transformation or recrystallization. We have done

some preliminary tests, but it is definitely not enough to understand the fate of Fe associated carbon under reducing environment. The carbon distribution and bioavailability during Fe mineral transformation or recrystallization will be needed to better predict the fate of NOM associated with Fe minerals.

In addition to carbon, the NOM-Fe mineral association is also important sink for many trace metals and nutrients in soil. In our study, we investigated the fate of Ni during Fe(II)-catalyzed transformation of ferrihydrite associated with NOM. Similar investigation with other trace metals is needed, as they may behave differently in the nature. More spectroscopy and microscopy evidence are also needed to tell the distribution of trace metal between NOM and Fe minerals. May be more interestingly, with elemental mapping techniques (such as STXM), we can see how these trace metals will redistribute during Fe mineral transformation or crystallization in the presence of NOM.

There still have many other Fe minerals can transform to secondary Fe minerals similar as we observed in ferrihydrite, such as vivianite, siderite, etc.. They all have important implications for us to understand the elements geochemical cycle in soil. However, little was known about their transformation under more complicated environment. Additional studies focused on these overlooked Fe minerals were expected for the better understanding of Fe dynamics in the real environment.

APPENDIX A: THE ROLE OF FREEZE DRYING IN FE(II)-CATALYZED FERRIHYDRITE TRANSFORMATION

Data Report

Fe(II)-catalyzed ferrihydrite transformation has been widely investigated and many factors have been found to alter the rate and species of secondary Fe mineral formation (55, 62, 65). The results from different studies, however, get confusion when further compared the experimental conditions and species of secondary Fe minerals. In addition, the transformation pathways from ferrihydrite to lepidocrocite, goethite or magnetite are still in debate. To further explore this Fe(II)-catalyzed ferrihydrite transformation, wet and freeze dried ferrihydrite were used and compared for mineral transformation in this study. From the Mössbauer temperature profiles (**Figure A.1**), the unreacted freeze dried ferrihydrite was well ordered at 25 K while wet ferrihydrite only partially ordered, difference still exist even at 14 K. This observation indicates freeze dried ferrihydrite has stronger Fe-Fe interactions and higher crystallinity compared to wet ferrihydrite. I further fitted the 14 K spectroscopies (**Figure A.2**) and got the hyperfine field distribution in the two solids (**Figure A.3**). Freeze dried ferrihydrite has more narrow hyperfine field distribution compared to wet ferrihydrite, and bigger average hyperfine field value (47.5 T compared to 44.4 T). The result of freeze dried ferrihydrite is consistent with others reported before (95).

Wet ferrihydrite and freeze dried ferrihydrite were treated by aqueous Fe(II) under similar Fe(II)/Fe(III) ratios at pH 7.0 over time. From the XRD results of wet ferrihydrite reactors (**Figure A.4**), diffraction peaks that consistent with goethite started to form within 2 hours and their intensity improved over time. Over 1 day reaction, extra diffraction peaks appeared that can be attributed to magnetite. No other secondary Fe minerals were found even with longer reaction time. The Fe(II) mass distribution was also tracked over time (**Figure A.5**). A good Fe(II) mass balance was achieved during the reaction, indicates no net Fe(II) loss due to accidental oxidation. Aqueous Fe(II) sorption by Fe minerals normally reach equilibrium over hours (40, 190), but a continuing

aqueous Fe(II) lose was observed in ferrihydrite reactor over 14 days, accompanied with an increase in residual Fe(II). It is consistent with the formation of magnetite as it consumes Fe(II) and incorporates them into mineral structure, which made them less susceptible to the mild extraction. The presence of goethite and magnetite is consistent with other studies under high Fe(II)/Fe(III) ratio (55, 64). The tardy appearance of magnetite after goethite, however, is an interesting observation that may indicate goethite as the precursor or catalyst for magnetite to form. Magnetite that has higher crystallinity and stability was found to form during goethite dehydration in other study (191).

To investigate the effect of freeze drying on ferrihydrite transformation, I also reacted freeze dried ferrihydrite with aqueous Fe(II) under same initial Fe(II)/Fe(III) ratio and pH. Different from the magnetite and goethite observed in wet ferrihydrite, only lepidocrocite was found in freeze dried ferrihydrite after 1 day reaction (**Figure A.6**). It indicates freeze dried ferrihydrite is less active or susceptible to mineral transformation as lepidocrocite has lower crystallinity than goethite and was regard as intermediate product during ferrihydrite transformation to goethite (113, 142). Magnetite, however, was also found in freeze dried ferrihydrite after 14 days reaction (**Figure A.6**). It took longer for magnetite to form in freeze dried ferrihydrite, and it is surprising to see no goethite as it has lower crystallinity than magnetite and would be expected easier to form. The dominance of lepidocrocite in freeze dried ferrihydrite may also be contributed by the anion existed in the Fe(II) stock solution. In this experiment, the Fe(II) stock solution was made by dissolving Fe metal in HCl, abundant Cl^- was introduced with Fe(II), which is in favor of lepidocrocite to form (55, 100).

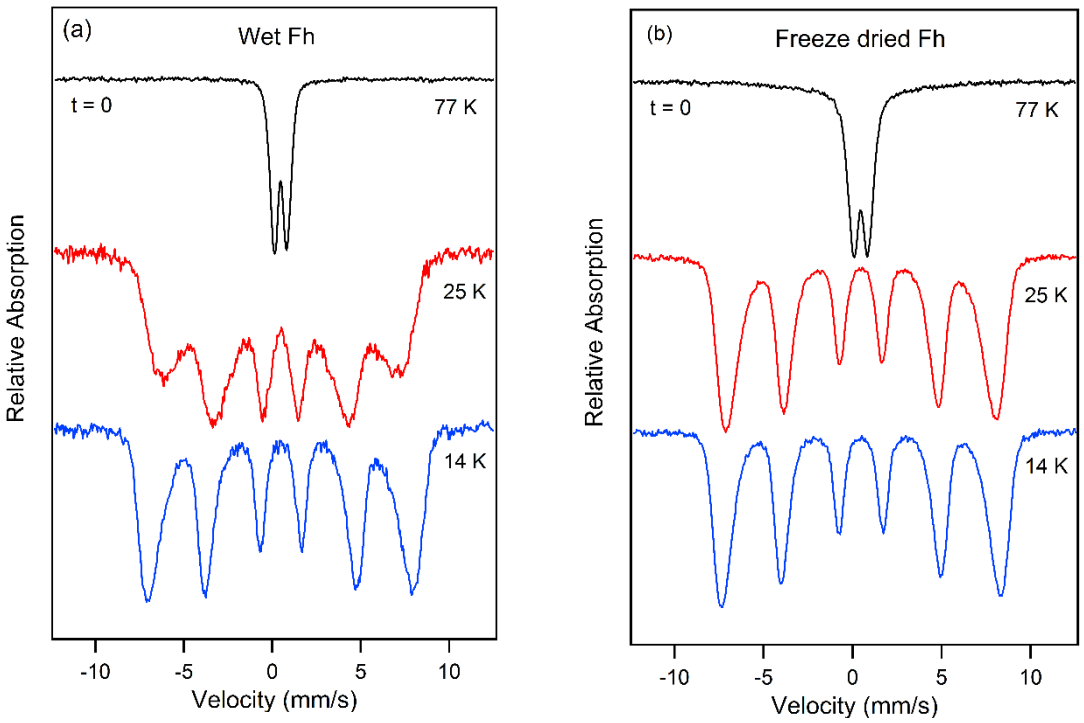

Figure A.1. Mössauer spectroscopies of (a) wet ferrihydrite and (b) freeze dried ferrihydrite at 77 K, 25 K and 14 K.

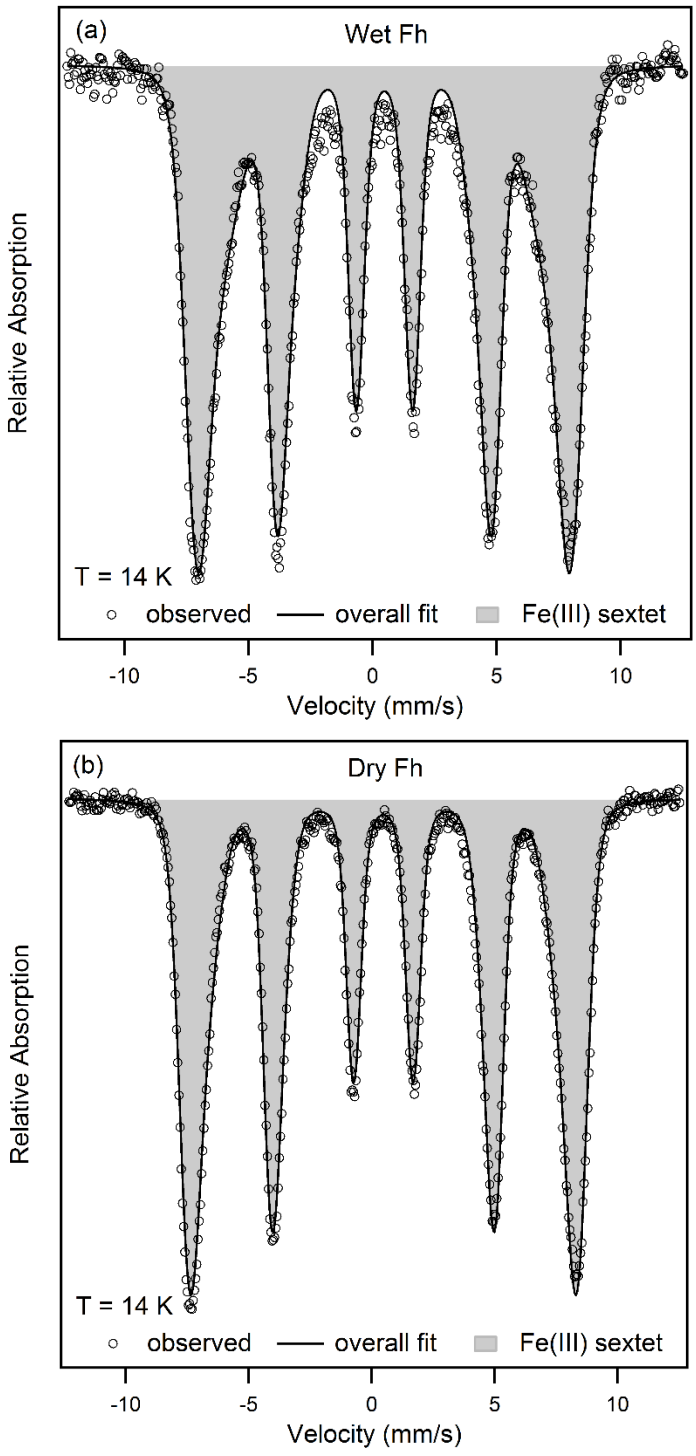

Figure A.2. Mössbauer spectroscopy and fitting of (a) wet ferrihydrite and (b) freeze dried ferrihydrite at 14 K. Both with center shift value 0.47 mm/s, the average hyperfine field value in wet ferrihydrite is 44.4 T, and in freeze dried ferrihydrite is 47.5 T.

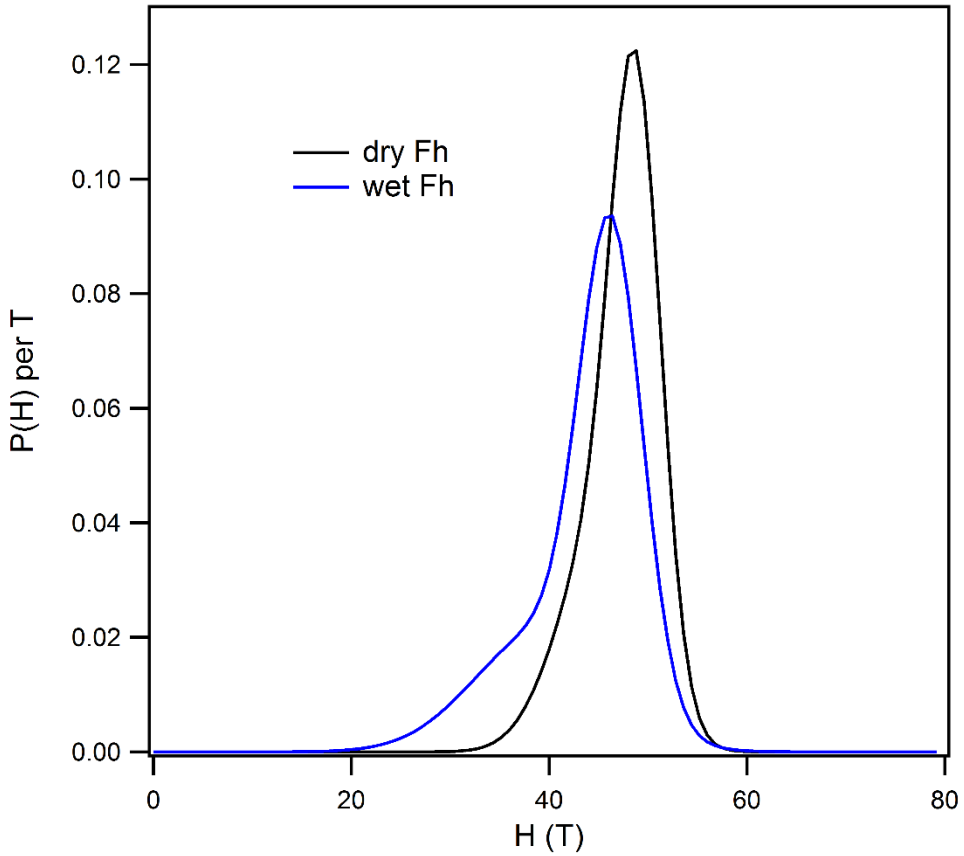

Figure A.3. Hyperfine field distribution of wet and freeze dried ferrihydrite at 14 K.

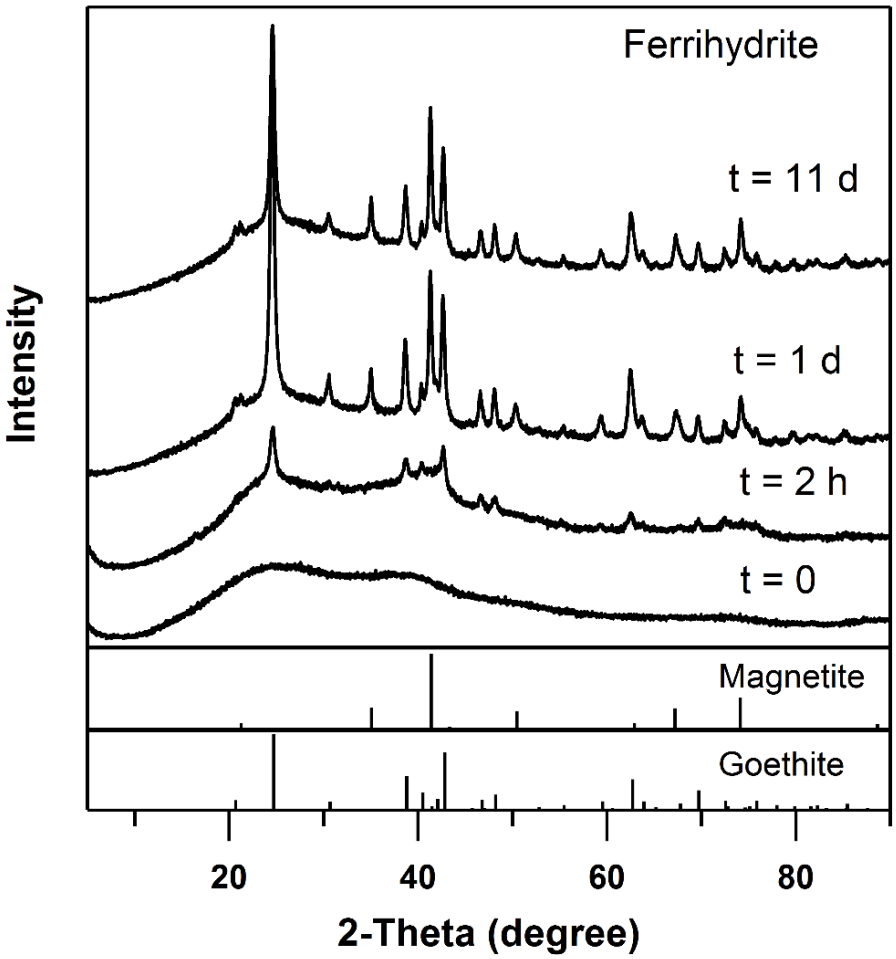

Figure A.4. X-ray diffraction pattern of wet ferrihydrite reacted with 2 mM Fe(II) in 10 mM PIPES (pH 7.0) over time. The identical peaks of secondary Fe mineral are consistent with goethite and magnetite.

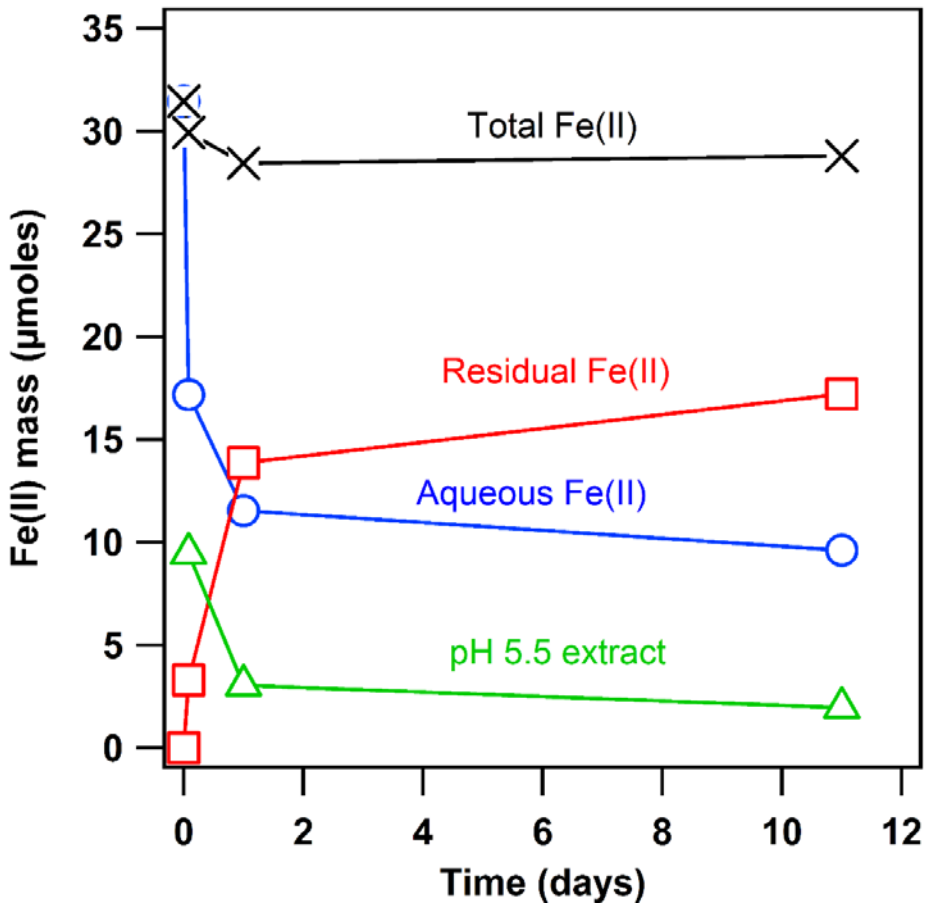

Figure A.5. Fe(II) mass distribution during 2 mM Fe(II) catalyzed wet ferrihydrite transformation in 10 mM PIPES buffer (pH 7.0) over time. The “pH 5.5 extract” indicates the sorbed Fe(II) that can be extracted by 10 mM MES buffer at pH 5.5. Residual Fe(II) reflects the Fe(II) in the post-extraction solids measured by dissolving the solid with 4 M HCl.

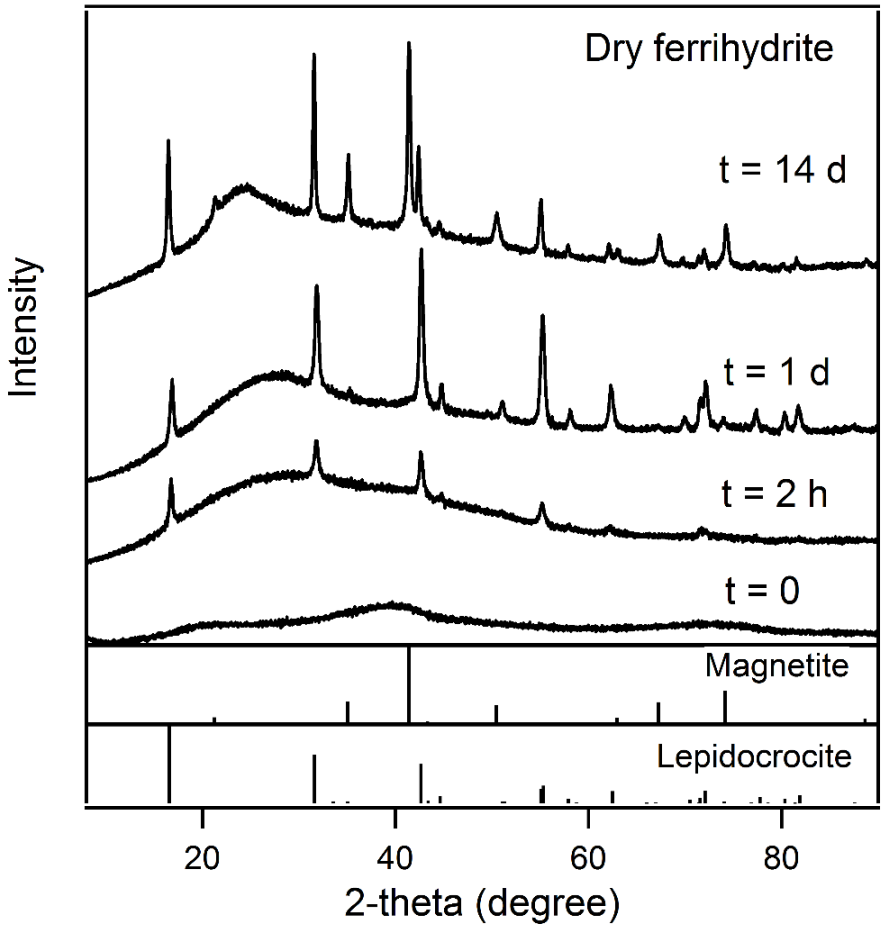

Figure A.6. Freeze dried ferrihydrite reacted with 4 mM Fe(II) in PIPES buffer (pH 7.0) over time. The Fe(II)/Fe(III) ratio is similar with wet ferrihydrite. Lepidocrocite was the main secondary Fe mineral found in the early stage, but after longer reaction time magnetite start to form.

APPENDIX B: THE ROLE OF DEFECTS IN NI SORPTION BY GOETHITE

Data Report

Our group has shown the defects in goethite may facilitate the electron transfer between aqueous Fe(II) and structural Fe(III) (107). To further investigate if the defects in goethite impact metal sorption, we did Ni sorption experiments with as-synthesized goethite (As-Goethite) and hydro-thermal treated goethite (HT-Goethite) that has less defects. ^{57}Fe enriched aqueous Fe(II) (99.37% of ^{57}Fe) was added to investigate the effect of Fe atom exchange on Ni sorption by goethite. The surface area of As-goethite is 28 m^2/g, slightly higher than 22 m^2/g in HT-goethite.

Around 85 μM Ni was equilibrated in 25 mM HEPES buffer at pH 7.5, then different goethite were added into the solution to achieve 2 g/L solid loading. For the reactors with Fe(II), aqueous Ni (~85 μM) and 1 mM Fe(II) were equilibrated in buffer before the adding of goethite (2 g/L). Triplicate reactors were set for each time point. The aqueous Ni concentrations were measured over time (**Table B.1**). Over 20 days, 71.3% of aqueous Ni was adsorbed by As-goethite, while only 57.2% was adsorbed by HT-goethite. After normalized by the surface area, the sorption capacity is 1.09 $\mu mol/m^2$ with As-goethite and 1.11 $\mu mol/m^2$ with HT-goethite, very consistent with each other. In the absence of Fe(II), the different Ni adsorption by two types of goethite was mainly caused by the difference in surface area.

The presence of Fe(II) inhibited the Ni adsorption by As-goethite and HT-goethite (**Figure B.1**), which is contradict with the observation of Coughlin et al. that 1 mM Fe(II) slightly enhanced Ni(II) sorption around pH 7.0 (28). But note the Ni concentration used in their study (4.47 μM) is much lower than our situation (85 μM), the surface available for ion sorption in their study was still plenty and the competition between Fe(II) and Ni(II) for adsorption points may not impact Ni(II) adsorption. To further characterize the adsorbed Ni, we did mild extraction to the solid with 0.4 M HCl. In As-goethite reactors, we extracted 60% of Ni associated with solid in the absence

of Fe(II), and it decreased to 37% with the presence of Fe(II). Similar in HT-goethite, the percent of extractable Ni in solid phase decreased from 49% to 40% with the presence of Fe(II). Aqueous Fe(II) inhibited the amount of Ni(II) adsorbed by goethite, but increased the stability of associated Ni.

To investigate the role of Fe(II) in Ni adsorption by As-goethite and HT-goethite, we measured the Fe(II) concentration and isotope composition in the aqueous phase over time. Around 39% of Fe(II) was sorbed by As-goethite and only 27% by HT-goethite (**Figure B.2**). More Fe(II) sorbed by As-goethite than HT-goethite. We also observed bigger ^{57}Fe percent change in As-goethite than HT-goethite (Figure B.3), indicates more Fe atom exchange occurred in As-goethite reactors. The amount of Fe(II) sorbed may explain the different extent of Fe atom exchange. The extractable Ni in As-goethite decreased 23% in the presence of Fe(II), but only decreased 9% in HT-goethite, it may be related to the different extent of Fe atom exchange we observed between As-goethite and HT-goethite.

Table B.1. Ni adsorption by As-synthesized goethite and hydro-thermal treated goethite.

Time (d)		Aqueous Ni (μM)		Extracted Ni (μM)		Adsorbed Ni(uM)		Percent of extracted (%)	
		As-Gt	HT-Gt	As-Gt	HT-Gt	As-Gt	HT-Gt	As-Gt	HT-Gt
0		85.43(2.58)	85.43(2.58)			0	0		
1	No Fe(II)	35.20(4.51)	48.92(3.42)			50.23	36.51		
	With Fe(II)	52.93(1.35)	63.69(0.59)			32.50	21.74		
20	No Fe(II)	24.51(6.51)	36.54(4.60)	36.81(0.50)	24.11(0.60)	60.92	48.89	60	49
	With Fe(II)	36.05(0.71)	48.65(1.49)	18.45(0.96)	14.74(1.54)	49.38	36.78	37	40

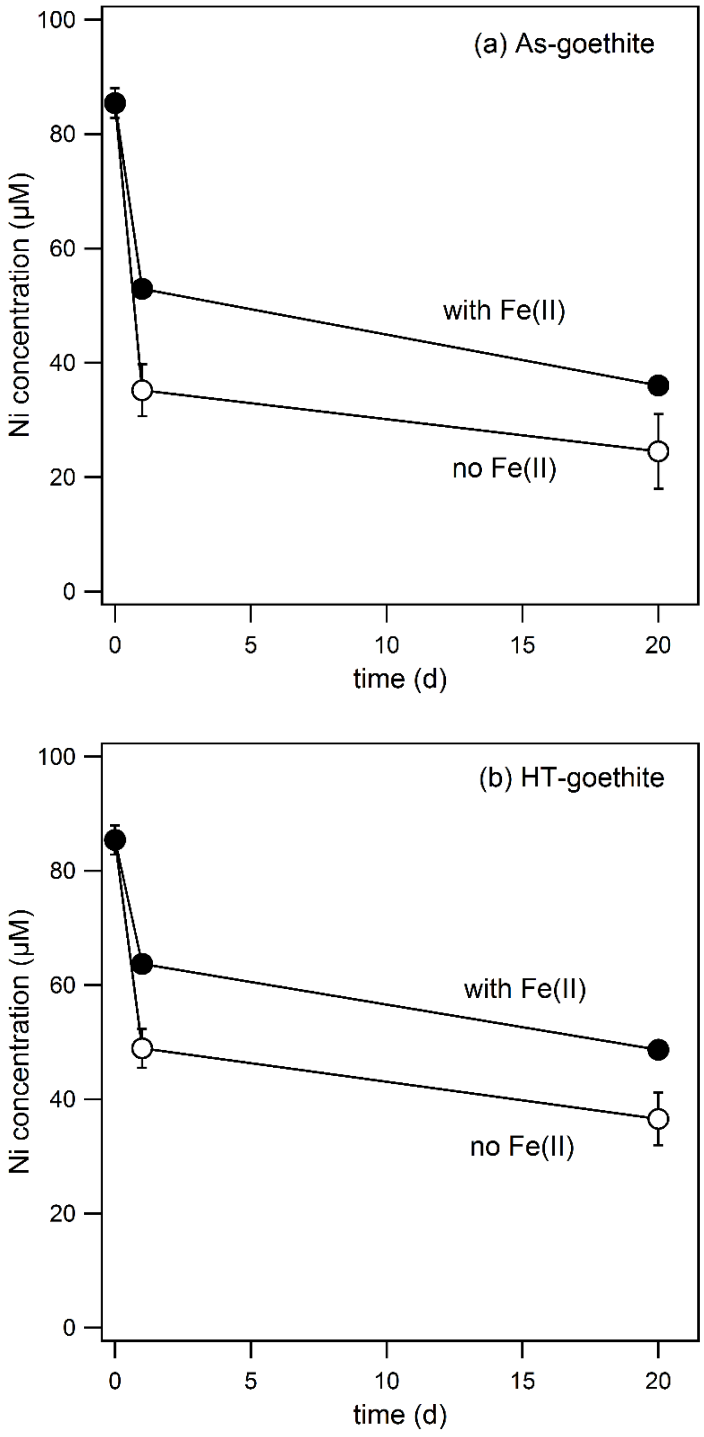

Figure B.1. The aqueous Ni concentration change over time in (a) As-goethite and (b) HT-goethite with or without Fe(II).

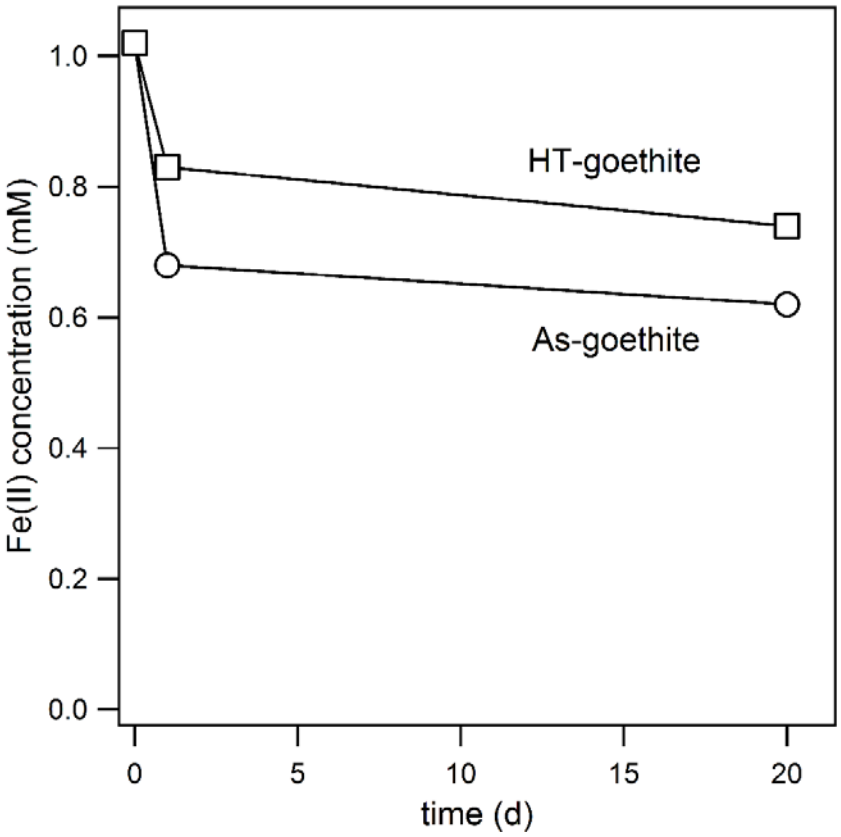

Figure B.2. Aqueous Fe(II) concentration in the reactors over time. Each data point indicates the average value of triplicate reactors.

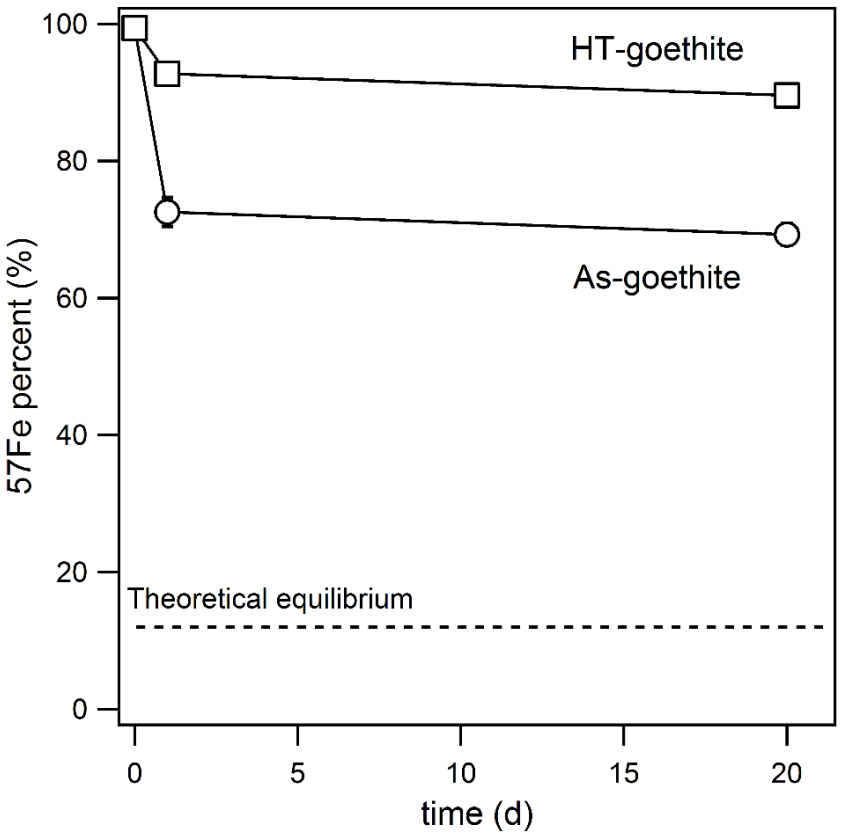

Figure B.3. The percent of ^{57}Fe isotope in aqueous phase over time. Due to the interruption of ^{58}Ni, we did not count ^{58}Fe in the Fe isotope composition, only ^{54}Fe, ^{56}Fe and ^{57}Fe were considered.

APPENDIX C: EFFECT OF ORGANIC C ON STABLE FE ISOTOPE FRACTIONATION AND ISOTOPE EXCHANGE KINETICS BETWEEN AQUEOUS FE(II) AND FERRIHYDRITE AT NEUTRAL PH

Effect of organic C on stable Fe isotope fractionation and isotope exchange kinetics between aqueous Fe(II) and ferrihydrite at neutral pH [1]

Abstract

Ferrihydrite is ubiquitous in soil and sediments, and because of its co-existence with organic matter, ferrihydrite plays an important role in regulating geochemical cycles of Fe, C, nutrients, and toxic metals in nature. Although pure ferrihydrite is easily transformed to more stable iron oxides upon interaction with aqueous Fe(II), mineralogical transformation is inhibited in the presence of structural impurities such as C and Si. Therefore, understanding the factors controlling the reactivity of ferrihydrite, especially in the presence of organic C and Si, is critical to understanding the role of ferrihydrite in geochemical cycles. Equilibrium stable Fe isotope fractionations, expressed as $^{56}Fe/^{54}Fe$ ratios, are fundamental thermodynamic properties and therefore reflect the nature of Fe bonding in ferrihydrite. In this study, we investigated stable Fe isotope fractionation between aqueous Fe(II) and ferrihydrite that was coprecipitated with natural organic matter to evaluate whether inhibition of mineralogical transformation by organic C also influences the reactivity and Fe-bonding in ferrihydrite. Experiments conducted using Suwannee River natural organic matter (SRNOM) coprecipitated with ferrihydrite (molar C:Fe =1.2) produced an equilibrium $^{56}Fe/^{54}Fe$ fractionation of -2.42 ± 0.17‰ between aqueous Fe(II) and Ferrihydrite-SRNOM coprecipitates. This fractionation factor differs from that previously determined between $Fe(II)_{aq}$ and pure ferrihydrite (-3.20‰), but is similar to that measured for $Fe(II)_{aq}$–Si-ferrihydrite, -2.58 ± 0.14‰, at a Fe:Si molar ratio of unity. Furthermore, the addition of C markedly increased the Fe isotope exchange rates to a similar degree as was found with Si-

[1] This work is in preparation for submission to a peer-reviewed journal, in which I am the second author and contribute to experimental design and conduction. Isotope data collection and analysis were carried out in University of Wisconsin-Madison.

substituted ferrihydrite, suggesting similar effects on both bonding and reactivity upon addition of similar amounts of C and Si. Because ferrihydrite often occurs with organic matter in soils (e.g., wetlands) and sediments, these results are important in the interpretation of Fe isotope fractionation and exchange kinetics during mineral-fluid interactions in natural ferrihydrite-bearing systems.

APPENDIX D: EFFECT OF BICARBONATE AND PHOSPHATE ON ARSENIC RELEASE FROM MINING-IMPACTED SEDIMENTS IN THE CHEYENNE RIVER WATERSHED, SOUTH DAKOTA, USA

Effect of bicarbonate and phosphate on arsenic release from mining-impacted sediments in the Cheyenne River watershed, South Dakota, USA [2]

Abstract

The mobilization of arsenic (As) from riverbank sediments affected by gold mining legacy in north-central South Dakota was examined using aqueous speciation chemistry, spectroscopy, and diffraction analyses. Gold mining resulted in the discharge of approximately 109 metric tons of mine waste into Whitewood Creek (WW) near the Homestake Mine and Cheyenne River at Deal Ranch (DR), 241 km downstream. The highest concentrations of acid-extractable As measured from solid samples was 2,020 mg kg-1 at WW and 385 mg kg-1 at DR. Similar sediment mineralogy between WW and DR was identified using XRD, with the predominance of alumino-silicate and iron-bearing minerals. Alkalinity measured in surface water at both sites ranged from 1,000 to 2,450 mg-1 as $CaCO_3$ (10-20 mM HCO_3^- at pH 7). Batch laboratory experiments were conducted under oxidizing conditions to evaluate the effects of $NaHCO_3$ (0.2 mM and 20 mM) and NaH_2PO_3 (0.1 and 10 mM) on the mobilization of As. These ions are relevant for the site due to the alkaline nature of the river and nutrient mobilization from the ranch. The range of As(V) release with the NaHCO3 treatment was 17-240 µg L-1. However, the highest release (6,234 µg L-1) occurred with 10 mM NaH2PO3, suggesting that As release is favored by competitive ion displacement with phosphate compared to bicarbonate. Although higher total As was detected in WW solids, the As(V) present in DR solids was labile when reacted with NaHCO3 and NaH2PO3, which is a relevant finding for communities living close to the river bank. The results from this study aid in a better understanding of As mobility in surface water sites affected by mining legacy.

[2] This work has been submitted to Environmental Science: Processes & Impacts, in which I am the coauthor and contributed to data collection and analyses of Mössbauer spectroscopy.

REFERENCES

1. Swift DC, Eggert J, Hicks DG, Hamel S, Caspersen K, Schwegler E, et al. Mass-radius relationships for exoplanets. The Astrophysical Journal. 2011;744(1):59.
2. Morgan JW, Anders E. Chemical composition of earth, Venus, and Mercury. Proceedings of the National Academy of Sciences. 1980;77(12):6973-7.
3. Sheftel AD, Mason AB, Ponka P. The long history of iron in the Universe and in health and disease. Biochimica et Biophysica Acta (BBA)-General Subjects. 2012;1820(3):161-87.
4. McDonough WF, Sun S-S. The composition of the Earth. Chem Geol. 1995;120(3-4):223-53.
5. Tagliabue A, Bowie AR, Boyd PW, Buck KN, Johnson KS, Saito MA. The integral role of iron in ocean biogeochemistry. Nature. 2017;543(7643):51.
6. Sung W, Morgan JJ. Kinetics and product of ferrous iron oxygenation in aqueous systems. Environ Sci Technol. 1980;14(5):561-8.
7. Davison W, Seed G. The kinetics of the oxidation of ferrous iron in synthetic and natural waters. Geochim Cosmochim Acta. 1983;47(1):67-79.
8. Makita H. Iron-oxidizing bacteria in marine environments: recent progresses and future directions. World Journal of Microbiology and Biotechnology. 2018;34(8):110.
9. Emerson D, Moyer C. Isolation and characterization of novel iron-oxidizing bacteria that grow at circumneutral pH. Applied and environmental microbiology. 1997;63(12):4784-92.
10. Bryce C, Blackwell N, Schmidt C, Otte J, Huang Y, Kleindienst S, et al. Microbial anaerobic Fe (II) oxidation–ecology, mechanisms and environmental implications. Environmental microbiology. 2018.
11. Melton ED, Swanner ED, Behrens S, Schmidt C, Kappler A. The interplay of microbially mediated and abiotic reactions in the biogeochemical Fe cycle. Nature Reviews Microbiology. 2014;12:797.
12. Lovley DR, Phillips EJ. Novel mode of microbial energy metabolism: organic carbon oxidation coupled to dissimilatory reduction of iron or manganese. Applied and environmental microbiology. 1988;54(6):1472-80.
13. Lovley DR, Stolz JF, Nord GL, Phillips EJ. Anaerobic production of magnetite by a dissimilatory iron-reducing microorganism. Nature. 1987;330(6145):252-4.
14. Barbeau K. Photochemistry of organic iron (III) complexing ligands in oceanic systems. Photochemistry and photobiology. 2006;82(6):1505-16.
15. Lovley DR, Coates JD, Blunt-Harris EL, Phillips EJ, Woodward JC. Humic substances as electron acceptors for microbial respiration. Nature. 1996;382(6590):445.
16. Roden EE, Kappler A, Bauer I, Jiang J, Paul A, Stoesser R, et al. Extracellular electron transfer through microbial reduction of solid-phase humic substances. Nature geoscience. 2010;3(6):417.
17. Canfield DE. Reactive iron in marine sediments. Geochim Cosmochim Acta. 1989;53(3):619-32.
18. Schwertmann U. The effect of pedogenic environments on iron oxide minerals. Advances in soil science: Springer; 1958. p. 171-200.
19. Laufer K, Nordhoff M, Røy H, Schmidt C, Behrens S, Jørgensen BB, et al. Coexistence of microaerophilic, nitrate-reducing, and phototrophic Fe (II) oxidizers and Fe (III) reducers in coastal marine sediment. Appl Environ Microbiol. 2016;82(5):1433-47.
20. Gorski CA, Scherer MM. Fe2+ sorption at the Fe oxide-water interface: A revised conceptual framework. Aquatic Redox Chemistry. 2011;1071:315-43.

21. Jenne EA. Controls on Mn, Fe, Co, Ni, Cu, and Zn Concentrations in Soils and Water: the Significant Role of Hydrous Mn and Fe Oxides. Trace Inorganics In Water. Advances in Chemistry. 73: AMERICAN CHEMICAL SOCIETY; 1968. p. 337-87.
22. Murray GC, Hesterberg D. Iron and phosphate dissolution during abiotic reduction of ferrihydrite-boehmite mixtures. Soil Sci Soc Am J. 2006;70(4):1318-27.
23. Coughlin BR, Stone AT. Nonreversible Adsorption of Divalent Metal Ions (MnII, CoII, NiII, CuII, and PbII) onto Goethite: Effects of Acidification, FeII Addition, and Picolinic Acid Addition. Environ Sci Technol. 1995;29(9):2445-55.
24. Macalady DL, Tratnyek PG, Grundl TJ. Abiotic reduction reactions of anthropogenic organic chemicals in anaerobic systems: a critical review. Journal of Contaminant Hydrology. 1986;1(1-2):1-28.
25. Roden EE, Urrutia MM. Influence of biogenic Fe (II) on bacterial crystalline Fe (III) oxide reduction. Geomicrobiology journal. 2002;19(2):209-51.
26. Pedersen HD, Postma D, Jakobsen R, Larsen O. Fast transformation of iron oxyhydroxides by the catalytic action of aqueous Fe(II). Geochim Cosmochim Acta. 2005;69(16):3967-77.
27. Klausen J, Troeber SP, Haderlein SB, Schwarzenbach RP. Reduction of substituted nitrobenzenes by Fe (II) in aqueous mineral suspensions. Environ Sci Technol. 1995;29(9):2396-404.
28. Coughlin BR, Stone AT. Nonreversible Adsorption of Divalent Metal-Ions (Mn-Ii, Co-Ii Ni-Ii Cu-Ii and Pb-Ii) onto Goethite - Effects of Acidification, Fe-Ii Addition, and Picolinic-Acid Addition. Environ Sci Technol. 1995;29(9):2445-55.
29. Sørensen J, Thorling L. Stimulation by lepidocrocite (7-FeOOH) of Fe (II)-dependent nitrite reduction. Geochim Cosmochim Acta. 1991;55(5):1289-94.
30. White AF, Peterson ML. Reduction of aqueous transition metal species on the surfaces of Fe (II)-containing oxides. Geochim Cosmochim Acta. 1996;60(20):3799-814.
31. Sørensen J, Thorling L. Stimulation by lepidocrocite (7-FeOOH) of Fe(II)-dependent nitrite reduction. Geochim Cosmochim Acta. 1991;55(5):1289-94.
32. STUMM WA. Aquatic surface chemistry: Chemical processes at the particle-water interface: John Wiley & Sons; 1987.
33. Stumm W, Sulzberger B. The cycling of iron in natural environments: considerations based on laboratory studies of heterogeneous redox processes. Geochim Cosmochim Acta. 1992;56(8):3233-57.
34. Charlet L, Silvester E, Liger E. N-compound reduction and actinide immobilisation in surficial fluids by Fe (II): the surface FeIIIOFeIIOH° species, as major reductant. Chem Geol. 1998;151(1-4):85-93.
35. Tronc E, Jolivet J-P, Lefebvre J, Massart R. Ion adsorption and electron transfer in spinel-like iron oxide colloids. Journal of the Chemical Society, Faraday Transactions 1: Physical Chemistry in Condensed Phases. 1984;80(10):2619-29.
36. Jeon B-H, Dempsey BA, Burgos WD, Royer RA. Sorption kinetics of Fe(II), Zn(II), Co(II), Ni(II), Cd(II), and Fe(II)/Me(II) onto hematite. Water Research. 2003;37(17):4135-42.
37. Jeon B-H, Dempsey BA, Burgos WD. Kinetics and mechanisms for reactions of Fe (II) with iron (III) oxides. Environ Sci Technol. 2003;37(15):3309-15.
38. Williams AG, Scherer MM. Spectroscopic evidence for Fe (II)− Fe (III) electron transfer at the iron oxide− water interface. Environ Sci Technol. 2004;38(18):4782-90.

39. Géhin A, Greneche J-M, Tournassat C, Brendle J, Rancourt DG, Charlet L. Reversible surface-sorption-induced electron-transfer oxidation of Fe (II) at reactive sites on a synthetic clay mineral. Geochim Cosmochim Acta. 2007;71(4):863-76.
40. Larese-Casanova P, Scherer MM. Fe (II) sorption on hematite: New insights based on spectroscopic measurements. Environ Sci Technol. 2007;41(2):471-7.
41. Gorski CA, Scherer MM. Influence of magnetite stoichiometry on FeII uptake and nitrobenzene reduction. Environ Sci Technol. 2009;43(10):3675-80.
42. Jones AM, Collins RN, Rose J, Waite TD. The effect of silica and natural organic matter on the Fe(II)-catalysed transformation and reactivity of Fe(III) minerals. Geochim Cosmochim Acta. 2009;73(15):4409-22.
43. Gorski CA, Handler RM, Beard BL, Pasakarnis T, Johnson CM, Scherer MM. Fe atom exchange between aqueous Fe2+ and magnetite. Environ Sci Technol. 2012;46(22):12399-407.
44. Handler RM, Beard BL, Johnson CM, Scherer MM. Atom exchange between aqueous Fe (II) and goethite: an Fe isotope tracer study. Environ Sci Technol. 2009;43(4):1102-7.
45. Beard BL, Handler RM, Scherer MM, Wu L, Czaja AD, Heimann A, et al. Iron isotope fractionation between aqueous ferrous iron and goethite. Earth and Planetary Science Letters. 2010;295(1):241-50.
46. Frierdich AJ, Helgeson M, Liu C, Wang C, Rosso KM, Scherer MM. Iron atom exchange between hematite and aqueous Fe (II). Environ Sci Technol. 2015;49(14):8479-86.
47. ThomasArrigo LK, Mikutta C, Byrne J, Kappler A, Kretzschmar R. Iron (II)-Catalyzed Iron Atom Exchange and Mineralogical Changes in Iron-rich Organic Freshwater Flocs: An Iron Isotope Tracer Study. Environ Sci Technol. 2017;51(12):6897-907.
48. Rosso KM, Yanina SV, Gorski CA, Larese-Casanova P, Scherer MM. Connecting Observations of Hematite (α-Fe2O3) Growth Catalyzed by Fe(II). Environ Sci Technol. 2010;44(1):61-7.
49. Zarzycki P, Kerisit S, Rosso KM. Molecular Dynamics Study of Fe(II) Adsorption, Electron Exchange, and Mobility at Goethite (α-FeOOH) Surfaces. J Phys Chem C. 2015;119(6):3111-23.
50. Joshi P, Gorski CA. Anisotropic Morphological Changes in Goethite during Fe2+-Catalyzed Recrystallization. Environ Sci Technol. 2016;50(14):7315-24.
51. Gorski CA, Scherer MM. Fe2+ sorption at the Fe oxide-water interface: A revised conceptual framework. Aquatic Redox Chemistry. 2011;1071:477-517.
52. Handler RM, Frierdich AJ, Johnson CM, Rosso KM, Beard BL, Wang C, et al. Fe (II)-catalyzed recrystallization of goethite revisited. Environ Sci Technol. 2014;48(19):11302-11.
53. Gorski CA, Fantle MS. Stable mineral recrystallization in low temperature aqueous systems: A critical review. Geochim Cosmochim Acta. 2017;198:439-65.
54. Joshi P, Fantle MS, Larese-Casanova P, Gorski CA. Susceptibility of Goethite to Fe2+-Catalyzed Recrystallization over Time. Environ Sci Technol. 2017;51(20):11681-91.
55. Hansel CM, Benner SG, Fendorf S. Competing Fe (II)-induced mineralization pathways of ferrihydrite. Environ Sci Technol. 2005;39(18):7147-53.
56. Schwertmann Ut, Fischer W. Natural “amorphous” ferric hydroxide. Geoderma. 1973;10(3):237-47.
57. Cornell R, Schwertmann U. The iron oxides. Structure, properties. 1998.
58. Das S, Hendry MJ, Essilfie-Dughan J. Transformation of two-line ferrihydrite to goethite and hematite as a function of pH and temperature. Environ Sci Technol. 2010;45(1):268-75.

59. Cudennec Y, Lecerf A. The transformation of ferrihydrite into goethite or hematite, revisited. Journal of Solid State Chemistry. 2006;179(3):716-22.
60. Langner HW, Inskeep WP. Microbial reduction of arsenate in the presence of ferrihydrite. Environ Sci Technol. 2000;34(15):3131-6.
61. Hansel CM, Benner SG, Neiss J, Dohnalkova A, Kukkadapu RK, Fendorf S. Secondary mineralization pathways induced by dissimilatory iron reduction of ferrihydrite under advective flow. Geochim Cosmochim Acta. 2003;67(16):2977-92.
62. Boland DD, Collins RN, Miller CJ, Glover CJ, Waite TD. Effect of Solution and Solid-Phase Conditions on the Fe(II)-Accelerated Transformation of Ferrihydrite to Lepidocrocite and Goethite. Environ Sci Technol. 2014;48(10):5477-85.
63. Jones AM, Collins RN, Waite TD. Redox characterization of the Fe (II)-catalyzed transformation of ferrihydrite to goethite. Geochim Cosmochim Acta. 2017;218:257-72.
64. Yang L, Steefel CI, Marcus MA, Bargar JR. Kinetics of Fe (II)-catalyzed transformation of 6-line ferrihydrite under anaerobic flow conditions. Environ Sci Technol. 2010;44(14):5469-75.
65. Yee N, Shaw S, Benning LG, Nguyen TH. The rate of ferrihydrite transformation to goethite via the Fe (II) pathway. American Mineralogist. 2006;91(1):92-6.
66. Burleson DJ, Penn RL. Two-Step Growth of Goethite from Ferrihydrite. Langmuir. 2006;22(1):402-9.
67. Houghton R. Aboveground forest biomass and the global carbon balance. Global Change Biology. 2005;11(6):945-58.
68. Zhuang Q, McGuire A, Melillo J, Clein JS, Dargaville R, Kicklighter D, et al. Carbon cycling in extratropical terrestrial ecosystems of the Northern Hemisphere during the 20th century: a modeling analysis of the influences of soil thermal dynamics. Tellus B: Chemical and Physical Meteorology. 2011;55(3):751-76.
69. Lalonde K, Mucci A, Ouellet A, Gelinas Y. Preservation of organic matter in sediments promoted by iron. Nature. 2012;483(7388):198-200.
70. Qian Zhao, Poulson SR, Dynes JJ, McBeth JM. Iron-bound organic carbon in forest soils: quantification and characterization. Biogeosciences. 2016;13(16):4777.
71. Kramer MG, Sanderman J, Chadwick OA, Chorover J, Vitousek PM. Long-term carbon storage through retention of dissolved aromatic acids by reactive particles in soil. Global Change Biology. 2012;18(8):2594-605.
72. Baldock J, Skjemstad J. Role of the soil matrix and minerals in protecting natural organic materials against biological attack. Org Geochem. 2000;31(7-8):697-710.
73. Eusterhues K, Wagner FE, Häusler W, Hanzlik M, Knicker H, Totsche KU, et al. Characterization of ferrihydrite-soil organic matter coprecipitates by X-ray diffraction and Mossbauer spectroscopy. Environ Sci Technol. 2008;42(21):7891-7.
74. Chen K-Y, Chen T-Y, Chan Y-T, Cheng C-Y, Tzou Y-M, Liu Y-T, et al. Stabilization of Natural Organic Matter by Short-Range-Order Iron Hydroxides. Environ Sci Technol. 2016.
75. Chen CM, Dynes JJ, Wang J, Sparks DL. Properties of Fe-Organic Matter Associations via Coprecipitation versus Adsorption. Environ Sci Technol. 2014;48(23):13751-9.
76. Gu B, Schmitt J, Chen Z, Liang L, McCarthy JF. Adsorption and desorption of different organic matter fractions on iron oxide. Geochim Cosmochim Acta. 1995;59(2):219-29.
77. Meier M, Namjesnik-Dejanovic K, Maurice PA, Chin Y-P, Aiken GR. Fractionation of aquatic natural organic matter upon sorption to goethite and kaolinite. Chem Geol. 1999;157(3-4):275-84.

78. Chorover J, Amistadi MK. Reaction of forest floor organic matter at goethite, birnessite and smectite surfaces. Geochim Cosmochim Acta. 2001;65(1):95-109.
79. Vindedahl A. Iron Oxide Nanoparticle Aggregation and Reactivity in Simulated Natural Environments [Ph.D. Dissertation]: University of Minnesota, Minneapolis, MN; 2015.
80. Vindedahl AM, Arnold WA, Penn RL. Impact of pahokee peat humic acid and buffer identity on goethite aggregation and reactivity. Environmental Science: Nano. 2015;2(5):509-17.
81. Vindedahl AM, Stemig MS, Arnold WA, Penn RL. Character of humic substances as a predictor for goethite nanoparticle reactivity and aggregation. Environ Sci Technol. 2016;50(3):1200-8.
82. Henneberry YK, Kraus TE, Nico PS, Horwath WR. Structural stability of coprecipitated natural organic matter and ferric iron under reducing conditions. Org Geochem. 2012;48:81-9.
83. Mikutta R, Lorenz D, Guggenberger G, Haumaier L, Freund A. Properties and reactivity of Fe-organic matter associations formed by coprecipitation versus adsorption: Clues from arsenate batch adsorption. Geochim Cosmochim Acta. 2014;144:258-76.
84. Pokrovsky O, Schott J. Iron colloids/organic matter associated transport of major and trace elements in small boreal rivers and their estuaries (NW Russia). Chem Geol. 2002;190(1-4):141-79.
85. Schwertmann U. Inhibitory effect of soil organic matter on the crystallization of amorphous ferric hydroxide. Nature. 1966;212(5062):645.
86. Chen CM, Kukkadapu R, Sparks DL. Influence of Coprecipitated Organic Matter on Fe(aq)(2+)-Catalyzed Transformation of Ferrihydrite: Implications for Carbon Dynamics. Environ Sci Technol. 2015;49(18):10927-36.
87. Zhou Z, Latta DE, Noor N, Thompson A, Borch T, Scherer MM. Fe (II)-catalyzed transformation of organic matter-ferrihydrite coprecipitates: A closer look using Fe isotopes. Environ Sci Technol. 2018.
88. Torn MS, Trumbore SE, Chadwick OA, Vitousek PM, Hendricks DM. Mineral control of soil organic carbon storage and turnover. Nature. 1997;389(6647):170-3.
89. Baldock J, Skjemstad J. Role of the soil matrix and minerals in protecting natural organic materials against biological attack. Org Geochem. 2000;31(7):697-710.
90. Lal R. Soil carbon sequestration impacts on global climate change and food security. science. 2004;304(5677):1623-7.
91. Schmidt MW, Torn MS, Abiven S, Dittmar T, Guggenberger G, Janssens IA, et al. Persistence of soil organic matter as an ecosystem property. Nature. 2011;478(7367):49-56.
92. Singh M, Sarkar B, Sarkar S, Churchman J, Bolan N, Mandal S, et al. Chapter Two - Stabilization of Soil Organic Carbon as Influenced by Clay Mineralogy. In: Sparks DL, editor. Adv Agron. 148: Academic Press; 2018. p. 33-84.
93. Jambor JL, Dutrizac JE. Occurrence and constitution of natural and synthetic ferrihydrite, a widespread iron oxyhydroxide. Chemical Reviews. 1998;98(7):2549-86.
94. Cismasu AC, Michel FM, Tcaciuc AP, Tyliszczak T, Brown JGE. Composition and structural aspects of naturally occurring ferrihydrite. Comptes Rendus Geoscience. 2011;343(2–3):210-8.
95. Cornell RM, Schwertmann U. The iron oxides: structure, properties, reactions, occurrences and uses: John Wiley & Sons; 2003.
96. Eusterhues K, Wagner FE, Hausler W, Hanzlik M, Knicker H, Totsche KU, et al. Characterization of Ferrihydrite-Soil Organic Matter Coprecipitates by X-ray Diffraction and Mossbauer Spectroscopy. Environ Sci Technol. 2008;42(21):7891-7.

97. Schwertmann U, Wagner F, Knicker H. Ferrihydrite–humic associations. Soil Sci Soc Am J. 2005;69(4):1009-15.
98. Cornell R, Schwertmann U. Influence of organic anions on the crystallization of ferrihydrite. Clays Clay Miner. 1979;27(6):402-10.
99. Weiner S, Addadi L. Crystallization pathways in biomineralization. Annual review of materials research. 2011;41:21-40.
100. Liu H, Guo H, Li P, Wei Y. The transformation of ferrihydrite in the presence of trace Fe (II): the effect of the anionic media. Journal of Solid State Chemistry. 2008;181(10):2666-71.
101. Eusterhues K, Hädrich A, Neidhardt J, Küsel K, Keller T, Jandt K, et al. Reduction of ferrihydrite with adsorbed and coprecipitated organic matter: microbial reduction by Geobacter bremensis vs. abiotic reduction by Na-dithionite. Biogeosciences. 2014;11(18):4953.
102. Poggenburg C, Mikutta R, Sander M, Schippers A, Marchanka A, Dohrmann R, et al. Microbial reduction of ferrihydrite-organic matter coprecipitates by Shewanella putrefaciens and Geobacter metallireducens in comparison to mediated electrochemical reduction. Chem Geol. 2016;447:133-47.
103. ThomasArrigo LK, Mikutta C, Byrne J, Kappler A, Kretzschmar R. Iron(II)-Catalyzed Iron Atom Exchange and Mineralogical Changes in Iron-rich Organic Freshwater Flocs: An Iron Isotope Tracer Study. Environ Sci Technol. 2017;51(12):6897-907.
104. Shimizu M, Zhou J, Schröder C, Obst M, Kappler A, Borch T. Dissimilatory reduction and transformation of ferrihydrite-humic acid coprecipitates. Environ Sci Technol. 2013;47(23):13375-84.
105. Cooper RE, Eusterhues K, Wegner C-E, Totsche KU, Küsel K. Ferrihydrite-associated organic matter (OM) stimulates reduction by Shewanella oneidensis MR-1 and a complex microbial consortia. Biogeosciences. 2017;14(22):5171.
106. Society IHS. Elemental Compositions and Stable Isotopic Ratios of IHSS Samples http://www.humicsubstances.org2018 [updated May 16, 2018.
107. Notini L, Latta DE, Neumann A, Pearce CI, Sassi M, N'Diaye AT, et al. The Role of Defects in Fe (II)–Goethite Electron Transfer. Environ Sci Technol. 2018;52(5):2751-9.
108. Tamura H, Goto K, Yotsuyanagi T, Nagayama M. Spectrophotometric determination of iron (II) with 1, 10-phenanthroline in the presence of large amounts of iron (III). Talanta. 1974;21(4):314-8.
109. Rancourt D, Ping J. Voigt-based methods for arbitrary-shape static hyperfine parameter distributions in Mössbauer spectroscopy. Nuclear Instruments and Methods in Physics Research Section B: Beam Interactions with Materials and Atoms. 1991;58(1):85-97.
110. Handler RM, Frierdich AJ, Johnson CM, Rosso KM, Beard BL, Wang CM, et al. Fe(II)-Catalyzed Recrystallization of Goethite Revisited. Environ Sci Technol. 2014;48(19):11302-11.
111. Frierdich AJ, Beard BL, Scherer MM, Johnson CM. Determination of the Fe (II) aq–magnetite equilibrium iron isotope fractionation factor using the three-isotope method and a multi-direction approach to equilibrium. Earth and Planetary Science Letters. 2014;391:77-86.
112. Gu B, Schmitt J, Chen Z, Liang L, McCarthy JF. Adsorption and desorption of natural organic matter on iron oxide: mechanisms and models. Environ Sci Technol. 1994;28(1):38-46.
113. Jones AM, Griffin PJ, Collins RN, Waite TD. Ferrous iron oxidation under acidic conditions – The effect of ferric oxide surfaces. Geochim Cosmochim Acta. 2014;145:1-12.
114. Chen C, Thompson A. Ferrous Iron Oxidation under Varying pO2 Levels: the Effect of Fe (III)/Al (III) Oxide Minerals and Organic Matter. Environ Sci Technol. 2017;52(2):597-606.

115. Daugherty EE, Gilbert B, Nico PS, Borch T. Complexation and redox buffering of iron (II) by dissolved organic matter. Environ Sci Technol. 2017;51(19):11096-104.
116. Leenheer JA, Croué J-P. Characterizing aquatic dissolved organic matter. Environ Sci Technol. 2003;37(1):18A-26A.
117. Louie SM, Spielman-Sun ER, Small MJ, Tilton RD, Lowry GV. Correlation of the Physicochemical Properties of Natural Organic Matter Samples from Different Sources to Their Effects on Gold Nanoparticle Aggregation in Monovalent Electrolyte. Environ Sci Technol. 2015;49(4):2188-98.
118. Buffle J, Wilkinson KJ, Stoll S, Filella M, Zhang J. A Generalized Description of Aquatic Colloidal Interactions: The Three-colloidal Component Approach. Environ Sci Technol. 1998;32(19):2887-99.
119. Vindedahl AM, Stemig MS, Arnold WA, Penn RL. Character of Humic Substances as a Predictor for Goethite Nanoparticle Reactivity and Aggregation. Environ Sci Technol. 2016;50(3):1200-8.
120. Bowen LH. Mössbauer Spectroscopy: An Introduction for Inorganic Chemists and Geochemists. New York: Halsted Press; 1973.
121. Pasakarnis T, McCormick ML, Parkin GF, Thompson A, Scherer MM. Fe II aq–Fe III oxide electron transfer and Fe exchange: effect of organic carbon. Environmental Chemistry. 2015;12(1):52-63.
122. Latta DE, Bachman JE, Scherer MM. Fe electron transfer and atom exchange in goethite: Influence of Al-substitution and anion sorption. Environ Sci Technol. 2012;46(19):10614-23.
123. Greffié C, Amouric M, Parron C. HRTEM study of freeze-dried and untreated synthetic ferrihydrites: consequences of sample processing. Clay Minerals. 2001;36(3):381-7.
124. Mikutta C, Wiederhold JG, Cirpka OA, Hofstetter TB, Bourdon B, Von Gunten U. Iron isotope fractionation and atom exchange during sorption of ferrous iron to mineral surfaces. Geochim Cosmochim Acta. 2009;73(7):1795-812.
125. Zarzycki P, Rosso KM. Stochastic simulation of isotopic exchange mechanisms for Fe (II)-catalyzed recrystallization of goethite. Environ Sci Technol. 2017;51(13):7552-9.
126. Taylor SD, Liu J, Arey BW, Schreiber DK, Perea DE, Rosso KM. Resolving Iron (II) Sorption and Oxidative Growth on Hematite (001) Using Atom Probe Tomography. J Phys Chem C. 2018;122(7):3903-14.
127. Guyodo Y, Banerjee SK, Penn RL, Burleson D, Berquo TS, Seda T, et al. Magnetic properties of synthetic six-line ferrihydrite nanoparticles. Physics of the Earth and Planetary Interiors. 2006;154(3-4):222-33.
128. Thelma SB, Jasmine JE, Anna L, Penn RL, Subir KB. Effects of magnetic interactions in antiferromagnetic ferrihydrite particles. J Phys: Condens Matter. 2009;21(17):176005.
129. Berquó TS, Erbs JJ, Lindquist A, Penn RL, Banerjee SK. Effects of magnetic interactions in antiferromagnetic ferrihydrite particles. Journal of Physics: Condensed Matter. 2009;21(17):176005.
130. Berquó TS, Banerjee SK, Ford RG, Penn RL, Pichler T. High crystallinity Si-ferrihydrite: an insight into its Néel temperature and size dependence of magnetic properties. Journal of Geophysical Research: Solid Earth. 2007;112(B2).
131. Kleber M, Eusterhues K, Keiluweit M, Mikutta C, Mikutta R, Nico PS. Mineral–organic associations: formation, properties, and relevance in soil environments. Adv Agron. 130: Elsevier; 2015. p. 34-100.

132. Kaiser K, Mikutta R, Guggenberger G. Increased stability of organic matter sorbed to ferrihydrite and goethite on aging. Soil Sci Soc Am J. 2007;71(3):711-9.
133. Thompson A, Chadwick OA, Rancourt DG, Chorover J. Iron-oxide crystallinity increases during soil redox oscillations. Geochim Cosmochim Acta. 2006;70(7):1710-27.
134. Frierdich AJ, Luo Y, Catalano JG. Trace element cycling through iron oxide minerals during redox-driven dynamic recrystallization. Geology. 2011;39(11):1083-6.
135. Latta DE, Gorski CA, Scherer MM. Influence of Fe2+-catalysed iron oxide recrystallization on metal cycling. Biochem Soc Trans. 2012;40:1191-7.
136. Swift MJ, Heal OW, Anderson JM, Anderson J. Decomposition in terrestrial ecosystems: Univ of California Press; 1979.
137. Lehmann J, Kleber M. The contentious nature of soil organic matter. Nature. 2015;528(7580):60.
138. Tanaka F, Fukushima M, Kikuchi A, Yabuta H, Ichikawa H, Tatsumi K. Influence of chemical characteristics of humic substances on the partition coefficient of a chlorinated dioxin. Chemosphere. 2005;58(10):1319-26.
139. Vindedahl AM, Strehlau JH, Arnold WA, Penn RL. Organic matter and iron oxide nanoparticles: aggregation, interactions, and reactivity. Environmental Science: Nano. 2016;3(3):494-505.
140. Kaiser K, Guggenberger G. The role of DOM sorption to mineral surfaces in the preservation of organic matter in soils. Org Geochem. 2000;31(7-8):711-25.
141. Pasakarnis TS. Effects of carbon during Fe (II)-catalyzed Fe oxide recrystallization: implications for Fe and carbon cycling: University of Iowa; 2013.
142. Boland DD, Collins RN, Miller CJ, Glover CJ, Waite TD. Effect of solution and solid-phase conditions on the Fe (II)-accelerated transformation of ferrihydrite to lepidocrocite and goethite. Environ Sci Technol. 2014;48(10):5477-85.
143. Zachara JM, Kukkadapu RK, Fredrickson JK, Gorby YA, Smith SC. Biomineralization of poorly crystalline Fe (III) oxides by dissimilatory metal reducing bacteria (DMRB). Geomicrobiology Journal. 2002;19(2):179-207.
144. Theis TL, Singer PC. Complexation of iron (II) by organic matter and its effect on iron (II) oxygenation. Environ Sci Technol. 1974;8(6):569-73.
145. Nurmi JT, Tratnyek PG. Electrochemical properties of natural organic matter (NOM), fractions of NOM, and model biogeochemical electron shuttles. Environ Sci Technol. 2002;36(4):617-24.
146. Kappler A, Benz M, Schink B, Brune A. Electron shuttling via humic acids in microbial iron (III) reduction in a freshwater sediment. FEMS Microbiology Ecology. 2004;47(1):85-92.
147. Lipson DA, Jha M, Raab TK, Oechel WC. Reduction of iron (III) and humic substances plays a major role in anaerobic respiration in an Arctic peat soil. Journal of Geophysical Research: Biogeosciences. 2010;115(G4).
148. Kaiser K, Guggenberger G. The role of DOM sorption to mineral surfaces in the preservation of organic matter in soils. Org Geochem. 2000;31(7):711-25.
149. Yang Y, Lohwacharin J, Takizawa S. Analysis of adsorption processes of dissolved organic matter (DOM) on ferrihydrite using surrogate organic compounds. Environmental Science and Pollution Research. 2017;24(27):21867-76.
150. Vu HP, Shaw S, Brinza L, Benning LG. Partitioning of Pb (II) during goethite and hematite crystallization: Implications for Pb transport in natural systems. Applied geochemistry. 2013;39:119-28.

151. Eusterhues K, Rennert T, Knicker H, Kogel-Knabner I, Totsche KU, Schwertmann U. Fractionation of Organic Matter Due to Reaction with Ferrihydrite: Coprecipitation versus Adsorption. Environ Sci Technol. 2011;45(2):527-33.
152. Katoh M, Murase J, Hayashi M, Matsuya K, Kimura M. Nutrient leaching from the plow layer by water percolation and accumulation in the subsoil in an irrigated paddy field. Soil science and plant nutrition. 2004;50(5):721-9.
153. Riedel T, Zak D, Biester H, Dittmar T. Iron traps terrestrially derived dissolved organic matter at redox interfaces. Proceedings of the National Academy of Sciences. 2013;110(25):10101-5.
154. Weber KA, Achenbach LA, Coates JD. Microorganisms pumping iron: anaerobic microbial iron oxidation and reduction. Nature Reviews Microbiology. 2006;4(10):752.
155. Voelker BM, Morel FM, Sulzberger B. Iron redox cycling in surface waters: effects of humic substances and light. Environ Sci Technol. 1997;31(4):1004-11.
156. Li Y, Yu S, Strong J, Wang H. Are the biogeochemical cycles of carbon, nitrogen, sulfur, and phosphorus driven by the “Fe III–Fe II redox wheel” in dynamic redox environments? Journal of Soils and Sediments. 2012;12(5):683-93.
157. Van Cappellen P, Wang Y. Cycling of iron and manganese in surface sediments; a general theory for the coupled transport and reaction of carbon, oxygen, nitrogen, sulfur, iron, and manganese. American Journal of Science. 1996;296(3):197-243.
158. Singh B, Gilkes R. Properties and distribution of iron oxides and their association with minor elements in the soils of south-western Australia. Journal of soil Science. 1992;43(1):77-98.
159. Bradl HB. Adsorption of heavy metal ions on soils and soils constituents. Journal of colloid and interface science. 2004;277(1):1-18.
160. Lee G, Bigham JM, Faure G. Removal of trace metals by coprecipitation with Fe, Al and Mn from natural waters contaminated with acid mine drainage in the Ducktown Mining District, Tennessee. Applied Geochemistry. 2002;17(5):569-81.
161. Latta DE, Gorski CA, Scherer MM. Influence of Fe2+-catalysed iron oxide recrystallization on metal cycling. Portland Press Limited; 2012.
162. Dixit S, Hering JG. Comparison of arsenic (V) and arsenic (III) sorption onto iron oxide minerals: implications for arsenic mobility. Environ Sci Technol. 2003;37(18):4182-9.
163. Kumpiene J, Lagerkvist A, Maurice C. Stabilization of As, Cr, Cu, Pb and Zn in soil using amendments - A review. Waste Manage. 2008;28(1):215-25.
164. Frierdich AJ, Hasenmueller EA, Catalano JG. Composition and structure of nanocrystalline Fe and Mn oxide cave deposits: Implications for trace element mobility in karst systems. Chem Geol. 2011;284(1-2):82-96.
165. Borch T, Kretzschmar R, Kappler A, Van Cappellen P, Ginder-Vogel M, Voegelin A, et al. Biogeochemical Redox Processes and their Impact on Contaminant Dynamics. Environ Sci Technol. 2010;44(1):15-23.
166. Frierdich AJ, Catalano JG. Controls on Fe (II)-activated trace element release from goethite and hematite. Environ Sci Technol. 2012;46(3):1519-26.
167. Frierdich AJ, Scherer MM, Bachman JE, Engelhard MH, Rapponotti BW, Catalano JG. Inhibition of trace element release during Fe (II)-activated recrystallization of Al-, Cr-, and Sn-substituted goethite and hematite. Environ Sci Technol. 2012;46(18):10031-9.
168. Flynn E, Catalano JG. Influence of Oxalate on Ni Fate during Fe (II)-Catalyzed Recrystallization of Hematite and Goethite. Environ Sci Technol. 2018.

169. Hinkle MA, Catalano JG. Effect of phosphate and sulfate on Ni repartitioning during Fe (II)-catalyzed Fe (III) oxide mineral recrystallization. Geochimica et Cosmochimica Acta. 2015;165:62-74.
170. Tronc E, Belleville P, Jolivet JP, Livage J. TRANSFORMATION OF FERRIC HYDROXIDE INTO SPINEL BY FE(II) ADSORPTION. Langmuir. 1992;8(1):313-9.
171. Martinez CE, McBride MB. Coprecipitates of Cd, Cu, Pb and Zn in iron oxides: solid phase transformation and metal solubility after aging and thermal treatment. Clays and Clay minerals. 1998;46(5):537-45.
172. Liu C, Zhu Z, Li F, Liu T, Liao C, Lee J-J, et al. Fe (II)-induced phase transformation of ferrihydrite: The inhibition effects and stabilization of divalent metal cations. Chem Geol. 2016;444:110-9.
173. Mitsunobu S, Muramatsu C, Watanabe K, Sakata M. Behavior of antimony (V) during the transformation of ferrihydrite and its environmental implications. Environ Sci Technol. 2013;47(17):9660-7.
174. Bolanz RM, Wierzbicka-Wieczorek M, Čaplovičová Mr, Uhlík P, Göttlicher Jr, Steininger R, et al. Structural incorporation of As5+ into hematite. Environ Sci Technol. 2013;47(16):9140-7.
175. Muramatsu C, Sakata M, Mitsunobu S. Immobilization of arsenic (V) during the transformation of ferrihydrite: A direct speciation study using synchrotron-based XAFS spectroscopy. Chemistry Letters. 2012;41(3):270-1.
176. Marshall TA, Morris K, Law GT, Livens FR, Mosselmans JFW, Bots P, et al. Incorporation of uranium into hematite during crystallization from ferrihydrite. Environ Sci Technol. 2014;48(7):3724-31.
177. Jang J-H, Dempsey BA, Catchen GL, Burgos WD. Effects of Zn (II), Cu (II), Mn (II), Fe (II), NO3−, or SO42− at pH 6.5 and 8.5 on transformations of hydrous ferric oxide (HFO) as evidenced by Mössbauer spectroscopy. Colloids and Surfaces A: Physicochemical and Engineering Aspects. 2003;221(1-3):55-68.
178. von Lutzow M, Kogel-Knabner I, Ekschmitt K, Matzner E, Guggenberger G, Marschner B, et al. Stabilization of organic matter in temperate soils: mechanisms and their relevance under different soil conditions - a review. Eur J Soil Sci. 2006;57(4):426-45.
179. Scheinost AC, Abend S, Pandya KI, Sparks DL. Kinetic Controls on Cu and Pb Sorption by Ferrihydrite. Environ Sci Technol. 2001;35(6):1090-6.
180. Davis JA. Complexation of trace metals by adsorbed natural organic matter. Geochim Cosmochim Acta. 1984;48(4):679-91.
181. Tessier A, Fortin D, Belzile N, DeVitre R, Leppard G. Metal sorption to diagenetic iron and manganese oxyhydroxides and associated organic matter: narrowing the gap between field and laboratory measurements. Geochim Cosmochim Acta. 1996;60(3):387-404.
182. Bruemmer G, Gerth J, Tiller K. Reaction kinetics of the adsorption and desorption of nickel, zinc and cadmium by goethite. I. Adsorption and diffusion of metals. Journal of Soil Science. 1988;39(1):37-52.
183. Vu HP, Shaw S, Brinza L, Benning LG. Crystallization of Hematite (α-Fe2O3) under Alkaline Condition: The Effects of Pb. Crystal Growth & Design. 2010;10(4):1544-51.
184. Ford RG, Kemner K, Bertsch PM. Influence of sorbate-sorbent interactions on the crystallization kinetics of nickel-and lead-ferrihydrite coprecipitates. Geochim Cosmochim Acta. 1999;63(1):39-48.

185. Chengshuai L, Fangbai L, Manjia C, Changzhong L, Hui T, Jian H. Adsorption and Stabilization of Lead during Fe (II)-catalyzed Phase Transformation of Ferrihydrite. ACTA CHIMICA SINICA. 2017;75(6):621-8.
186. Du H, Huang Q, Lei M, Tie B. Sorption of Pb (II) by Nanosized Ferrihydrite Organo-Mineral Composites Formed by Adsorption versus Coprecipitation. ACS Earth and Space Chemistry. 2018.
187. Eickhoff M, Obst M, Schröder C, Hitchcock AP, Tyliszczak T, Martinez RE, et al. Nickel partitioning in biogenic and abiogenic ferrihydrite: The influence of silica and implications for ancient environments. Geochim Cosmochim Acta. 2014;140:65-79.
188. Cornell R. Simultaneous incorporation of Mn, Ni and Co in the goethite (α-FeOOH) structure. Clay Minerals. 1991;26(3):427-30.
189. Ford RG, Bertsch PM, Farley KJ. Changes in transition and heavy metal partitioning during hydrous iron oxide aging. Environ Sci Technol. 1997;31(7):2028-33.
190. Elsner M, Schwarzenbach RP, Haderlein SB. Reactivity of Fe (II)-bearing minerals toward reductive transformation of organic contaminants. Environ Sci Technol. 2004;38(3):799-807.
191. Oëzdemir O, Dunlop DJ. Intermediate magnetite formation during dehydration of goethite. Earth and Planetary Science Letters. 2000;177(1-2):59-67.